INFORMATION ONLY



USGS-OFR-85-540

USGS-OFR-85-540



# Uranium-Trend Dating of Quaternary Deposits in the Nevada Test Site Area, Nevada and California

by

J. N. Rosholt, C. A. Bush, W. J. Carr, D. L. Hoover,
W C Swadley, and J. R. Dooley, Jr.

U. S. Geological Survey
Lakewood, Colorado
Open-File Report 85-540
1985

Prepared in cooperation with the
Nevada Operations Office
U.S. Department of Energy
(Interagency Agreement DE-AI08-78ET44802)

## CONTENTS



### TABLES



### ILLUSTRATIONS

## ABSTRACT

The uranium-trend dating method has been used to estimate the ages of alluvium, colluvium, altered volcanic ash, and eolian deposits in the Nevada Test Site area. For dating of deposits of 5,000 to 800,000 years age, the open-system technique consists of determining a linear trend from analyses of four to ten channel samples collected at different depths in a depositional unit, or in the soil profile formed in a depositional unit. The concentrations of $^{238}U$, $^{234}U$, $^{230}Th$, and $^{232}Th$ are accurately determined for each sample where analyses are made on subsamples of the less-than-2 mm-size fraction. Isotopic concentrations are determined by alpha spectrometry utilizing radioisotope dilution techniques. The analytical results are plotted as ratios of $(^{230}U-^{230}Th)/^{238}U$ versus $(^{234}U-^{238}U)/^{238}U$. Ideally these data points yield a linear array in which the slope of the line of best fit changes predictably for increasingly older deposits. The rate of change of slope is determined by the half-period of uranium flux, F(0). An empirical model compensates for differing values of F(0) in response to climate and other local and regional environmental factors.

Analyses of deposits of known ages are required to calibrate the empirical model; calibrations were provided by correlations with deposits dated by the radiocarbon and K-Ar methods. Deposits used for calibration are alluvium of mid-Holocene age (5 Ka) in Colorado, loess of Late Wisconsin age (12 Ka) in Minnesota, glacial till and loess of Bull Lake age (150 Ka) near West Yellowstone, Montana, till of Bull Lake age (150 Ka) near Pinedale, Wyoming, and zeolitized volcanic ash from Lake Tecopa, California (Tuff A, 600 Ka, and Tuff B, 740 Ka). Tuff A and Tuff B are the distal facies of the Lava Creek ash and the Bishop ash, respectively. At best, the uranium-trend ages have an estimated accuracy of about ±10 percent for depositional units between 60,000 and 600,000 years old; however, the uncertainty in the slope is strongly dependent on the quality of the linear trend regarding scatter of data points and the length of the line defined by the points.

Analyses of 36 sample suites are included in this report; U-trend dates were determined on 31 of these suites establishing the age ranges for deposition of four major stratigraphic units at the Nevada Test Site. Median ages for these deposits indicate ages of 40 ± 15 Ka for Q2a sediments, 170 ± 40 Ka for Q2b sediments, 270 · 50 Ka for the younger Q2c stratigraphic unit and 440 ± 60 Ka for the older Q2c unit. Q2s stratigraphic units range in age from about 200 to 500 Ka. Uranium-trend ages of laminar carbonate deposits indicate the time of strong calcium carbonate development rather than the time of deposition of their older host sediments.


## INTRODUCTION

Uranium-series disequilibrium dating methods described by Ku and others (1979) used conventional closed system $^{230}Th/^{234}U$ ratios for dating pedogenic carbonates which form rinds on alluvial gravel. These ages provide reasonable estimates of the minimum age of the alluvium. For conventional uranium-series dating (Ku, 1976), a closed system exists throughout the history of a deposit only if there has been no postdepositional migration of $^{238}U$ or of its daughter products ($^{234}U$ and $^{230}Th$). However, open-system conditions impose no restrictions on postdepositional migration of these radioisotopes within and between deposits. Results of other studies of uranium-series disequilibria

indicate that uranium commonly exhibits an open-system behavior (Ivanovich and Harmon, 1982).

An open-system variation of uranium-series dating called uranium-trend has been tested extensively over the past decade. A preliminary model for uranium-trend dating was described by Rosholt (1980) with samples collected from a variety of Quaternary deposits including alluvium, eolian sediments, glacial deposits, and devitrified volcanic ash. A revised model for uranium-trend systematics is described by Rosholt (1985). The empirical model requires time calibration based on analyses of known age deposits; results of these calibrations are included in Rosholt and others (1985). An abbreviated discussion of the mechanisms of uranium migration in surficial deposits is included in this report.

For uranium-trend dating, the distribution of associated uranium-series members in the geochemical environment during and after sedimentation must have been controlled by open-system behavior. Sediments and geochemical precipitates interact with materials carried in water that moves through these deposits. This water usually contains at least small amounts of uranium, and as this uranium decays, it produces a trail of radioactive daughter products that are readily adsorbed on solid matrix material. If the trail of the daughter products, $^{234}U$ and $^{230}Th$, is distributed through the deposits in a predictable pattern, then a model for uranium-trend dating can be developed. The large number of geochemical variables in an open system precludes the definition of a rigorous mathematical model for uranium migration. Instead, an empirical model is used to define the parameters that can reasonably explain the patterns of isotopic distribution. This model requires independent time calibration with known-age deposits and careful evaluation of the stratigraphic relationships of the deposits to be dated.

In the geologic environment, uranium occurs chiefly in two different phases: (1) as a resistate or fixed phase (solids are dominant) where uranium is structurally incorporated in matrix minerals, (2) a mobile phase (water is dominant) which includes the uranium flux that migrates through a deposit. This mobile-phase uranium is responsible for an isotopic fractionation process in the $^{234}U$-$^{230}Th$ series (daughter emplacement) that enables the uranium-trend dating technique to work. Another fractionation process is the preferential leaching of $^{234}U$ from the fixed phase. Many of the deposits analyzed in this study are slightly moist and typically not wet or saturated. Nevertheless, uranium migration occurs, perhaps seasonally, either in solution or on colloids that slowly move through void spaces between mineral grains. In arid and semiarid environments, much of the mobile-phase uranium resides on the surface of dry mineral grains most of the time, and only a small amount of the time it is in solution or in suspension moving through a deposit. As a deposit undergoes interstratal alteration, some uranium isotopes are released from the fixed phase and enter the mobile phase; this process results in another form of isotope fractionation ($^{234}U$ displacement).

Analyses of the isotopic abundances of $^{238}U$, $^{234}U$, $^{232}Th$, and $^{230}Th$ in a single sample do not establish a meaningful time-related pattern of distribution in an open-system environment. However, analyses of several samples, each of which has slightly different physical properties and slightly different chemical compositions, may provide a useful pattern in the distribution of these isotopes. Analyses of 6 to 8 samples per unit, from a relatively large number of alluvial, colluvial, glacial, and eolian deposits has shown that time-related patterns exist.



The purpose of this investigation is to determine the reliability of an empirical radiometric dating technique (uranium-trend), extending from a few thousand to more than one-half million years, to aid in the geologic study of surficial deposits. This uranium-trend dating method has been applied to the Nevada Test Site region where a major effort is underway to define and date late Cenozoic stratigraphic deposits under the U.S. Department of Energy Nevada Nuclear Waste Storage Investigations project. Numerous trenches excavated in the surficial deposits of the area have provided excellent sites for sampling the deposits (Swadley and Hoover, 1983; Swadley and others, 1984). Stratigraphic units defined by Hoover and others, (1981) were collected for this investigation.

## EMPIRICAL MODEL

The very long-lived $^{238}U$ isotope (half life of $4.5 \times 10^9$ years) upon radioactive decay, produced long-lived daughter products, $^{234}U$ and $^{230}Th$. Because the half-life of $^{234}U$ is 248 Ka, this isotope has a potential as a geochemical tracer in deposits that are as old as 800 Ka. The half-life of $^{230}Th$ is 75 Ka; because of its daughter-parent relation to $^{234}U$, it is a key isotope used in nearly all uranium-series dating models (Ku, 1976). The system equilibrium of the parent material is disturbed during transport, and the attainment of a new, readjusted, system equilibrium starts in the sediment at the time of deposition. Thus, for surficial deposits, the starting point for the uranium-trend clock is the initiation of movement of water through the sediment rather than initiation of soil development, although both of these processes may start at essentially the same time.

The empirical model incorporates a component called uranium flux, F(0). The physical significance of F(0) is not well understood; it is related to the effective concentration of uranium moving through a deposit, which in turn is a function of climate, texture of sediment, and the amount of uranium in the mobile phase. In the model, the effect of this flux on isotopic variations decreases exponentially with time. The following is an oversimplified example of the uranium flux in alluvium. At the time of deposition, large volumes of water pass through the alluvium. However, once the surface becomes geomorphically stable, the sediment compacts and soils subsequently develops; during these phases, the volume of water that passes through the alluvium is significantly less. Both the quantity of water passing through and affecting a deposit, and the concentration of uranium in this water are components of the flux; its magnitude is a function of the concentration of uranium in the mobile phase relative to the concentration of uranium in the fixed phase.

Because of the large number of variables in a system that is completely open with respect to migration of uranium, a rigorous mathematical model based on simple equations for radioactive growth and decay of daughter products cannot be constructed. Instead, an empirical model is based on results obtained from several alluvial, colluvial, glacial, and eolian deposits of different ages. The model requires calibration of both the uranium-trend slope and the uranium-flux factor, F(0), based on analytical results from deposits of known age.

The isotopic composition of several samples from the same deposit, expressed in activity units, is required for solution of the model. The uranium-trend value from which ages are calculated is the slope of the line representing

$$\frac{\Delta(^{234}U - ^{238}U)}{\Delta(^{234}U - ^{230}Th)}$$

To accommodate measured isotopic data, the variations are normalized to $^{238}U$ and the uranium-trend model can be written in the following form,

$$\frac{Y}{X} = \frac{\Delta(^{234}U - ^{238}U)/^{238}U}{\Delta(^{234}U - ^{230}Th)/^{238}U} = \frac{C_1 e^{-\lambda_0 t} + C_2 e^{-\lambda_2 t}}{C_3 e^{-\lambda_0 t} + C_4 e^{-\lambda_2 t} + C_5 e^{-\lambda_3 t}}$$

$$C_1 = \frac{-\lambda_0\lambda_2}{\lambda_2-\lambda_0}; \quad C_2 = \frac{\lambda_2\lambda_2}{\lambda_2-\lambda_0}; \quad C_3 = \frac{3\lambda_0\lambda_2\lambda_3}{(\lambda_2-\lambda_0)(\lambda_3-\lambda_0)};$$

$$C_4 = \frac{3\lambda_2\lambda_2\lambda_3}{(\lambda_0-\lambda_2)(\lambda_3-\lambda_2)} + 2\lambda_2; \quad C_5 = \frac{3\lambda_2\lambda_3\lambda_3}{(\lambda_0-\lambda_3)(\lambda_2-\lambda_3)} - \lambda_3$$

where (1) $\lambda_0$ is the decay constant of F(0)=ln 2/(half period of F(0)], (2) $\lambda_2$ is the decay constant of $^{234}U$, and (3) $\lambda_3$ is the decay constant of $^{230}Th$. These are equations that define the empirical model and the numerical constants in the coefficients preceding the exponential terms were determined by computer to provide a model with the best fits for deposits of known age. The alternative uranium-trend slope represented by the equation

$$\frac{Y}{X} = \frac{\Delta(^{234}U - ^{238}U)/^{238}U}{\Delta(^{238}U - ^{230}Th)/^{238}U}$$

is used to solve for the age. An example of this uranium-trend plot is shown in Figure 1 where a York fit (Ludwig, 1979) is used to obtain the least squares regression line.

An additional parameter in the uranium-trend plot is the intercept of the slope line on the X-axis, $x_i$, represented by the equations

$$y = mx + b$$

$$x_i = -b/m$$

where m is the measured slope of the line, b is the intercept on the Y-axis, and $x_i$ is the intercept on the X-axis. The value of $x_i$ is used to obtain the calibration for the uranium-trend model.

A different type of plot is used to determine if all the samples included in the uranium-trend slope describe a reasonable linear array on a thorium plot. This plot serves as a useful criterion to determine if all of the samples are likely to be from the same depositional unit and if any samples contain a significant amount of foreign material.

The thorium plot of the isotopic data can be constructed when the $^{234}U/^{230}Th$ ratios of the samples are plotted on the X-axis versus the $^{232}Th/^{230}Th$ ratios plotted on the Y-axis as shown in Figure 2.



The half period of F(0) and its decay constant, $\lambda_0$, are strictly empirical values that allow selection of the proper exponential coefficient in the equation for the uranium-trend model. For deposits of unknown age, a method is required to determine the proper value of $\lambda_0$ to be used in the equation; this value is determined from a calibration curve based on $\lambda_0$ values obtained for units of known age. For this calibration, the values of $x_i$ are plotted against the half periods of F(0) as shown on the log-log graph in Figure 3. The calibration curve is defined by the proper $\lambda_0$ values that yield the known ages for calibration units using the model equation. The $x_i$ values for deposits of known-age are used for calibration. These values are plotted against the half periods of F(0) equivalent to their $\lambda_0$ values. The solution of the empirical equation, using any given half period of F(0) yields a fan-like array of uranium-trend slopes representing various ages. These slopes rotate counterclockwise from the first to second quadrant of the uranium-trend plots. For deposits whose analyses are included in this paper, the F(0) value is determined from the calibration graph (Fig. 3) using the $x_i$ value measured on the uranium-trend plot of the data for each depositional unit.

Four primary points based on different radiometric dating techniques were used for the calibrations: (1) a radiocarbon age of 12 Ka (Frye, 1973) was used for loess of Late Wisconsin age in Minnesota, (2) an obsidian hydration age of 150 Ka (Pierce, 1979) was used for deposits of Bull Lake age near West Yellowstone, Montana, and in northwestern Wyoming, (3) a K-Ar age of 0.6 Ma was used for calibration of the Lava Creek ash bed, which correlates with the zeolitized ash in Tuff A, Lake Tecopa, California (Izett and others, 1970), and (4) a K-Ar age of 0.73 Ma was used for Bishop ash bed (Dalrymple and others, 1965) which correlates with Tuff B at Lake Tecopa.

## GEOLOGIC SETTING

The Nevada Test Site is in the southern part of the Great Basin, an area characterized by north-trending linear mountain ranges that are flanked by extensive alluvial fans and separated by broad alluvial basins. The geographic area including the location of sampling sites for uranium-trend dating is shown in Figure 4. The climate is arid and vegetation is limited to sparse desert plants. Quaternary surficial deposits in the NTS region primarily include alluvial deposits of coarse material, fluvial deposits of sand derived from eolian material, eolian sheets and dunes, and debris flows. Surficial units present in the region are summarized by Swadley and others (1984, Fig. 3).

### Late Cenozoic Stratigraphy

The late Tertiary and Quaternary deposits of the study area consist of alluvium, eolian sands, colluvium, lake sediments, and volcanic deposits. These range in age from greater than 3 m.y. old for some of the lake sediments to less than about 150 years old for the youngest alluvial unit (Hoover and others, 1981). Hoover and others (1981) described the stratigraphy of these deposits and defined characteristics by which they can be mapped and correlated across the region on the basis of age, lithology, and depositional environment. The following brief descriptions of the map units are based mainly on their work. The deposits are grouped herein into four major units: (1) late Pliocene and Pleistocene, (2) Pliocene(?) and early Pleistocene, (3) middle and late Pleistocene, and (4) Holocene.

## Late Pliocene and Pleistocene Deposits

The oldest surficial deposits investigated are predominantly of late Pliocene age and consist of lacustrine sediments. These lacustrine deposits are mainly unconsolidated to moderately indurated marl and silt that locally contain beds of limestone, sand, and fine-grained volcanic ash. They were deposited in Lake Amargosa, which occupied much of what is now the Amargosa Desert valley (Fig. 4) during the late Pliocene; remnants of the lake probably persisted into the early Quaternary.

The age of the lacustrine deposits is not precisely known; however, an ash bed near the middle of the unit yielded radiometric ages of about 3 Ma (fission-track method, C. W. Naeser, U. S. Geological Survey, written commun., 1980) and 3.8 Ma (K-Ar method on biotite; R. L. Hay, University of California, Berkeley, written commun., 1979). A second ash bed near the top of the unit was dated at 2.1 ± 0.4 Ma by the fission-track method (C. W. Naeser, written commun., 1982). A slightly younger age is suggested for the upper part of the deposits by mammoth remains that are considered to be less than 2 Ma (C. A. Repenning, U. S. Geological Survey, written commun., 1982); these deposits are beyond the range of uranium-trend dating.

## Pliocene(?) and Early Pleistocene Deposits

These deposits consist of alluvium that mainly is early Pleistocene but in some areas may be as old as latest Pliocene. Unit QTa, generally older than about 0.74 Ma, is largely coarse debris flows, but talus, colluvium (QTc) and pediment gravel (QTg) are present in some areas. The QTa deposits are commonly eroded and dissected, and normally exhibit strong calcic soils, which locally result in low permeability.

The approximate age of unit QTa is limited by the ages of enclosing units; there are no dated materials within the unit. QTa unconformably overlies lacustrine deposits at several localities in the area (Swadley, 1983), indicating the QTa deposits locally are less than 2 Ma. Unit QTa is overlain by unit Q2e, that locally contains lenses of volcanic ash correlated with the Bishop ash by Izett (1982) on the basis of their similar chemistry. Radiometric dates for samples from the Bishop ash indicate that it is 0.74 Ma old (Izett, 1982). The lower part of unit Q2e is considered approximately 0.74 Ma old on the basis of the correlation with the Bishop ash. A period of erosion and weathering occurred following the deposition of QTa but prior to deposition of Q2e (Hoover and others, 1981), suggesting that QTa deposits may be substantially older than the 0.74 Ma old limit implied by its stratigraphic position below Q2e deposits containing the Bishop ash. Basalt ash deposits in fractures within unit QTa exposed in two fault trenches in eastern Crater Flat are inferred to be approximately 1.2 Ma (Swadley and others, 1984), possibly restricting further the upper limit for the age of unit QTa. One QTa deposit was sampled, analyzed, and found to be beyond the range of the U-trend method.

## Middle and Late Pleistocene Deposits

Middle and late Pleistocene deposits (unit Q2) consist of fan alluvium, fluvial and eolian sands, and volcanic ash. These deposits have been subdivided into five mappable units on the basis of relative age and lithology: three alluvial units, Q2c, Q2b, and Q2a (in order of decreasing age); eolian dunes and sand sheets, Q2e, and fluvial sand sheets, Q2s. The lithologies, stratigraphic relations, and soil development of these units are described in more detail by Hoover and others (1981, p. 15).



Unit Q2c consists of fluvial fan deposits and some debris flows. These deposits typically are unconsolidated, poorly to well-sorted, nonbedded to well-bedded, angular to rounded gravel with sand and silt in the matrix. Interbeds of silty sand are locally common. Alluvial fans of Q2c generally are deposited on unit QTa on the middle and upper valley slopes; Q2c also occurs as terrace deposits in larger stream valleys. Eight age determinations were made on fluvial deposits of unit Q2c.

Eolian deposits of unit Q2e occur as dunes and sand sheets in and adjacent to the Amargosa Desert valley. Ramps of fine, well-sorted sand as much as 50 m thick flank many of the hills bordering the Amargosa Desert on the north. Unit Q2e is locally interbedded with the lower part of Q2c and is clearly older than Q2b. One Q2e deposit analyzed for this study was beyond the range of the U-trend method.

The inferred age of 0.74 Ma old for lenses of volcanic ash in the lower part of unit Q2e discussed above is considered the approximate lower age limit for both units Q2e and Q2c. Younger Q2c gravels locally overlie and contain reworked cinders from the Big Dune basalt center 11 km northwest of Lathrop Wells (Fig. 4), which has yielded K-Ar dates ranging from 230,000 to 300,000 years old (Vaniman and others, 1982), indicating the approximate age for the younger part of Q2c deposition.

Fluvial sand sheets of unit Q2s occur along major streams and drainages downstream from dunes. The sheets consist of water-laid fine to medium gravelly sand or stream-reworked windblown sand, and commonly rest on Q2c fans. Three Q2s deposits were dated in this study.

Unit Q2b is similar to Q2c in depositional environment and lithology. It occurs as terrace deposits that are inset in Q2c and underlies lower slope fans. These Q2b fans commonly merge upslope with Q2c fan deposits. Six suites of samples from unit Q2b were dated in this study.

The youngest fluvial part of Q2, unit Q2a, consists of debris flow deposits that are large enough to be mapped at only three localities in this study area. Q2a is poorly sorted, unconsolidated sand- to clay-size material that contains some gravel. Nine age determinations were made on the fluvial part of unit Q2a.

Overlying unit Q2a (and older units) is a thin unit of eolian silt which probably is desert loess. This unit is not present in Holocene deposits (unit Q1) in the study area, indicating a probable age of pre Holocene, but post Q2a (late Pleistocene). Two sample suites were collected and analyzed in this material; only one U-trend age estimate was obtained from these suites.

## Holocene Deposits

Unit Q1, Holocene in age, is principally coarse fluvial material and local debris flows in and along present drainages. It has little or no soil development and, mainly on the basis of topography, may be divided locally into as many as three units (Q1a, b, and c). In addition, Q1 contains local eolian deposits (Q1e) and sand sheets (Q1s). No U-trend ages were attempted on Q1 deposits because of the large percentage error limitations inherent in the method for deposits as young as Holocene.

## EXPERIMENTAL PROCEDURES

### Sample Collection, Preparation, and Chemical Procedures

To obtain a uranium-trend date, several channel samples, about 1 kg each, are collected from a vertical section of each depositional unit. The required number of samples for a reliable trend plot depends on the variation in ratios of uranium and thorium that define the trend line. The minimum number of samples needed is not known until analyses are completed; therefore, subdividing the unit into a larger number of samples usually will increase the likelihood of better defining the uranium-trend line. A minimum of three samples is required, but it is desirable to have 5 to 8 samples in a given sampling unit to determine a reliable slope. It is not always possible to determine, in the field, the exact boundary between depositional units. To help alleviate this problem, collection of a larger number of samples is required to determine the boundary between some depositional units. For soils, sampling by horizon or subhorizon usually is appropriate. Differences in mineralogy and particle size of the sediment also are good field criteria for selecting samples that are likely to have a suitable spread of values to provide a well-defined linear trend. It is preferable to sample a channel through deposits exposed in a trench wall or a relatively fresh, well-exposed, outcrop. Examples of sampled sections are shown in the sketch of collection sites in Yucca Mountain Trench 14 (Fig. 5).

Depositional units at the Nevada Test Site commonly contain pebbles and larger fragments and a subsample of less-than-2 mm size is retained for analysis, pulverized to less-than-0.2 mm size, homogenized, and processed. In deposits where the isotopic composition is similar in each sample, additional data can be obtained by analyzing that part of the unpulverized subsample that is less-than-0.3 mm size. Both <2 mm and <0.3 mm size fractions were analyzed for samples from six localities at the NTS (TSV396, SCF1, SCF2, CF2, YM2 and YM13).

Chemical procedures used for separating uranium and thorium for alpha spectrometry measurements are those described by Rosholt (1985). Spikes of $^{232}U$ and $^{229}Th$ are used in the radioisotope-dilution technique to determine the concentrations of uranium and thorium. For defining uranium-trend slopes, a uranium separate is counted four different times in the alpha spectrometer and a thorium separate is counted three different times. The procedure of determining the isotopic abundances of $^{230}Th$, $^{235}U$, and $^{233}U$ is described by Rosholt (1984).

## DISCUSSION OF RESULTS

Uranium-trend analyses for 28 sample sections at or near the Nevada Test Site, some of which include deposits of more than one age, are included in this report. Site locations are shown on Figure 4, and descriptions of the 37 depositional units analyzed are listed in Table 1. Table 2 contains a generalized description of each sampled unit, including selected soil data and lithologic characteristics, depths below the surface, and uranium and thorium content for each sample. Uranium and thorium concentrations are accurate to within ±2 percent of the reported value. Five sample sequences (SFF, Q2E, SCF1, SCF2, and SCF3) were not datable using the uranium-trend model. Two of



the undatable units are eolian sand and the remaining three are fluvial sand. The isotopic ratios required for the plots are listed in Table 3. Also included with the isotopic ratios are error values (2 standard deviation) required for computer calculation of the slope and uncertainty of the slope of the linear regression line. An additional significant figure for these data (Table 3) is retained for the slope calculation to avoid premature arithmetic rounding. Uranium-trend and thorium plots for each deposit listed in Table 2 are shown in Figures 6-34.

Some data were not included in the calculations of uranium-trend age. A few of the units sampled and analyzed at the beginning of this investigation included near-surface materials at depths of less than 8 cm. Data for these near-surface samples have been excluded from the calculation of the linear regression line because of the likelihood of contamination by dust and other foreign material that is significantly younger than the main deposit. In some other cases, samples were excluded from the uranium-trend line if, on the thorium plot, they did not fit the linear array defined by the other samples from the deposit. One reason that a sample may depart from linearity is that it is composed in part or entirely of material from an older or younger deposit. This problem usually is encountered only with the upper or lower sampled part of a deposit. Another reason for the above discrepancies is that the porosity and permeability characteristics of layers within the depositional unit may be sufficiently different so that very different effective uranium fluxes may have occurred in the same deposit. For instance, the effective flux rate is different for an open-work gravel in which the mobile-phase uranium has a short residence time compared to that for a clayey layer through which fluids move more slowly. Assimilation of uranium in a deposit during a late stage of alteration can cause anomalous variations in the isotopic system, such as the incorporation of uraniferous opal. Examples of samples excluded from uranium-trend slope calculations include: those from the upper horizons in FFPG, 31, RV1-J, 39, CF1, YM13, and YM14; those with anomalous uranium content in TSV-307E and YM14B-2; and sample SCF4-5 that contains a mixture of two different depositional facies in the section. On the basis of the fit of data on the thorium plot, it appears possible to identify samples in the profile that do not belong to the same stratigraphic unit or that have mineralogic or grain-sized components that are not comparable to the whole of the unit.

The uranium-trend model parameters for 33 dated units from NTS are shown in Table 4. These parameters include the values for X-intercept, half period of F(0), uranium-trend slope, and age for each unit. The uncertainty for each age determination listed is one standard deviation, and includes scatter as defined by Ludwig (1979). A unit number for each dated deposit is included in Table 4 and shown on the calibration curve (Fig. 3).

Specific results for each geographic area (Table 1) generally are described below in order of increasing age (Q2a, Q2b, Q2c, QTa). The five samples in unit SFF, collected from a silty, vesicular A horizon in a trench on the edge of Frenchman Flat tend to form a circular array rather than a linear relationship on the U-trend plot (Fig. 6); no U-trend age could be calculated for these samples. A similar eolian sediment with underlying CCa horizon was recollected; 10 samples in section FFPG gave a U-trend age of 30 Ka with large error of ± 30 Ka. The top sample (FFPG-1) was not included in the U-trend slope (Fig. 7) because of possible infiltration of material from the surface. The uppermost sample of 6 samples of the underlying alluvium in

the Q2b deposit (S1) also was not included in the U-trend line because of probable infiltration of material from the overlying deposits. Unit S1 yielded a trend line with limited range (Fig. 8) and gives an age of 80 ± 60 Ka. However, an extensive resampling of the alluvium in the trench at Frenchman Flat (represented by units F2 and F3) gave more defined U-trend ages (Figs. 9 and 10) of 200 ± 80 Ka and 190 ± 70 Ka for the upper and lower parts of unit Q2b, respectively.

Units with three different U-trend ages were identified in Rock Valley trench RV1 (Ander and others, 1984, Fig. 8). The upper Q2a units of slope wash (RV1 A-D, Fig. 11) and a buried B horizon (RV1 J-O, Fig. 12) give ages in the 20–50 Ka range. The underlying Q2b unit, represented by the calcareous B horizon (RV1 P-U, Fig. 13), has a U-trend age of 180 ± 40 Ka. The lowest parts of the two RV1 sections consist of the Q2c unit; these deposits gave similar ages of 310 ± 40 Ka (RV1 E-I, Fig. 11) and 270 ± 30 Ka (RV1 V-Z, Fig. 13).

The upper Q2a units sampled in Rock Valley trench RV2 gave U-trend ages of 38 ± 10 Ka (TSV-307, Fig. 14) and 36 ± 20 Ka (RV2-U, Fig. 15); these units are equivalent to the upper units in the nearby Rock Valley trench RV1. The lower gravel alluvium of the Q2c unit in the RV2 section, which was sampled at a greater depth than the RV1 sections, yields an age of 390 ± 100 Ka (RV2-L, Fig. 15).

Initially, only four samples were collected for dating a reddish-brown soil in a sand sheet exposed in a trench near the Jackass Flats Engine Test Stand (ETS, Fig. 4); these samples were insufficient to determine a U-trend age (Fig. 16). Nine samples from a channel through a thicker part of the argillic B horizon in the Q2a sheet sand was resampled; a U-trend slope (Fig. 17) gives an age of 160 Ka with a relatively large error of 90 Ka. This poor U-trend value should be closer to the upper limit of about 250 Ka.

Eight samples of alluvium (S9) were collected from a 1.6 m-thick unit in the upper part of the Jackass Divide trench (JD, Fig. 4). The uranium and thorium isotopic ratios of the upper two samples resemble that of samples from deposits of unit Q2a in other trenches, therefore the values for these two samples were excluded from the U-trend slope of the underlying Q2c unit. The lower six samples yielded an age of 270 ± 50 Ka (Fig. 18); the upper two samples also have a wide divergence from the regression line on the thorium plot of the lower 6 samples. A 1.2 m-thick unit of older alluvium was collected from the lower part of Jackass Divide trench. The 8 samples in this unit provide well defined U-trend and thorium plots (Fig. 19) that indicate an age of 830 ± 40 Ka. This age corresponds to those determined for older deposits of unit Q2c.

A series of 8 samples (SCF1) of pebbly fluvial gravel in unit Q2b was collected in the west trench in South Crater Flat. Both the less-than-2-mm and less-than-0.3 mm size fractions were analyzed in each sample; however, no U-trend age could be calculated from either set of plots (Fig. 20). Another series of 5 samples (SCF3) was recollected from the trench, but a U-trend age could not be calculated for the less-than-2 mm size fraction (Fig. 21). A 0.8 m-thick sequence of 9 samples in fluvial sand and pebble gravel (SCF2) was collected in unit Q2c exposed in the west trench at South Crater Flat. These samples did not provide a U-trend age because of the excessive scatter of the points for both the less-than-2 mm and the less-than-0.3 mm size fractions in



all samples (Fig. 22). Eight samples from a 1.2 m-thick section (SCF4) of unit Q2c was recollected from the trench. The upper 4 samples of sandy sediment defined a different trend line than the lower 3 samples of pebbly alluvium; the intermediate sample (SCF4-5) appears to be a mixture of both units (Fig. 23). Uranium-trend ages for the upper and lower parts are 400 and 480 Ka, respectively. These values provide an estimated average age of 440 ± 60 Ka for this Q2c deposit.

A group of 6 samples consisting mainly of calcium carbonate (TSV 396) was collected from trench 1 in Crater Flat. Both the less-than-2-mm and less-than-0.3 mm were analyzed for each subsample. Each size fraction yielded similar ages with an average age of 48 ± 20 Ka as obtained from the U-trend plots shown in Figure 24. These results suggest significant calcium carbonate accumulation and K-horizon development over the past 50 Ka; U-trend ages in this kind of enriched carbonate material reflect the time of strong calcium carbonate development in older sediments.

Eight samples (CF1) of the upper alluvium (Q2a) were collected from trench 3 in Crater Flat. On the thorium plot (Fig. 25), sample CF1-2 diverges from the regression line defined by the remaining samples, therefore it was excluded from the U-trend slope that gives an estimated age of 40 ± 10 Ka. A 25 cm thick buried argillic B horizon in unit Q2a also was collected in this trench (CF6) which yielded a U-trend plot of 5 samples (Fig. 26) with an approximate age of 190 ± 50 Ka. Seven samples (CF2) of alluvium in unit Q2c underlying the argillic B horizon were collected from the trench; both less-than-2 mm and less-than-0.3 mm size fractions gave similar U-trend plots (Fig. 27) and an age of 270 ± 30 Ka.

The YM2 section in Yucca Mountain Trench 2 consists of 4 samples from a thin buried B horizon formed in alluvium (YM2U) and 6 samples from the underlying calcareous gravelly alluvium (YM2L). Plots for the less-than-2-mm and the less-than-0.3 mm size fractions for these deposits are shown in Figure 28. The U-trend age of the upper (Q2a) unit is 47 ± 18 Ka and that of the lower (Q2b) unit is 145 ± 25 Ka.

The YM13 section collected from Yucca Mountain Trench 13 contained deposits of two different ages; an upper Q2a unit (6 samples), and a lower Q2c unit (6 samples). The upper sample in each unit was not included in the U-trend plot because both samples contained admixtures of material from the overlying deposit (Fig. 29). The fractions finer than 2 mm and finer than 0.3 mm were analyzed for each sample in the section. Ages of 35 Ka and 46 Ka for these fractions, respectively, provide an age of about 40 ± 10 Ka for the upper unit (Q2a); and ages of 220 Ka and 250 Ka respectively, provide an age estimate of 240 ± 50 Ka for the lower unit (Q2c).

Two superposed B horizons are exposed in the upper 90 cm of Yucca Mountain Trench 14 (Fig. 5). A 30 cm-thick channel (YM14B) consisting of the lower B horizon only was sampled from the north wall of the trench. Sample YM14B-2 had a higher uranium content than the other samples in this unit, which reflects recent addition of uranium; this sample is not compatible with the other samples in the unit and it was excluded from the U-trend line. The age calculated from the remaining 8 samples representing unit Q2a (Fig. 30) is 38 ± 10 Ka. A 60 cm-thick section (YM14U) containing both the upper and lower B horizons formed in Q2a sand was collected from the south wall in the trench (Fig. 5). The upper sample (YM14-1) is not included in the U-trend slope

(Fig. 31) because it contains material from the overlying sediment. The age obtained from the remaining 8 samples is 90 ± 50 Ka; however, this age is considered to be inaccurate because the section includes two B horizons that may be formed in deposits of different ages. A more reliable U-trend age for the lower 3 samples in the lower B horizon of unit Q2a is 55 ± 20 Ka. A 1.7 m-thick section was collected in the lower Q2c alluvium in the Yucca Mountain Trench 14 (Fig. 5). Three types of Q2c deposits are exposed in the trench: (1) a layer of laminar carbonate in the upper 0.6 m (YM14M, 10-14), (2) a calcareous-sandy sediment in the middle 0.35 m (YM14L, 15-17), and (3) calcite-cemented gravel in the lower 0.75 m (YM14L, 18-22). The U-trend dates for these samples (Fig. 31) suggest that the carbonate accumulation started in the middle part of this section about 270 ± 90 Ka ago. The underlying sandy and gravelly alluvium of unit Q2c has ages of 420 ± 50 Ka and 480 ± 90 Ka, respectively.

A 1.2 m-thick channel in alluvial unit Q2b (CBQ) was collected from the Charlie Brown Quarry northeast of Shoshone, California. The results of the analyses of 8 samples are shown in Figure 32, which gave U-trend age of 160 ± 25 Ka. It unconformably overlies the Tuff A ash bed found in nearby Lake Tecopa (Shepard and Gude, 1968) which has been correlated with the 600 Ka Lava Creek ash (Izett, 1982).

The FHA unit consists of volcanic ash which has been partially altered to clay that was sampled at an outcrop at Fairbanks Hills, Nevada (Fig. 4). A minimum age of 600 Ka was calculated from the poorly defined U-trend plot shown in Figure 33.

Eight samples were collected from an 80 cm-thick channel in a trench on the Eleana Pediment (Fig. 4). The carbonate-cemented alluvium is equivalent to unit QTa but its age is beyond the limits of the dating technique. The U-trend age calculated from the from the measured slope (Fig. 34) yields a minimum age of 800 Ka.

## SUMMARY

Uranium-trend dating is a useful method of determining the approximate age of Quaternary deposits in the Nevada Test Site area. The method is the most accurate in the range of 60,000 to 600,000 years. Samples that have a wide spread of data points and minimum scatter about the uranium-trend slope at best may be accurate within ± 10 percent. Relative errors are large near the lower and upper limits of the age range of the method. Age resolution for deposits less than 20,000 years old have errors equal to or greater than the reported age. With respect to the maximum age limit of deposits (greater than 600,000 years), the error usually is greater than 20 percent, thus the limit on the possible maximum age becomes uncertain for ages greater than 700,000 years. Dating of deposits from the Nevada Test Site and in New Mexico (J. N. Rosholt, unpublished data) indicate that age resolution is better for calcareous deposits than for noncalcareous deposits such as carbonate-free till and loess. Poorly sorted alluvial deposits of mixed mineralogy usually yield a better spread of the data points on the uranium-trend plot than do eolian sand or other quartz-rich sand deposits that have little or no soil development.

A tabulation of 31 uranium-trend ages determined on alluvial and fluvial units at NTS are included in Table 5 modified from Swadley and others



(1984). The results are listed according to stratigraphic units defined by Hoover and others (1981). A sample suite (FFPC) containing a loess deposit dated at approximately 30 Ka. The age range in the remaining Q2a deposits of slope wash sand and fluvial gravel is 31 ± 10 to 55 ± 20 Ka. A poor age of sample suite 31 is replaced by results from recollected samples in Frenchman Flat (F2 and F3); thus, the age range of Q2b deposits is considered to be 145 ± 25 to 200 ± 80 Ka. Two groups of Q2c deposits have been found. The younger Q2c stratigraphic unit ranges from 240 ± 50 Ka in the Yucca Mountain area to 310 ± 40 Ka at Rock Valley. The older Q2c stratigraphic unit, sampled in Rock Valley, Jackass Divide, and South Crater Flat, has a range of 390 ± 100 to 440 ± 60 Ka. Q2a deposits dated from 160 ± 90 to 480 ± 90 Ka; however, the younger age is a less reliable value with a large error plot and it should be considered as closer to a 250 Ka value. The laminar carbonate (YM14M) reflects the time of strong calcium carbonate development, about 270 ± 90 Ka, rather than the older age of the host fluvial sand in Trench 14.

A histogram showing 30 U-trend age determinations from alluvial units at NTS are shown in Figure 35. Results of the first sampling of Frenchman Flat alluvium (31) are excluded from the histogram. Median ages for these deposits indicate the following times of widespread depositions: About 80 ± 15 Ka for Q2a sediments, 170 ± 40 Ka for Q2b sediments, 270 ± 50 and 440 ± 60 Ka for younger and older Q2c deposits. These results are reasonably consistent with other age determinations, stratigraphic constraints, and with estimates based on geomorphic evidence. In this geographic area, most of the late to middle Pleistocene sediments appear to have been deposited in these time frames.

## REFERENCES CITED


Ander, M. D., Byers, F. M., and Orkild, P. P., 1984, Nevada Test Site field trip guidebook, 1984, Geol. Soc. of America and MacKay School of Mines, University of Nevada-Reno, 1984 Annual Meeting, Reno, p. 1-35.

Dalrymple, G. B., Cox, Allan, and Doell, R. R., 1965, Potassium-argon age and paleomagnetism of the Bishop Tuff, California: Geol. Soc. America Bull., v. 76, p. 665-674.

Frye, J. C., 1978, Pleistocene succession of the central interior United States: Quaternary Research, v. 3, p. 275-283.

Ivanovich, M., and Harmon, R. S., 1982, Uranium Series Disequilibrium: Applications to Environmental Problems, Clarendon Press, Oxford, 571 p.

Izett, G. A., 1982, The Bishop ash bed and some older compositionally similar ash beds in California, Nevada, and Utah: U.S. Geological Survey Open-File Report 82-582, 44 p.

Izett, G. A., Wilcox, R. E., Powers, H. A., and Desborough, G. A., 1970, The Bishop ash bed, a Pleistocene marker bed in the western United States: Quaternary Research, v. 1, p. 122-132.

Ku, T. L., 1976, The uranium-series methods of age determination: Annual Rev. Earth and Planetary Science Letters, v. 4, p. 347-379.

Ku, T. L., Bull, W. B., Freeman, S. T., and Knauss, K. G., 1979, $Th^{230}$-$U^{234}$ dating of pedogenic carbonates in gravely desert soils of Vidal Valley, Southeastern California: Geol. Soc. America Bull., v. 90, p. 1063-1073.

Ludwig, K. R., 1979, A program in Hewlett-Packard BASIC for X-Y plotting and line-fitting of isotopic and other data: U. S. Geol. Survey Open-File Report, 79-1641, 28 p.

Pierce, K. L., 1979, History and dynamics of glaciation in the northern Yellowstone National Park area: U. S. Geological Survey Prof. Paper 729-F, p. F1-F90.

Rosholt, J. N., 1980, Uranium-trend dating of Quaternary sediments: U. S. Geol. Survey Open-File Report 80-1087, 65 p.

Rosholt, J. N., 1984, Isotope dilution analyses of uranium and thorium in geologic samples using $^{233}U$ and $^{229}Th$: Nuclear Instr. and Methods, v. 223, p. 572-576.

Rosholt, J. N., 1985, Uranium-trend systematics for dating Quaternary sediments: U.S. Geological Survey Open-File Report 85-298, 34 p.

Rosholt, J. N., Bush, C. A., Shroba, R. R., Pierce, K. L., and Richmond, G. M., 1985, Uranium-trend dating and calibrations for Quaternary sediments: U.S. Geological Survey Open-File Report 85-299, 48 p.

Sheppard, R. A., and Gude, A. J., 1968, Distribution and genesis of authigenic silicate minerals in tuffs of Pleistocene Lake Tecopa, Inyo County, California: U.S. Geological Survey Professional Paper 597, 38 p.

Swadley, W. C., 1983, Map showing surficial geology of the Lathrop Wells quadrangle, Nye County, Nevada: U.S. Geological Survey Miscellaneous Investigations Series Map I-1361, scale 1:48,000.

Swadley, W C, and Hoover, D. L., 1983, Geology of faults exposed in trenches in Crater Flat, Nye County, Nevada: U.S. Geological Survey Open-File Report 83-608, 15 p.

Swadley, W C, Hoover, D. L., Rosholt, J. N., 1984, Preliminary report on late Cenozoic faulting and stratigraphy in the vicinity of Yucca Mountain, Nye County, Nevada: U.S. Geological Survey Open-File Report 84-788, 42 p.

Vaniman, D. T., Crowe, B. M., and Gladney, E. S., 1982, Petrology and geochemistry of Hawaiite lavas from Crater Flat, Nevada: Contributions to Mineralogy and Petrology, v. 80, p. 341-357.




Table 1. Locations, distances from end of trench wall, stratigraphic descriptions, and depths below the surface for all deposits analyzed

| Sample Suite (number of samples) | Trench | Location | Material | Stratigraphic Unit | Depth (cm) |
|---|---|---|---|---|---|
| SFF | S.W. Frenchman Flat Trench 36°45.1'N 115°59.3'W | East Wall 13 m north | Eolian sediment | Q2a? | 2-87 |
| (5) | | East Wall 13 m north | Eolian and sediment | Q2a? | 2-22 |
| FFPG (10) | | East Wall 23 m north | Alluvium | Q2b | 9-85 |
| SI (6) | | East Wall 9 m north | Buried B horizon | Q2a | 37-57 |
| F2 (8) | | East Wall 9 m north | Pebbly Fan gravel | Q2a | 60-170 |
| F3 (12) | | | | | |
| RVI-AD (4) | Rock Valley Trench 1 36°43.4'N 116°7.7'W | West Wall 14 m south | Slope wash | Q2a | 10-90 |
| RVI-EI (5) | | West Wall 14 m south | Underlying alluvium | Q2a | 90-190 |
| RVI-JO (6) | | East Wall 12 m north | Buried B horizon | Q2a | 35-58 |
| RVI-PU (6) | | East Wall 23 m north | Calcareous B horizon | Q2b | 58-81 |
| RVI-VZ (6) | | East Wall 23 m north | K horizon | Q2c | 81-100 |
| TSV-307 (7) | Rock Valley Trench 2 36°43.5'N 116°7.6'W | East Wall 20 m north | Gravel alluvium | Q2a | 30-170 |
| RV2-U (8) | | East Wall 23 m north | Buried B horizon | Q2a | 50-90 |
| RV2-L (8) | | East Wall 23 m north | Gravel alluvium | Q2c | 120-227 |
| Q2L (8) | Jackass Flats Engine Test Stand Trench 36°47.8'N 116°20.0'W | West Wall | Sand sheet deposit | Q2b | 90-110 |
| Q2S (9) | | West Wall | Sand sheet argillic B horizon | Q2a | 45-135 |
| S9 (8) | Jackass Divide Trench 36°47.8'N 116°19.0'W | West Wall 8.5 m south | Upper alluvium | Q2c | 8-168 |
| JD (8) | | West Wall 18.5 m south | Lower alluvium | Q2e | 120-240 |
| SCF1 (8) | South Crater Flat West Trench 36°43.6'N 116°33.8'W | East Wall 21.5 m north | Upper alluvium | Q2b | 23-84 |
| SCF3 (5) | | East Wall 28 m north | Upper alluvium | Q2b | 30-106 |
| SCF2 (9) | | East Wall 0.5 m north | Lower alluvium | Q2c | 23-91 |
| SCF4 (8) | | East Wall 3 m north | Lower alluvium | Q2e | 61-181 |

Table 1. Locations, distances from end of trench wall, stratigraphic descriptions, and depths below the surface for all deposits analyzed (cont'd.)

| Sample Suite (number of samples) | Trench | Location | Material | Stratigraphic Unit | Depth (cm) |
|---|---|---|---|---|---|
| TSV396 (6) | Crater Flat Trench 1 36°47.3'N 116°30.6'W | North wall about 3 m west of fault zone | Upper carb. enriched zone | --- | 50-170 |
| CF1 (8) CF6 (5) CF2 (7) | Crater Flat Trench 3 36°47.0'N 116°30.6'W | South Wall 11.3 m east<br>North Wall 24.9 m east<br>South Wall 25.5 m east | Upper alluvium<br>Argillic B horizon<br>Lower alluvium | Q2a<br>Q2b<br>Q2c | 23-84<br>58-79<br>69-157 |
| YM2U (4) YM2L (6) | Yucca Mtn. Trench 2 36°51.5'N 116°38.8'W | North Wall 25 m east<br>North Wall 25 m east | Buried B horizon<br>Gravel alluvium | Q2a<br>Q2b | 91-142<br>142-231 |
| YM13U (6) YM13L (5) | Yucca Mtn. Trench 13 36°52.9'N 116°35.2'W | South Wall 15 m east<br>South Wall 15 m east | Buried B horizon<br>Gravel alluvium | Q2a<br>Q2c | 30-107<br>107-182 |
| YM14B (9) YM14U (9) YM14M (5) YM14L (8) | Yucca Mtn. Trench 14 36°50.8'N 116°45.0'W | North Wall 21.5 m west<br>South Wall 28 m west<br>North Wall 15 m west<br>North Wall 15 m west | Lower B horizon below stone line<br>Upper and lower B horizon<br>Laminar carbonate K horizon<br>Cca horizon overlying gravel | Q2a<br>Q2a<br>Q2a<br>Q2a | 50-77<br>30-93<br>90-146<br>146-257 |
| CBQ (8) | Charlie Brown Quarry, Sho-Shone, CA 35°58.2'N 116°15.2'W | North Wall | Alluvium unconformably overlies Lava Creek ash | Q2b | 8-128 |
| FHA (5) | Fairbanks Hills NW 36°31.7'N 116°20.1'W | Outcrop | Altered Volcanic ash | -- | 0-96 |
| SJ (8) | Eleana Pediment Trench 37°11.0'N 116°5.4'W | South Wall | Gravel carbonate cemented | QTa | 10-90 |



Table 2. Uranium and thorium concentration and Th/U ratio in Quaternary deposits

| Sample | Depth (cm) | Description | U (ppm) | Th (ppm) | Th/U |
|---|---|---|---|---|---|
| **SFF unit, Frenchman Flat eolian unit** | | | | | |
| SFF-1 | 2-11 | All samples analyzed in this section of vesicular A horizon are silt and clay | 2.12 | 13.07 | 6.17 |
| SFF-2 | 11-20 | | 1.97 | 11.56 | 5.86 |
| SFF-3 | 20-29 | | 1.66 | 10.37 | 6.25 |
| SFF-4 | 29-38 | | 1.60 | 9.79 | 6.11 |
| SFF-5 | 38-47 | | 1.53 | 8.84 | 5.78 |
| **FFPG unit, Frenchman Flat patterned ground eolian unit** | | | | | |
| FFPG-1 | 2-4 | All samples analyzed in this section are fine-grained sand, silt and clay. | 2.59 | 16.43 | 6.35 |
| FFPG-2 | 4-6 | | 2.39 | 15.56 | 6.52 |
| FFPG-3 | 6-8 | | 1.96 | 11.83 | 6.04 |
| FFPG-4 | 8-10 | | 1.82 | 11.24 | 6.19 |
| FFPG-5 | 10-12 | | 1.71 | 11.25 | 6.56 |
| FFPG-6 | 12-14 | | 1.75 | 11.02 | 6.30 |
| FFPG-7 | 14-16 | | 1.78 | 11.71 | 6.57 |
| FFPG-8 | 16-18 | | 1.72 | 11.29 | 6.56 |
| FFPG-9 | 18-20 | | 1.59 | 10.70 | 6.74 |
| FFPG-10 | 20-22 | | 1.62 | 11.15 | 6.87 |
| **S1 unit, Frenchman Flat alluvium** | | | | | |
| S1-A | 9-23 | All samples analyzed in section are fine- to medium-grained sand, silt and clay. | 1.73 | 10.93 | 6.31 |
| S1-B | 20-33 | | 1.69 | 11.33 | 6.72 |
| S1-C | 33-46 | | 1.68 | 11.52 | 6.84 |
| S1-D | 46-59 | | 1.55 | 10.72 | 6.93 |
| S1-E | 59-72 | | 1.47 | 10.50 | 7.16 |
| S1-F | 72-85 | | 1.43 | 9.84 | 6.86 |
| **F2/3 Section, Frenchman Flat alluvium** | | | | | |
| F2-1 | 37-39 | Samples in this unit represent the 3Btca soil horizon. | 1.54 | 7.01 | 4.57 |
| F2-2 | 39-42 | | 1.50 | 6.62 | 4.40 |
| F2-3 | 42-44 | | 1.47 | 6.34 | 4.31 |
| F2-4 | 44-47 | | 1.50 | 6.03 | 4.03 |
| F2-5 | 47-50 | | 1.46 | 5.85 | 4.01 |
| F2-6 | 50-53 | | 1.39 | 6.13 | 4.41 |
| F2-7 | 53-56 | | 1.22 | 5.80 | 4.77 |
| F2-8 | 56-59 | | 1.29 | 6.00 | 4.64 |
| F3-1 | 60-69 | Samples in this unit of pebbly fan gravel represent the 4Cca. soil horizon. | 1.37 | 5.91 | 4.30 |
| F3-2 | 69-78 | | 1.40 | 5.80 | 4.14 |
| F3-3 | 78-87 | | 1.37 | 5.15 | 3.75 |
| F3-4 | 87-96 | | 1.58 | 5.58 | 3.53 |
| F3-5 | 96-105 | | 1.54 | 7.44 | 4.85 |
| F3-6 | 105-114 | | 1.62 | 7.01 | 4.34 |
| F3-7 | 114-123 | | 1.53 | 7.15 | 4.68 |
| F3-8 | 123-132 | | 1.57 | 7.41 | 4.72 |
| F3-9 | 132-141 | | 1.48 | 7.79 | 5.26 |
| F3-10 | 141-150 | | 1.55 | 7.26 | 4.67 |
| F3-11 | 150-160 | | 1.42 | 7.22 | 5.08 |
| F3-12 | 160-170 | | 1.49 | 7.18 | 4.80 |

Table 2. Uranium and thorium concentration and Th/U ratio in Quaternary deposits, (Cont'd.)

| Sample | Depth (cm) | Description | U (ppm) | Th (ppm) | Th/U |
|---|---|---|---|---|---|
| RV1 section, (RV1-AD and RV1-EI sample suites) Rock Valley Trench 1 | | | | | |
| RV1-A | 10-30 | Fine to coarse sand | 2.18 | 13.02 | 5.97 |
| RV1-B | 30-50 | Fine to coarse sand | 2.63 | 12.58 | 4.79 |
| RV1-C | 50-70 | Caliche-rich portion | 4.95 | 8.13 | 1.64 |
| RV1-D | 70-90 | Fine to coarse sand | 2.83 | 9.59 | 3.36 |
| RV1-E | 90-110 | All samples analyzed in | 2.46 | 10.06 | 4.09 |
| RV1-F | 110-130 | unit are fine to coarse | 2.13 | 9.16 | 4.29 |
| RV1-G | 130-150 | sand. | 2.25 | 9.96 | 4.43 |
| RV1-H | 150-170 | | 2.13 | 9.79 | 4.60 |
| RV1-I | 170-190 | | 2.25 | 10.06 | 4.47 |
| RV1 Section (RV1-JO, RV1-PU, and RV1-VZ sample suites) Rock Valley Trench 1 | | | | | |
| RV1-J | 35-58 | Samples in this unit represent | 1.99 | 13.51 | 6.79 |
| RV1-K | 38-42 | a buried B horizon | 1.88 | 12.69 | 6.76 |
| RV1-L | 42-46 | | 1.78 | 12.53 | 7.06 |
| RV1-M | 46-50 | | 1.82 | 13.00 | 7.15 |
| RV1-N | 50-54 | | 1.70 | 12.67 | 7.43 |
| RV1-O | 54-58 | | 1.87 | 12.61 | 6.75 |
| RV1-P | 58-62 | Samples in this unit repre- | 2.22 | 11.99 | 5.40 |
| RV1-Q | 62-66 | sent the calcareous B | 2.15 | 12.06 | 5.60 |
| RV1-R | 66-69 | horizon | 2.06 | 12.59 | 6.11 |
| RV1-S | 69-73 | | 1.97 | 12.09 | 6.13 |
| RV1-T | 73-77 | | 2.05 | 11.99 | 5.86 |
| RV1-U | 77-81 | | 2.11 | 11.82 | 5.61 |
| RV1-V | 81-85 | Samples in this unit repre- | 2.57 | 10.46 | 4.08 |
| RV1-W | 85-89 | sent he K horizon | 2.27 | 10.11 | 4.45 |
| RV1-X | 89-92 | | 2.25 | 9.58 | 4.25 |
| RV1-Y | 92-96 | | 2.61 | 9.22 | 3.53 |
| RV1-Z | 96-100 | | 2.85 | 8.25 | 2.90 |
| TSV 307 unit, Rock Valley Trench 2 | | | | | |
| 307-A | 30-50 | Fine to coarse sand with | 2.00 | 11.76 | 5.87 |
| 307-B | 50-70 | profile extending across | 2.10 | 12.70 | 6.05 |
| 307-C | 70-90 | orange B zone in Q2 | 2.01 | 12.76 | 6.36 |
| 307-D | 90-110 | alluvium. | 2.05 | 11.38 | 5.52 |
| 307-E | 110-130 | Caliche horizon | 3.23 | 13.96 | 4.32 |
| 307-F | 130-150 | Upper part of lower | 2.64 | 8.49 | 3.22 |
| 307-G | 150-170 | Q2 alluvium. | 2.40 | 7.16 | 2.99 |



Table 2. Uranium and thorium concentration and Th/U ratio in Quaternary deposits, (cont'd)

| Sample | Depth (cm) | Description | U (ppm) | Th (ppm) | Th/U |
|---|---|---|---|---|---|
| RV2 section, Rock Valley Trench 2 | | | | | |
| RV2-1 | 50-55 | Samples in this unit | 2.15 | 13.16 | 6.11 |
| RV2-2 | 55-60 | represent the 2Bt horizon | 1.99 | 12.53 | 6.29 |
| RV2-3 | 60-65 | | 1.97 | 12.77 | 6.48 |
| RV2-4 | 65-70 | | 1.92 | 12.75 | 6.65 |
| RV2-5 | 65-70 | | 1.82 | 12.67 | 6.96 |
| RV2-6 | 75-70 | | 1.88 | 12.74 | 6.77 |
| RV2-7 | 80-85 | | 1.86 | 11.99 | 6.46 |
| RV2-8 | 85-90 | | 2.02 | 11.81 | 5.84 |
| RV2-9 | 120-133 | This unit is poorly sorted, | 2.16 | 9.84 | 4.53 |
| RV2-10 | 133-146 | nonbedded, sandy gravel | 2.28 | 9.64 | 4.22 |
| RV2-11 | 146-159 | | 2.47 | 9.80 | 3.97 |
| RV2-12 | 159-172 | | 2.24 | 10.07 | 4.53 |
| RV2-13 | 172-185 | | 2.77 | 9.79 | 3.54 |
| RV2-14 | 185-198 | | 2.52 | 9.39 | 3.73 |
| RV2-15 | 198-211 | | 2.70 | 9.60 | 3.54 |
| RV2-16 | 211-224 | | 2.33 | 9.66 | 4.15 |
| Q2E unit, eolian sand, Jackass Flats Engine Test Stand Trench | | | | | |
| Q2E-1 | 50-65 | All samples in this unit | 1.90 | 12.39 | 6.53 |
| Q2E-2 | 65-80 | are reddish-brown oxidized | 1.83 | 12.01 | 6.58 |
| Q2E-3 | 80-95 | medium to coarse sand. | 1.84 | 11.65 | 6.34 |
| Q2E-4 | 95-110 | | 2.21 | 11.81 | 5.36 |
| Q2S unit, sand section, Jackass Flats Engine Test Stand Trench | | | | | |
| Q2S-1 | 45-55 | All samples in this unit | 1.74 | 10.90 | 6.27 |
| Q2S-2 | 55-65 | are reddish-brown oxidized | 1.71 | 11.07 | 6.48 |
| Q2S-3 | 65-75 | medium to coarse sand | 1.69 | 10.57 | 6.26 |
| Q2S-4 | 75-85 | | 1.68 | 10.20 | 6.06 |
| Q2S-5 | 85-95 | | 1.72 | 10.59 | 6.16 |
| Q2S-6 | 95-105 | | 1.68 | 10.20 | 6.06 |
| Q2S-7 | 105-115 | | 1.90 | 11.01 | 5.79 |
| Q2S-8 | 115-125 | | 1.91 | 11.11 | 5.82 |
| Q2S-9 | 125-135 | | 2.13 | 11.82 | 5.55 |
| S9 unit, Jackass Divide Trench, upper part | | | | | |
| S9-A | 8-28 | All samples analyzed in this | 2.28 | 14.14 | 6.74 |
| S9-B | 28-48 | section are fine to | 2.10 | 13.55 | 6.47 |
| S9-C | 48-68 | coarse sand with | 2.41 | 13.67 | 5.68 |
| S9-D | 68-88 | some silt and clay. | 2.52 | 12.39 | 4.92 |
| S9-E | 88-108 | | 3.07 | 9.83 | 3.21 |
| S9-F | 108-128 | | 2.75 | 12.62 | 4.59 |
| S9-G | 128-148 | | 3.18 | 13.04 | 4.11 |
| S9-H | 148-168 | | 2.93 | 13.19 | 4.51 |

Table 2. Uranium and thorium concentration and Th/U ratio in Quaternary deposits, (cont'd.)

| Sample | Depth (cm) | Description | U (ppm) | Th (ppm) | Th/U |
|---|---|---|---|---|---|
| | | JD unit, Jackass Divide Trench, lower part | | | |
| JD-1 | 120-135 | All samples analyzed in this | 3.24 | 10.39 | 3.21 |
| JD-2 | 135-150 | section are fine to | 3.11 | 12.05 | 3.87 |
| JD-3 | 150-165 | coarse sand with some | 3.68 | 11.65 | 3.17 |
| JD-4 | 165-180 | silt and clay. | 3.33 | 12.04 | 3.62 |
| JD-5 | 180-195 | | 2.91 | 12.10 | 4.15 |
| JD-6 | 195-210 | | 2.97 | 12.92 | 4.35 |
| JD-7 | 210-225 | | 3.30 | 12.67 | 3.84 |
| JD-8 | 225-240 | | 3.69 | 12.94 | 3.51 |
| | | SCF1 unit, upper alluvium in South Crater Flat West Trench | | | |
| SCF1m-1 | 23-30 | Fluvial sandy pebble | 2.63 | 15.68 | 5.95 |
| SCF1m-2 | 30-38 | deposit. All samples in | 2.76 | 15.06 | 5.46 |
| SCF1m-3 | 38-46 | this part were less | 2.86 | 15.46 | 5.41 |
| SCF1m-4 | 46-53 | than 2 mm fraction. | 2.58 | 14.76 | 5.73 |
| SCF1m-5 | 53-61 | | 2.61 | 13.77 | 5.28 |
| SCF1m-6 | 61-69 | | 2.62 | 13.95 | 5.32 |
| SCF1m-7 | 69-76 | | 2.69 | 14.24 | 5.29 |
| SCF1m-8 | 76-84 | | 2.69 | 14.38 | 5.34 |
| SCF1f-1 | 23-30 | Same horizons as | 2.52 | 15.26 | 6.06 |
| SCF1f-2 | 30-38 | above, less than | 2.61 | 14.83 | 5.69 |
| SCF1f-3 | 38-46 | 0.25 mm fraction. | 2.57 | 15.17 | 5.89 |
| SCF1f-4 | 46-53 | | 2.59 | 15.64 | 6.05 |
| SCF1f-5 | 53-61 | | 2.69 | 16.27 | 6.05 |
| SCF1f-6 | 61-69 | | 2.58 | 14.65 | 5.68 |
| SCF1f-7 | 69-76 | | 2.53 | 14.84 | 5.85 |
| SCF1f-8 | 76-84 | | 2.39 | 15.42 | 6.45 |
| | | SCF2 unit, lower alluvium in South Crater Flat West Trench | | | |
| SCF2m-1 | 23-30 | Sandy pebble deposit | 3.77 | 14.22 | 3.78 |
| SCF2m-2 | 30-38 | with samples 1-5 mainly | 4.50 | 13.83 | 3.08 |
| SCF2m-3 | 38-46 | sand, 6-9 mainly pebble, | 4.31 | 12.29 | 2.85 |
| SCF2m-4 | 46-53 | less than 2 mm fraction. | 4.55 | 9.26 | 2.03 |
| SCF2m-5 | 53-61 | | 4.08 | 10.27 | 2.52 |
| SCF2m-6 | 61-69 | | 3.58 | 14.38 | 4.02 |
| SCF2m-7 | 69-76 | | 3.72 | 15.43 | 4.15 |
| SCF2m-8 | 76-84 | | 4.47 | 15.60 | 3.49 |
| SCF2m-9 | 84-91 | | 4.51 | 14.68 | 3.26 |
| SCF2f-1 | 23-30 | Same fluvial deposit | 3.67 | 13.82 | 3.76 |
| SCF2f-2 | 30-38 | as above, less than | 4.55 | 12.72 | 2.80 |
| SCF2f-3 | 38-46 | 0.25 mm fraction. | 4.42 | 11.29 | 2.56 |
| SCF2f-4 | 46-53 | | 4.48 | 8.92 | 1.99 |
| SCF2f-5 | 53-61 | | 4.25 | 9.21 | 2.17 |
| SCF2f-6 | 61-69 | | 4.13 | 13.71 | 3.32 |
| SCF2f-7 | 69-76 | | 4.76 | 15.31 | 3.22 |
| SCF2f-8 | 76-84 | | 6.36 | 16.13 | 2.54 |
| SCF2f-9 | 84-91 | | 4.77 | 14.41 | 3.03 |



Table 2. Uranium and thorium concentration and Th/U ratio in Quaternary deposits, (cont'd.)

| Sample | Depth (cm) | Description | U (ppm) | Th (ppm) | Th/U |
|---|---|---|---|---|---|
| | | SCF3 unit, upper alluvium in South Crater Flat West Trench | | | |
| SCF3-1 | 30-46 | Sandy pebble, mainly | 2.58 | 15.01 | 5.82 |
| SCF3-2 | 46-61 | pebble deposit on | 2.73 | 15.54 | 5.69 |
| SCF3-3 | 61-76 | Qfb terrace. | 2.79 | 15.09 | 5.41 |
| SCF3-4 | 76-91 | | 2.75 | 15.30 | 5.56 |
| SCF3-5 | 91-106 | | 2.80 | 15.25 | 5.45 |
| | | SCF4 unit, lower alluvium in South Crater Flat West Trench | | | |
| SCF4-1 | 61-76 | Fluvial sand and | 3.61 | 13.15 | 3.64 |
| SCF4-2 | 76-91 | pebble deposit with | 3.40 | 13.15 | 3.87 |
| SCF4-3 | 91-106 | top half more sandy | 3.28 | 13.82 | 4.21 |
| SCF4-4 | 106-121 | and bottom half | 3.01 | 12.41 | 4.12 |
| SCF4-5 | 121-136 | more pebbly. Unit | 3.51 | 13.34 | 3.80 |
| SCF4-6 | 136-151 | is more sandy than | 3.95 | 14.06 | 3.56 |
| SCF4-7 | 151-166 | equivalent SCF2 | 3.69 | 14.88 | 4.03 |
| SCF4-8 | 166-181 | section. | 3.67 | 12.76 | 3.48 |
| | | SJ unit, Eleana pediment | | | |
| SJ-A | 10-20 | All samples analyzed | 2.90 | 8.50 | 2.93 |
| SJ-B | 20-30 | in this section were | 2.42 | 10.50 | 4.34 |
| SJ-C | 30-40 | medium to coarse sand, | 3.57 | 8.62 | 2.42 |
| SJ-D | 40-50 | with caliche. | 2.42 | 8.78 | 3.63 |
| SJ-E | 50-60 | | 2.25 | 8.83 | 3.92 |
| SJ-F | 60-70 | | 2.46 | 8.59 | 3.50 |
| SJ-G | 70-80 | | 2.33 | 8.37 | 3.59 |
| SJ-H | 80-90 | | 2.29 | 8.67 | 3.78 |
| | | TSV 396 unit, upper carbonate enriched zone in Crater Flat Trench 1 | | | |
| 396m-A | 50-70 | K-horizon gravel, moderately | 4.07 | 14.86 | 3.65 |
| 396m-B | 70-90 | cemented with Stage III to | 4.66 | 13.12 | 2.82 |
| 396m-C | 90-110 | Stage IV caliche. All | 3.75 | 13.79 | 3.68 |
| 396m-D | 110-130 | samples less than 2 mm | 5.55 | 10.84 | 1.95 |
| 396m-E | 130-150 | fraction | 6.73 | 11.54 | 1.71 |
| 396m-F | 150-170 | | 7.28 | 8.39 | 1.15 |
| 396f-A | 50-70 | Same horizons as above; | 4.11 | 14.07 | 3.42 |
| 396f-B | 70-90 | all samples less than | 4.57 | 12.05 | 2.64 |
| 396f-C | 90-110 | 0.3 mm fraction | 3.82 | 13.15 | 3.45 |
| 396f-D | 110-130 | | 5.46 | 11.54 | 2.12 |
| 396f-E | 130-150 | | 6.69 | 11.26 | 1.68 |
| 396f-F | 150-170 | | 7.16 | 8.36 | 1.17 |

Table 2. Uranium and thorium concentration and Th/U ratio in Quaternary deposits, (cont'd.)

| Sample | Depth (cm) | Description | U (ppm) | Th (ppm) | Th/U |
|---|---|---|---|---|---|
| **CF1 unit, alluvium in Crater Flat Trench 3** | | | | | |
| CF1-1 | 23-30 | All samples in this unit of sandy, pebble-cobble fluvial deposit were less than 0.33 mm fraction. No bedding or poor bedding is in the deposit. | 2.16 | 14.56 | 6.75 |
| CF1-2 | 30-38 | | 2.20 | 13.80 | 6.28 |
| CF1-3 | 38-46 | | 2.32 | 14.52 | 6.26 |
| CF1-4 | 46-53 | | 2.50 | 14.66 | 5.87 |
| CF1-5 | 53-61 | | 2.47 | 14.70 | 5.95 |
| CF1-6 | 61-69 | | 2.46 | 14.37 | 5.85 |
| CF1-7 | 69-76 | | 2.35 | 14.17 | 6.04 |
| CF1-8 | 76-84 | | 2.31 | 13.98 | 6.05 |
| **CF6 unit, older argillic B-horizon soil in Crater Flat Trench 3** | | | | | |
| CF6-1 | 58-59 | All samples of sandy clay were less than 2 mm fraction. | 2.65 | 16.10 | 6.07 |
| CF6-2 | 59-64 | | 2.70 | 16.61 | 6.14 |
| CF6-3 | 64-69 | | 2.24 | 13.68 | 6.12 |
| CF6-4 | 69-74 | | 2.51 | 14.46 | 5.76 |
| CF6-5 | 74-79 | | 2.59 | 15.75 | 6.08 |
| **CF2 unit, lower alluvium in Crater Flat Trench 3** | | | | | |
| CF2m-1 | 69-81 | All samples in this unit of pebble to boulder beds with poor bedding were less than 2 mm fraction. | 3.83 | 14.18 | 3.70 |
| CF2m-2 | 81-94 | | 4.23 | 12.83 | 3.04 |
| CF2m-3 | 94-107 | | 3.91 | 13.22 | 3.38 |
| CF2m-4 | 107-119 | | 3.23 | 14.22 | 4.40 |
| CF2m-5 | 119-132 | | 3.28 | 13.76 | 4.19 |
| CF2m-6 | 132-145 | | 3.29 | 14.69 | 4.47 |
| CF2m-7 | 145-157 | | 3.28 | 12.96 | 3.95 |
| CF2f-1 | 69-81 | Same unit as above with samples less than 0.25 mm fraction. | 3.54 | 12.85 | 3.63 |
| CF2f-2 | 81-94 | | 4.31 | 12.22 | 2.83 |
| CF2f-3 | 94-107 | | 3.79 | 11.71 | 3.09 |
| CF2f-4 | 107-119 | | 3.43 | 12.33 | 3.59 |
| CF2f-5 | 119-132 | | 2.90 | 12.99 | 4.47 |
| CF2f-6 | 132-145 | | 2.81 | 14.48 | 5.16 |
| CF2f-7 | 145-157 | | 2.85 | 11.95 | 4.19 |
| **YM2 section, alluvium in Yucca Mountain Trench 2** | | | | | |
| Upper unit | | | | | |
| YM2m-1 | 91-104 | B horizon at top, grading into pebble-gravel at base. Samples were less than 2 mm fraction. | 2.42 | 16.26 | 6.71 |
| YM2m-2 | 104-117 | | 2.35 | 16.75 | 7.12 |
| YM2m-3 | 117-130 | | 2.21 | 17.44 | 7.88 |
| YM2m-4 | 130-142 | | 2.72 | 16.50 | 6.06 |
| YM2f-1 | 91-104 | Same horizons as above. Less than 0.3 mm fraction. | 2.23 | 14.87 | 6.67 |
| YM2f-2 | 104-117 | | 2.17 | 15.38 | 7.09 |
| YM2f-3 | 117-130 | | 2.08 | 16.29 | 7.84 |
| YM2f-4 | 130-142 | | 2.53 | 14.59 | 5.76 |



Table 2. Uranium and thorium concentration and Th/U ratio in Quaternary deposits, (cont'd.)

| Sample | Depth (cm) | Description | U (ppm) | Th (ppm) | Th/U |
|---|---|---|---|---|---|
| Lower unit | | | | | |
| YM2m-5 | 142-155 | Mostly gravel, underlain by 1.4 m of similar gravel. Samples were less than 2 mm fraction. | 3.83 | 15.87 | 4.15 |
| YM2m-6 | 155-170 | | 3.31 | 17.14 | 5.18 |
| YM2m-7 | 170-185 | | 3.43 | 16.69 | 4.86 |
| YM2m-8 | 185-201 | | 3.58 | 13.76 | 3.89 |
| YM2m-9 | 201-216 | | 4.12 | 15.06 | 3.66 |
| YM2m-10 | 216-231 | | 3.43 | 12.24 | 3.56 |
| YM2f-5 | 142-155 | Same horizons as above. Less than 0.3 mm fraction. | 1.68 | 14.16 | 8.41 |
| YM2f-6 | 155-170 | | 3.09 | 14.44 | 4.67 |
| YM2f-7 | 170-185 | | 3.39 | 13.40 | 3.95 |
| YM2f-8 | 185-201 | | 3.46 | 11.98 | 3.46 |
| YM2f-9 | 201-216 | | 4.06 | 12.41 | 3.06 |
| YM2f-10 | 216-231 | | 3.68 | 12.80 | 3.48 |
| **YM13 section, alluvium in Yucca Mountain Trench 13** | | | | | |
| Upper part | | | | | |
| YM13m-1 | 30-38 | B horizon at top, grading into pebble-gravel at base. Samples were less than 2 mm fraction. | 2.18 | 15.28 | 7.00 |
| YM13m-2 | 38-51 | | 1.93 | 19.34 | 10.00 |
| YM13m-3 | 51-64 | | 1.97 | 17.97 | 9.14 |
| YM13m-4 | 64-76 | | 1.97 | 18.22 | 9.25 |
| YM13m-5 | 76-91 | | 2.54 | 17.06 | 6.72 |
| YM13m-6 | 91-107 | | 3.29 | 15.20 | 4.62 |
| YM13f-1 | 30-38 | Same horizons as above less than 0.3 mm fraction. | 2.29 | 15.92 | 6.94 |
| YM13f-2 | 38-51 | | 2.01 | 16.54 | 8.22 |
| YM13f-3 | 51-64 | | 1.99 | 18.28 | 9.17 |
| YM13f-4 | 64-76 | | 2.01 | 18.30 | 9.08 |
| YM13f-5 | 76-91 | | 2.30 | 15.77 | 6.85 |
| YM13f-6 | 91-107 | | 3.14 | 14.10 | 4.49 |
| Lower part | | | | | |
| YM13m-7 | 107-122 | Mostly gravel with abundant caliche rinds less than 2 mm fraction. | 2.90 | 16.15 | 5.58 |
| YM13m-8 | 122-137 | | 3.26 | 16.09 | 4.93 |
| YM13m-9 | 137-152 | | 2.60 | 15.95 | 6.13 |
| YM13m-10 | 152-167 | | 2.87 | 16.71 | 5.61 |
| YM13m-11 | 167-182 | | 4.12 | 15.93 | 3.86 |
| YM13f-7 | 107-122 | Same horizons as above less than 0.25 mm fraction. | 2.92 | 15.99 | 5.48 |
| YM13f-8 | 122-137 | | 3.51 | 14.15 | 4.03 |
| YM13f-9 | 137-152 | | 2.58 | 15.27 | 5.91 |
| YM13f-10 | 152-167 | | 2.90 | 16.22 | 5.60 |
| YM13f-11 | 167-182 | | 3.54 | 15.09 | 4.26 |

Table 2. Uranium and thorium concentration and Th/U ratio in Quaternary deposits

| Sample | Depth (cm) | Description | U (ppm) | Th (ppm) | Th/U |
|---|---|---|---|---|---|
| **YM14B section, Q2 sand and alluvium in Yucca Mountain Trench 14** | | | | | |
| *Upper unit* | | | | | |
| YM14B-1 | 50-53 | 3Bt soil horizon in lower part of Q2s loose sand | 2.31 | 15.84 | 6.86 |
| YM14B-2 | 53-56 | | 3.95 | 15.66 | 3.96 |
| YM14B-3 | 56-59 | | 2.36 | 15.65 | 6.63 |
| YM14B-4 | 59-62 | | 2.46 | 15.55 | 6.33 |
| YM14B-5 | 62-65 | | 2.46 | 15.46 | 6.28 |
| YM14B-6 | 65-68 | | 2.56 | 15.49 | 6.04 |
| YM14B-8 | 71-74 | | 2.82 | 15.35 | 5.45 |
| YM14B-9 | 74-77 | | 2.89 | 15.36 | 5.31 |
| | | | 3.30 | 14.77 | 4.48 |
| **YM14 section, Upper and lower B horizon in Yucca Mountain Trench 14** | | | | | |
| *Upper unit* | | | | | |
| YM14-1 | 30-37 | Unit consists of Q2s loose sand. | 2.09 | 12.84 | 6.14 |
| YM14-2 | 37-44 | | 2.08 | 14.82 | 7.11 |
| YM14-3 | 44-51 | | 2.10 | 14.90 | 7.09 |
| YM14-4 | 51-58 | | 2.26 | 15.32 | 6.79 |
| YM14-5 | 58-65 | | 2.20 | 15.42 | 7.02 |
| YM14-6 | 65-72 | | 2.28 | 15.06 | 6.60 |
| YM14-7 | 72-79 | | 2.39 | 15.72 | 6.58 |
| YM14-8 | 79-86 | | 2.74 | 15.00 | 5.48 |
| YM14-9 | 86-93 | | 3.05 | 14.49 | 4.74 |
| **YM14 section, Q2c alluvium in Yucca Mountain Trench 14** | | | | | |
| *Middle unit* | | | | | |
| YM14-10 | 90-100 | Laminar carbonate K-horizon | 4.63 | 12.50 | 2.70 |
| YM14-11 | 100-115 | | 4.44 | 9.90 | 2.24 |
| YM14-12 | 115-130 | | 5.60 | 6.12 | 1.09 |
| YM14-13 | 130-138 | | 5.83 | 5.73 | .98 |
| YM14-14 | 138-146 | | 4.26 | 1.16 | .27 |
| *Lower unit* | | | | | |
| YM14-15 | 146-154 | Sandy part Cca horizon | 2.46 | 7.60 | 3.09 |
| YM14-16 | 154-167 | | 2.39 | 8.80 | 3.69 |
| YM14-17 | 167-182 | | 2.67 | 9.46 | 3.55 |
| YM14-18 | 182-197 | Gravelly sand, calcite cemented, unit with reworked carbonate stringers. | 3.16 | 12.87 | 4.07 |
| YM14-19 | 197-212 | | 3.40 | 11.47 | 3.38 |
| YM14-20 | 212-227 | | 3.55 | 15.69 | 4.42 |
| YM14-21 | 227-242 | | 5.22 | 12.01 | 2.30 |
| YM14-22 | 242-257 | | 3.80 | 15.53 | 4.08 |



Table 2. Uranium and thorium concentration and Th/U ratio in Quaternary deposits, (cont'd.)

| Sample | Depth (cm) | Description | U (ppm) | Th (ppm) | Th/U |
|---|---|---|---|---|---|
| **CBQ unit, alluvium in Charlie Brown Quarry, Shoshone, California.** | | | | | |
| CBQ-1 | 8-23 | All samples analyzed in section are fine- to medium-grained sand with silt and clay. | 2.07 | 11.31 | 5.46 |
| CBQ-2 | 23-38 | | 2.46 | 11.07 | 4.51 |
| CBQ-3 | 38-53 | | 2.88 | 11.39 | 3.96 |
| CBQ-4 | 53-68 | | 2.99 | 10.74 | 3.60 |
| CBQ-5 | 68-83 | | 2.54 | 10.99 | 4.32 |
| CBQ-6 | 83-98 | | 2.98 | 9.08 | 3.16 |
| CBQ-7 | 98-113 | | 2.09 | 10.50 | 5.02 |
| CBQ-8 | 113-128 | | 2.78 | 10.11 | 3.64 |
| **FMA unit, altered volcanic ash, Fairmont Hills, Nevada.** | | | | | |
| A15-A | 0-15 | Ash mostly altered to clay | 4.79 | 20.89 | 4.36 |
| A15-B | 15-20 | Ash mostly altered to clay | 3.72 | 22.61 | 6.09 |
| A15-C | 20-30 | Slightly altered ash | 4.01 | 16.50 | 4.12 |
| A15-D | 85-93 | Slightly altered ash | 7.17 | 28.9 | 4.03 |
| A15-E | 93-96 | Ash altered to clay | 4.41 | 35.2 | 7.96 |
| **SJ unit, Elsana pediment Trench.** | | | | | |
| SJ-A | 10-20 | All samples analyzed in this section were medium to coarse sand, with caliche. | 2.90 | 8.50 | 2.93 |
| SJ-B | 20-30 | | 2.42 | 10.50 | 4.34 |
| SJ-C | 30-40 | | 3.57 | 8.62 | 2.42 |
| SJ-D | 40-50 | | 2.42 | 8.78 | 3.63 |
| SJ-E | 50-60 | | 2.25 | 8.83 | 3.92 |
| SJ-F | 60-70 | | 2.46 | 8.59 | 3.50 |
| SJ-G | 70-80 | | 2.33 | 8.37 | 3.59 |
| SJ-H | 80-90 | | 2.29 | 8.67 | 3.78 |

Table 3. Isotopic ratios of uranium and thorium required for U-trend plots

| Sample | U ppm | $^{234}U/^{238}U$ | $^{230}Th/^{238}U$ | $^{234}U/^{232}Th$ | $^{230}Th/^{232}Th$ | $(^{234}U-^{230}Th)/^{238}U$ | $(^{234}U-^{238}U)/^{238}U$ |
|---|---|---|---|---|---|---|---|
| **SFF unit (Fig. 6)** | | | | | | | |
| SFF-1 | 2.12 | 1.014 | 1.438 | 0.492±0.026 | 0.708±0.020 | -0.838±0.060 | +0.014±0.032 |
| SFF-2 | 1.97 | 1.032 | 1.416 | .518± .027 | .733± .023 | - .416± .059 | + .037± .033 |
| SFF-3 | 1.66 | 1.006 | 1.448 | .485± .025 | .712± .023 | - .468± .067 | + .006± .032 |
| SFF-4 | 1.60 | .982 | 1.417 | .497± .026 | .704± .023 | - .418± .060 | - .018± .032 |
| SFF-5 | 1.53 | .998 | 1.324 | .524± .027 | .695± .022 | - .324± .056 | - .002± .032 |
| **FFPG unit (Fig. 7)** | | | | | | | |
| FFPG-1 | 2.59 | .980 | 1.389 | .478± .025 | .663± .021 | - .389± .058 | - .020± .031 |
| FFPG-2 | 2.39 | 1.035 | 1.515 | .465± .024 | .705± .023 | - .515± .064 | + .035± .033 |
| FFPG-3 | 1.96 | 1.065 | 1.476 | .502± .026 | .742± .024 | - .476± .062 | + .065± .034 |
| FFPG-4 | 1.82 | 1.073 | 1.528 | .490± .025 | .739± .024 | - .528± .064 | + .064± .034 |
| FFPG-5 | 1.71 | 1.045 | 1.549 | .462± .024 | .716± .023 | - .549± .065 | + .045± .033 |
| FFPG-6 | 1.75 | 1.032 | 1.532 | .482± .025 | .738± .024 | - .532± .064 | + .032± .033 |
| FFPG-7 | 1.78 | 1.068 | 1.550 | .463± .024 | .718± .023 | - .550± .065 | + .068± .034 |
| FFPG-8 | 1.72 | 1.047 | 1.549 | .464± .024 | .716± .023 | - .549± .065 | + .047± .034 |
| FFPG-9 | 1.59 | 1.053 | 1.603 | .450± .023 | .722± .023 | - .603± .067 | + .053± .034 |
| FFPG-10 | 1.62 | 1.029 | 1.585 | .441± .023 | .698± .022 | - .585± .066 | + .029± .033 |
| **SI unit (Fig. 8)** | | | | | | | |
| SI-A | 1.73 | .972 | 1.561 | .481± .025 | .751± .024 | - .561± .066 | - .028± .031 |
| SI-B | 1.69 | .991 | 1.680 | .452± .024 | .759± .024 | - .680± .071 | - .009± .032 |
| SI-C | 1.68 | .992 | 1.687 | .444± .023 | .749± .024 | - .687± .071 | - .008± .032 |
| SI-D | 1.55 | 1.027 | 1.649 | .438± .023 | .722± .023 | - .649± .069 | + .027± .033 |
| SI-E | 1.47 | .993 | 1.699 | .423± .022 | .720± .023 | - .699± .071 | - .007± .032 |
| SI-F | 1.43 | 1.010 | 1.691 | .442± .023 | .748± .024 | - .691± .071 | + .010± .032 |
| **F2 unit (Fig. 9)** | | | | | | | |
| F2-1 | 1.54 | 1.086 | 1.019 | .676± .035 | .689± .019 | - .019± .043 | + .086± .035 |
| F2-2 | 1.50 | 1.085 | 1.051 | .702± .037 | .738± .021 | - .051± .044 | + .085± .035 |
| F2-3 | 1.47 | 1.084 | 1.026 | .716± .037 | .735± .021 | - .026± .043 | + .084± .035 |
| F2-4 | 1.50 | 1.104 | .954 | .767± .040 | .737± .020 | + .046± .040 | + .104± .035 |
| F2-5 | 1.46 | 1.080 | .978 | .770± .040 | .753± .021 | + .022± .041 | + .080± .035 |
| F2-6 | 1.39 | 1.088 | 1.010 | .701± .036 | .707± .020 | - .010± .042 | + .088± .035 |
| F2-7 | 1.22 | 1.051 | 1.091 | .647± .034 | .707± .020 | - .091± .046 | + .051± .034 |
| F2-8 | 1.29 | 1.040 | 1.058 | .665± .035 | .704± .020 | - .058± .044 | + .041± .033 |



Table 3. Isotopic ratios of uranium and thorium required for U-trend plots, (cont'd.)

| Sample | U ppm | $^{234}U/^{238}U$ | $^{230}Th/^{238}U$ | $^{234}U/^{232}Th$ | $^{230}Th/^{232}Th$ | $(^{234}U-^{230}Th)/^{238}U$ | $(^{234}U-^{238}U)/^{238}U$ |
|---|---|---|---|---|---|---|---|
| **F3 unit (Fig. 10)** | | | | | | | |
| F3-1 | 1.37 | 1.041 | 1.013 | .718±0.037 | .727±0.020 | - .013±0.043 | + .041±0.033 |
| F3-2 | 1.40 | 1.079 | 1.002 | .766± .039 | .748± .039 | - .002± .042 | + .079± .035 |
| F3-3 | 1.37 | 1.061 | 1.018 | .824± .043 | .838± .043 | - .018± .043 | + .061± .034 |
| F3-4 | 1.54 | 1.059 | 1.095 | .875± .045 | .958± .027 | - .095± .046 | + .059± .034 |
| F3-5 | 1.54 | 1.064 | .969 | .637± .033 | .618± .017 | + .031± .041 | + .064± .034 |
| F3-6 | 1.[illegible] | 1.043 | .971 | .712± .037 | .691± .019 | + .029± .041 | + .043± .034 |
| F3-7 | 1.53 | 1.036 | 1.041 | .660± .034 | .688± .019 | - .041± .044 | + .036± .033 |
| F3-8 | 1.57 | 1.095 | 1.104 | .655± .034 | .723± .020 | - .104± .046 | + .095± .035 |
| F3-9 | 1.48 | 1.008 | 1.137 | .587± .031 | .667± .019 | - .137± .048 | + .008± .032 |
| F3-10 | 1.55 | 1.014 | 1.136 | .662± .034 | .752± .021 | - .136± .048 | + .014± .032 |
| F3-11 | 1.42 | 1.012 | 1.141 | .608± .032 | .694± .019 | - .141± .048 | + .012± .032 |
| F3-12 | 1.49 | 1.001 | 1.161 | .644± .033 | .644± .021 | - .161± .049 | + .001± .032 |
| **RVI section (Fig. 11)** | | | | | | | |
| RVI-A | 2.18 | 1.055 | 1.503 | .509± .026 | .765± .021 | - .503± .063 | + .055± .034 |
| RVI-B | 2.63 | 1.104 | 1.192 | .634± .033 | .756± .021 | - .192± .050 | + .104± .035 |
| RVI-C | 4.95 | 1.288 | .567 | 1.851± .096 | 1.049± .029 | + .433± .024 | + .288± .041 |
| RVI-D | 2.83 | 1.166 | .864 | .903± .047 | .780± .022 | + .136± .036 | + .166± .037 |
| RVI-E | 2.46 | 1.077 | .906 | .741± .039 | .671± .019 | + .094± .048 | + .077± .034 |
| RVI-F | 2.13 | 1.065 | .945 | .708± .037 | .669± .019 | + .055± .040 | + .065± .034 |
| RVI-G | 2.25 | 1.050 | .948 | .686± .036 | .651± .018 | + .052± .040 | + .050± .034 |
| RVI-H | 2.13 | 1.029 | .984 | .650± .034 | .650± .018 | + .016± .041 | + .019± .033 |
| RVI-I | 2.25 | 1.031 | .991 | .680± .035 | .674± .019 | + .009± .042 | + .031± .033 |
| **RVI section (Fig. 12)** | | | | | | | |
| RVI-J | 1.99 | 1.047 | 1.566 | .455± .024 | .713± .020 | - .566± .066 | + .047± .033 |
| RVI-K | 1.88 | 1.025 | 1.483 | .457± .024 | .677± .019 | - .483± .062 | + .025± .032 |
| RVI-L | 1.78 | 1.005 | 1.504 | .438± .023 | .658± .018 | - .504± .063 | + .005± .032 |
| RVI-M | 1.82 | .998 | 1.519 | .432± .022 | .656± .018 | - .519± .064 | - .002± .032 |
| RVI-N | 1.70 | 1.005 | 1.518 | .416± .022 | .631± .018 | - .518± .064 | + .005± .032 |
| RVI-O | 1.87 | 1.027 | 1.393 | .458± .024 | .638± .018 | - .393± .059 | + .027± .033 |
| **RVI section (Fig. 13)** | | | | | | | |
| RVI-P | 2.22 | 1.141 | 1.096 | .572± .030 | .627± .018 | - .096± .046 | + .141± .037 |
| RVI-Q | 2.15 | 1.111 | 1.131 | .551± .029 | .623± .017 | - .131± .047 | + .111± .036 |
| RVI-R | 2.06 | 1.061 | 1.227 | .506± .026 | .621± .017 | - .227± .052 | + .061± .034 |
| RVI-S | 1.97 | 1.040 | 1.233 | .504± .026 | .621± .017 | - .233± .052 | + .040± .033 |
| RVI-T | 2.05 | 1.040 | 1.194 | .527± .027 | .629± .018 | - .194± .050 | + .040± .033 |
| RVI-U | 2.11 | 1.065 | 1.155 | .551± .029 | .636± .018 | - .155± .049 | + .065± .034 |
| RVI-V | 2.57 | 1.127 | .982 | .758± .039 | .744± .021 | + .018± .041 | + .127± .036 |
| RVI-W | 2.27 | 1.096 | 1.000 | .694± .036 | .694± .019 | + .000± .042 | + .096± .035 |
| RVI-X | 2.25 | 1.105 | .983 | .727± .038 | .714± .020 | + .017± .041 | + .105± .035 |
| RVI-Y | 2.61 | 1.171 | .863 | .875± .045 | .755± .021 | + .137± .036 | + .171± .037 |
| RVI-Z | 2.85 | 1.261 | .750 | 1.066± .055 | .800± .022 | + .250± .032 | + .261± .040 |

Table 3. Isotopic ratios of uranium and thorium required for U-trend plots, (cont'd.)

| Sample | U ppm | Activity Ratios: $\frac{^{234}U}{^{238}U}$ | $\frac{^{230}Th}{^{232}Th}$ | $\frac{^{234}U}{^{232}Th}$ | $\frac{^{230}Th}{^{232}Th}$ | $(\frac{^{234}U}{^{238}U}-\frac{^{230}Th}{^{232}Th})$ | $(\frac{^{234}U}{^{238}U}-1)$ |
|---|---|---|---|---|---|---|---|
| **307 unit (Fig. 14)** | | | | | | | |
| 307-A | 2.00 | 1.033 | 1.395 | .518±0.027 | .722±0.020 | - .395±0.059 | + .033±0.033 |
| 307-B | 2.10 | 1.064 | 1.329 | .502± .026 | .668± .019 | - .329± .056 | + .064± .034 |
| 307-C | 2.01 | 1.036 | 1.318 | .477± .025 | .629± .018 | - .318± .055 | + .036± .033 |
| 307-D | 2.05 | 1.062 | 1.183 | .550± .029 | .651± .018 | - .183± .050 | + .062± .034 |
| 307-E | 3.23 | 1.092 | .891 | .704± .037 | .627± .018 | + .109± .038 | + .092± .035 |
| 307-F | 2.64 | 1.168 | .824 | .944± .049 | .778± .022 | + .176± .035 | + .168± .037 |
| 307-G | 2.40 | 1.230 | .822 | 1.017± .053 | .836± .023 | + .178± .035 | + .230± .039 |
| **RV2 section (Fig. 15** | | | | | | | |
| RV2-1 | 2.15 | 1.057 | 1.314 | .506± .026 | .664± .019 | - .314± .055 | + .057± .034 |
| RV2-2 | 1.99 | 1.062 | 1.331 | .491± .026 | .654± .018 | - .331± .056 | + .062± .034 |
| RV2-3 | 1.97 | 1.069 | 1.328 | .477± .025 | .631± .018 | - .328± .056 | + .069± .034 |
| RV2-4 | 1.92 | 1.038 | 1.351 | .464± .024 | .627± .018 | - .351± .057 | + .038± .033 |
| RV2-5 | 1.82 | 1.019 | 1.452 | .444± .023 | .645± .018 | - .452± .061 | + .019± .033 |
| RV2-6 | 1.88 | 1.012 | 1.363 | .456± .024 | .622± .017 | - .363± .057 | + .012± .032 |
| RV2-7 | 1.86 | 1.021 | 1.331 | .478± .025 | .636± .018 | - .331± .056 | + .021± .033 |
| RV2-8 | 2.02 | 1.054 | 1.222 | .529± .027 | .646± .018 | - .222± .051 | + .054± .034 |
| RV2-9 | 2.16 | 1.059 | .986 | .682± .035 | .672± .019 | + .014± .041 | + .059± .034 |
| RV2-10 | 2.28 | 1.062 | .984 | .732± .038 | .720± .020 | + .016± .041 | + .062± .034 |
| RV2-11 | 2.47 | 1.102 | .963 | .779± .041 | .750± .021 | + .037± .040 | + .102± .035 |
| RV2-12 | 2.24 | 1.049 | .971 | .687± .036 | .667± .019 | + .029± .041 | + .049± .034 |
| RV2-13 | 2.77 | 1.072 | .946 | .873± .045 | .826± .023 | + .054± .040 | + .072± .034 |
| RV2-14 | 2.52 | 1.070 | .949 | .828± .043 | .786± .022 | + .051± .040 | + .070± .034 |
| RV2-15 | 2.70 | 1.084 | .958 | .867± .045 | .831± .023 | + .042± .040 | + .084± .035 |
| RV2-16 | 2.33 | 1.053 | .956 | .744± .039 | .712± .020 | + .044± .040 | + .053± .034 |
| **Q2E unit (Fig. 16)** | | | | | | | |
| Q2E-1 | 1.90 | .978 | 1.283 | .465± .024 | .596± .017 | - .283± .054 | - .022± .031 |
| Q2E-2 | 1.83 | .996 | 1.246 | .461± .024 | .575± .016 | - .246± .052 | - .004± .032 |
| Q2E-3 | 1.84 | .982 | 1.253 | .479± .025 | .600± .017 | - .253± .053 | - .018± .031 |
| Q2E-4 | 2.21 | .972 | 1.112 | .567± .029 | .630± .018 | - .112± .047 | - .028± .031 |
| **Q2S unit (Fig. 17)** | | | | | | | |
| Q2S-1 | 1.74 | .981 | 1.254 | .484± .025 | .607± .017 | - .254± .053 | - .109± .031 |
| Q2S-2 | 1.71 | .979 | 1.270 | .468± .024 | .595± .017 | - .270± .054 | - .021± .031 |
| Q2S-3 | 1.69 | .995 | 1.231 | .485± .025 | .597± .017 | - .231± .052 | - .005± .032 |
| Q2S-4 | 1.68 | 1.013 | 1.198 | .501± .026 | .600± .017 | - .198± .050 | + .013± .032 |
| Q2S-5 | 1.72 | .984 | 1.217 | .493± .026 | .600± .017 | - .217± .051 | - .016± .031 |
| Q2S-6 | 1.68 | .997 | 1.207 | .501± .026 | .605± .017 | - .207± .051 | - .003± .032 |
| Q2S-7 | 1.90 | .984 | 1.189 | .524± .027 | .623± .017 | - .189± .050 | - .016± .031 |
| Q2S-8 | 1.91 | .994 | 1.172 | .521± .027 | .611± .017 | - .172± .049 | - .006± .032 |
| Q2S-9 | 2.13 | .992 | 1.126 | .587± .028 | .616± .017 | - .126± .047 | - .008± .032 |



Table 3. Isotopic ratios of uranium and thorium required for U-trend plots, (cont'd.)

| Sample | U ppm | Activity Ratios: $\frac{^{234}U}{^{238}U}$ | $\frac{^{230}Th}{^{232}Th}$ | $\frac{^{234}U}{^{232}Th}$ | $\frac{^{230}Th}{^{232}Th}$ | $(\frac{^{234}U}{^{238}U}-\frac{^{230}Th}{^{232}Th})$ | $(\frac{^{234}U}{^{238}U}-1)$ |
|---|---|---|---|---|---|---|---|
| **S9 unit (Fig. 18)** | | | | | | | |
| S9-A | 2.24 | .983 | 1.462 | .450± .023 | .658± .018 | - .462± .061 | - .017± .031 |
| S9-B | 2.10 | 1.030 | 1.373 | .464± .024 | .645± .018 | - .373± .058 | + .030± .033 |
| S9-C | 2.41 | 1.045 | 1.066 | .538± .028 | .570± .016 | - .066± .045 | + .045± .033 |
| S9-D | 2.52 | 1.108 | .979 | .617± .032 | .604± .017 | + .021± .041 | + .108± .036 |
| S9-E | 3.07 | 1.217 | .721 | .947± .049 | .682± .019 | + .279± .050 | + .217± .039 |
| S9-F | 2.75 | 1.095 | .978 | .661± .034 | .646± .018 | + .022± .041 | + .095± .035 |
| S9-G | 3.18 | 1.067 | .927 | .734± .038 | .681± .019 | + .073± .039 | + .067± .034 |
| S9-H | 2.93 | 1.032 | .998 | .673± .035 | .672± .019 | + .002± .042 | + .032± .033 |
| **JD unit (Fig. 19)** | | | | | | | |
| JD-1 | 3.24 | 1.137 | 1.079 | .946± .049 | 1.020± .029 | - .079± .045 | + .137± .036 |
| JD-2 | 3.11 | 1.116 | 1.059 | .785± .041 | .831± .023 | - .059± .044 | + .116± .036 |
| JD-3 | 3.68 | 1.125 | 1.078 | .958± .050 | 1.029± .029 | - .078± .045 | + .125± .036 |
| JD-4 | 3.33 | 1.106 | 1.027 | .839± .044 | .861± .024 | - .027± .043 | + .106± .036 |
| JD-5 | 2.91 | 1.056 | 1.061 | .731± .038 | .776± .022 | - .061± .045 | + .056± .034 |
| JD-6 | 2.97 | 1.010 | 1.024 | .698± .036 | .715± .020 | - .024± .043 | + .010± .032 |
| JD-7 | 3.30 | 1.047 | 1.069 | .791± .041 | .845± .024 | - .069± .045 | + .047± .034 |
| JD-8 | 3.69 | 1.076 | 1.051 | .865± .045 | .909± .025 | - .051± .044 | + .076± .034 |
| **SCF1m unit (Fig. 20)** | | | | | | | |
| SCF1m-1 | 2.63 | 1.038 | 1.386 | .510± .027 | .707± .020 | - .386± .058 | + .038± .033 |
| SCF1m-2 | 2.76 | 1.044 | 1.278 | .556± .029 | .708± .020 | - .278± .053 | + .044± .033 |
| SCF1m-3 | 2.86 | 1.024 | 1.213 | .561± .029 | .680± .019 | - .213± .051 | + .024± .033 |
| SCF1m-4 | 2.58 | 1.035 | 1.232 | .530± .028 | .653± .018 | - .232± .052 | + .035± .033 |
| SCF1m-5 | 2.61 | 1.039 | 1.111 | .575± .030 | .639± .018 | - .111± .047 | + .039± .033 |
| SCF1m-6 | 2.62 | 1.048 | 1.096 | .570± .030 | .625± .018 | - .096± .046 | + .048± .034 |
| SCF1m-7 | 2.69 | 1.019 | 1.069 | .573± .030 | .613± .017 | - .069± .045 | + .019± .033 |
| SCF1m-8 | 2.69 | .995 | 1.092 | .569± .030 | .621± .017 | - .092± .046 | - .005± .032 |
| **SCF1f unit (Fig. 20)** | | | | | | | |
| SCF1f-1 | 2.52 | 1.047 | 1.442 | .501± .026 | .723± .020 | - .442± .061 | + .047± .034 |
| SCF1f-2 | 2.61 | 1.106 | 1.447 | .539± .028 | .772± .022 | - .447± .061 | + .106± .035 |
| SCF1f-3 | 2.57 | 1.113 | 1.465 | .515± .027 | .750± .021 | - .465± .062 | + .113± .036 |
| SCF1f-4 | 2.59 | 1.108 | 1.440 | .502± .026 | .723± .020 | - .440± .060 | + .108± .035 |
| SCF1f-5 | 2.69 | 1.137 | 1.349 | .502± .026 | .677± .019 | - .349± .057 | + .137± .036 |
| SCF1f-6 | 2.58 | 1.130 | 1.215 | .535± .028 | .649± .018 | - .215± .051 | + .130± .036 |
| SCF1f-7 | 2.53 | 1.075 | 1.171 | .518± .027 | .607± .017 | - .171± .049 | + .075± .034 |
| SCF1f-8 | 2.39 | 1.063 | 1.227 | .470± .024 | .577± .016 | - .227± .052 | + .063± .034 |

Table 3. Isotopic ratios of uranium and thorium required for U-trend plots, (cont'd.)

| Sample | U ppm | Activity Ratios: $\frac{^{234}U}{^{238}U}$ | $\frac{^{230}Th}{^{238}U}$ | $\frac{^{234}U}{^{230}Th}$ | $\frac{^{230}Th}{^{234}Th}$ | $\frac{(^{234}U-^{230}Th)}{^{238}U}$ | $\frac{(^{234}U-^{238}U)}{^{238}U}$ |
|---|---|---|---|---|---|---|---|
| **SCF2m unit (Fig. 21)** | | | | | | | |
| SCF2m-1 | 3.77 | 1.343 | 1.286 | .804±0.042 | 1.033±0.029 | - .286±0.054 | + .343±0.043 |
| SCF2m-2 | 4.50 | 1.393 | 1.036 | .987± .051 | 1.022± .029 | - .036± .044 | + .393± .045 |
| SCF2m-3 | 4.31 | 1.455 | 1.165 | 1.063± .055 | 1.239± .035 | - .205± .051 | + .455± .047 |
| SCF2m-4 | 4.44 | 1.602 | 1.209 | 1.492± .078 | 1.797± .050 | - .275± .059 | + .581± .049 |
| SCF2m-5 | 4.08 | 1.581 | 1.215 | 1.206± .063 | 1.537± .043 | - .303± .055 | + .322± .042 |
| SCF2m-6 | 3.58 | 1.322 | 1.303 | .755± .039 | .984± .028 | - .205± .051 | + .320± .042 |
| SCF2m-7 | 3.72 | 1.320 | 1.205 | .732± .038 | .882± .025 | - .024± .043 | + .393± .045 |
| SCF2m-8 | 4.47 | 1.393 | 1.024 | .871± .045 | .892± .025 | - .048± .044 | + .811± .045 |
| SCF2m-9 | 4.51 | 1.411 | 1.048 | .932± .049 | .977± .027 | - .048± .044 | + .411± .045 |
| **SCF2f unit (Fig. 21)** | | | | | | | |
| SCF2f-1 | 3.67 | 1.378 | 1.318 | .847± .042 | 1.063± .030 | - .318± .055 | + .378± .044 |
| SCF2f-2 | 4.55 | 1.489 | 1.029 | 1.066± .056 | 1.117± .031 | - .029± .043 | + .489± .048 |
| SCF2f-3 | 4.42 | 1.549 | 1.195 | 1.187± .062 | 1.419± .040 | - .195± .050 | + .549± .050 |
| SCF2f-4 | 4.48 | 1.639 | 1.225 | 1.525± .079 | 1.868± .052 | - .225± .051 | + .639± .052 |
| SCF2f-5 | 4.25 | 1.604 | 1.325 | 1.398± .073 | 1.853± .052 | - .325± .056 | + .604± .051 |
| SCF2f-6 | 4.13 | 1.550 | 1.549 | .919± .048 | 1.423± .040 | - .549± .065 | + .550± .050 |
| SCF2f-7 | 4.76 | 1.560 | 1.415 | .958± .050 | 1.351± .038 | - .415± .059 | + .560± .050 |
| SCF2f-8 | 6.36 | 1.677 | 1.166 | 1.202± .062 | 1.402± .0-1 | - .166± .049 | + .677± .054 |
| SCF2f-9 | 4.76 | 1.512 | 1.097 | 1.003± .042 | 1.100± .031 | - .097± .046 | + .512± .048 |
| **SCF3 unit (Fig. 22)** | | | | | | | |
| SCF3-1 | 2.58 | 1.042 | 1.301 | .531± .028 | .690± .019 | - .301± .055 | + .042± .033 |
| SCF3-2 | 2.73 | 1.023 | 1.234 | .543± .028 | .670± .019 | - .234± .052 | + .023± .033 |
| SCF3-3 | 2.79 | 1.030 | 1.124 | .571± .030 | .642± .018 | - .124± .047 | + .030± .033 |
| SCF3-4 | 2.75 | 1.033 | 1.149 | .556± .029 | .638± .018 | - .149± .048 | + .033± .033 |
| SCF3-5 | 2.80 | 1.020 | 1.102 | .567± .030 | .625± .018 | - .102± .046 | + .020± .033 |
| **SCF4 unit (Fig. 23)** | | | | | | | |
| SCF4-1 | 3.61 | 1.383 | 1.204 | .849± .044 | 1.022± .029 | - .204± .051 | + .383± .044 |
| SCF4-2 | 3.40 | 1.318 | 1.184 | .799± .042 | .946± .026 | - .184± .050 | + .318± .042 |
| SCF4-3 | 3.28 | 1.315 | 1.164 | .734± .038 | .855± .024 | - .164± .049 | + .315± .042 |
| SCF4-4 | 3.01 | 1.265 | 1.139 | .750± .039 | .854± .024 | - .139± .048 | + .265± .040 |
| SCF4-5 | 3.51 | 1.385 | .976 | .814± .042 | .795± .022 | + .024± .041 | + .385± .043 |
| SCF4-6 | 3.95 | 1.414 | .840 | .869± .045 | .730± .020 | + .160± .035 | + .414± .045 |
| SCF4-7 | 3.69 | 1.302 | .877 | .767± .040 | .673± .019 | + .123± .037 | + .302± .042 |
| SCF4-8 | 3.67 | 1.376 | .825 | .888± .046 | .733± .021 | + .175± .035 | + .376± .044 |
| **TSV 396m (Fig. 24)** | | | | | | | |
| 396m-A | 4.07 | 1.258 | 1.008 | 0.846± .044 | 0.852± .024 | -0.008± .042 | +0.258± .040 |
| 396m-B | 2.90 | 1.274 | .908 | 1.104± .057 | 1.003± .028 | + .092± .038 | + .274± .041 |
| 396m-C | 3.25 | 1.197 | 1.129 | .840± .044 | .948± .027 | - .129± .047 | + .197± .038 |
| 396m-D | 5.55 | 1.258 | 1.048 | 1.581± .082 | 1.652± .046 | - .044± .044 | + .254± .040 |
| 396m-E | 2.85 | 1.271 | 1.031 | 1.803± .094 | 1.859± .052 | - .031± .043 | + .271± .041 |
| 396m-F | 2.92 | 1.240 | 1.053 | 2.680± .139 | 2.822± .079 | - .053± .044 | + .240± .040 |



Table 3. Isotopic ratios of uranium and thorium required for U-trend plots

| Sample | U ppm | Activity Ratios: $\frac{^{234}U}{^{238}U}$ | $\frac{^{230}Th}{^{238}U}$ | $\frac{^{234}U}{^{230}Th}$ | $\frac{^{230}Th}{^{234}Th}$ | $\frac{(^{234}U-^{230}Th)}{^{238}U}$ | $\frac{(^{234}U-^{238}U)}{^{238}U}$ |
|---|---|---|---|---|---|---|---|
| **TSV 396f (Fig. 24)** | | | | | | | |
| 396f-A | 4.12 | 1.259 | .980 | .888± .046 | .870± .024 | + .020± .041 | + .259± .040 |
| 396f-B | 4.57 | 1.296 | .866 | 1.151± .060 | .996± .028 | + .130± .036 | + .296± .041 |
| 396f-C | 3.82 | 1.192 | 1.083 | .881± .046 | .958± .027 | - .083± .045 | + .193± .038 |
| 396f-D | 5.46 | 1.253 | 1.041 | 1.434± .075 | 1.494± .042 | - .041± .044 | + .253± .040 |
| 396f-E | 6.69 | 1.270 | 1.015 | 1.803± .094 | 1.830± .051 | - .015± .043 | + .270± .041 |
| 396f-F | 7.16 | 1.267 | 1.027 | 2.590± .131 | 2.661± .075 | - .027± .043 | + .267± .041 |
| **CF1 unit (Fig. 25)** | | | | | | | |
| CF1-1 | 2.16 | 1.061 | 1.475 | .450± .023 | .664± .019 | - .475± .062 | + .061± .034 |
| CF1-2 | 2.20 | 1.069 | 1.567 | .488± .025 | .758± .021 | - .567± .066 | + .069± .034 |
| CF1-3 | 2.32 | 1.104 | 1.343 | .485± .025 | .651± .018 | - .343± .056 | + .104± .035 |
| CF1-4 | 2.50 | 1.117 | 1.236 | .517± .027 | .640± .018 | - .236± .052 | + .117± .036 |
| CF1-5 | 2.47 | 1.127 | 1.263 | .510± .027 | .643± .018 | - .263± .053 | + .127± .036 |
| CF1-6 | 2.46 | 1.148 | 1.249 | .519± .027 | .648± .018 | - .249± .052 | + .148± .037 |
| CF1-7 | 2.35 | 1.135 | 1.289 | .503± .026 | .648± .018 | - .289± .054 | + .135± .036 |
| CF1-8 | 2.31 | 1.118 | 1.272 | .502± .026 | .638± .018 | - .272± .053 | + .118± .036 |
| **CF6 unit (Fig. 26)** | | | | | | | |
| CF6-1 | 2.45 | 1.142 | 1.277 | .509± .026 | .650± .018 | - .277± .054 | + .142± .037 |
| CF6-2 | 2.70 | 1.142 | 1.288 | .507± .026 | .648± .018 | - .288± .054 | + .142± .037 |
| CF6-3 | 2.24 | 1.146 | 1.280 | .505± .026 | .647± .018 | - .280± .054 | + .146± .037 |
| CF6-4 | 2.51 | 1.135 | 1.231 | .537± .028 | .661± .019 | - .231± .052 | + .135± .036 |
| CF6-5 | 2.59 | 1.103 | 1.293 | .508± .026 | .657± .018 | - .293± .054 | + .103± .035 |
| **CF2m unit (Fig. 27)** | | | | | | | |
| CF2m-1 | 3.83 | 1.237 | .950 | .821± .043 | .780± .022 | + .050± .040 | + .237± .039 |
| CF2m-2 | 4.23 | 1.272 | .850 | 1.000± .052 | .850± .024 | + .150± .036 | + .272± .041 |
| CF2m-3 | 3.91 | 1.267 | .892 | .899± .047 | .801± .022 | + .108± .038 | + .267± .040 |
| CF2m-4 | 3.73 | 1.124 | 1.001 | .690± .036 | .691± .019 | - .001± .042 | + .124± .036 |
| CF2m-5 | 3.78 | 1.126 | 1.004 | .725± .038 | .728± .020 | - .004± .042 | + .125± .036 |
| CF2m-6 | 3.29 | 1.117 | 1.052 | .680± .035 | .715± .020 | - .052± .045 | + .117± .035 |
| CF2m-7 | 3.28 | 1.150 | 1.051 | .768± .040 | .808± .023 | - .051± .045 | + .150± .037 |
| **CF2f unit (Fig. 27)** | | | | | | | |
| CF2f-1 | 3.54 | 1.787 | .978 | .840± .044 | .822± .023 | + .022± .041 | + .287± .041 |
| CF2f-2 | 4.31 | 1.322 | .848 | 1.030± .053 | .873± .024 | + .152± .036 | + .322± .042 |
| CF2f-3 | 3.79 | 1.305 | .923 | .982± .051 | .907± .025 | + .077± .039 | + .305± .042 |
| CF2f-4 | 3.43 | 1.247 | .950 | .848± .044 | .805± .023 | + .050± .040 | + .247± .040 |
| CF2f-5 | 2.90 | 1.164 | 1.038 | .680± .035 | .706± .020 | - .038± .044 | + .164± .037 |
| CF2f-6 | 2.81 | 1.146 | 1.086 | .595± .031 | .646± .018 | - .086± .046 | + .146± .037 |
| CF2f-7 | 2.85 | 1.152 | 1.062 | .724± .038 | .770± .022 | - .062± .045 | + .152± .037 |

Table 3. Isotopic ratios of uranium and thorium required for U-trend plots

| Sample | U ppm | Activity Ratios: $\frac{^{234}U}{^{238}U}$ | $\frac{^{230}Th}{^{232}Th}$ | $\frac{^{234}U}{^{232}Th}$ | $\frac{^{230}Th}{^{232}Th}$ | $\frac{(^{234}U-^{230}Th)}{^{238}U}$ | $\frac{(^{234}U-^{238}U)}{^{238}U}$ |
|---|---|---|---|---|---|---|---|
| **TM2m section (Fig. 28)** | | | | | | | |
| TM2m-1 | 2.42 | 1.051 | 1.369 | 0.460± .024 | 0.630± .018 | -0.369± .057 | +0.051± .038 |
| TM2m-2 | 2.35 | 1.076 | 1.431 | .438± .023 | .621± .017 | - .431± .060 | + .076± .038 |
| TM2m-3 | 2.21 | 1.078 | 1.416 | .393± .020 | .556± .016 | - .416± .059 | + .078± .038 |
| TM2m-4 | 2.79 | 1.159 | 1.124 | .510± .027 | .573± .016 | - .124± .047 | + .159± .037 |
| TM2m-5 | 3.83 | 1.251 | .831 | .746± .039 | .619± .017 | + .169± .035 | + .251± .040 |
| TM2m-6 | 3.31 | 1.130 | 1.034 | .597± .031 | .617± .017 | - .034± .043 | + .130± .036 |
| TM2m-7 | 3.83 | 1.133 | 1.014 | .636± .033 | .645± .018 | - .014± .043 | + .133± .036 |
| TM2m-8 | 3.54 | 1.160 | 1.006 | .798± .041 | .799± .022 | - .006± .042 | + .160± .037 |
| TM2m-9 | 4.12 | 1.184 | .887 | .845± .044 | .749± .021 | + .113± .037 | + .184± .038 |
| TM2m-10 | 3.43 | 1.199 | .925 | .868± .045 | .803± .022 | + .075± .039 | + .199± .038 |
| **TM2f section (Fig. 28)** | | | | | | | |
| TM2f-1 | 2.23 | 1.059 | 1.402 | .454± .024 | .638± .018 | - .402± .059 | + .059± .038 |
| TM2f-2 | 2.17 | 1.104 | 1.413 | .428± .022 | .605± .017 | - .413± .059 | + .104± .035 |
| TM2f-3 | 2.08 | 1.089 | 1.428 | .387± .020 | .553± .015 | - .428± .060 | + .089± .035 |
| TM2f-4 | 2.53 | 1.215 | 1.137 | .527± .027 | .599± .017 | - .137± .048 | + .215± .039 |
| TM2f-5 | 3.68 | 1.283 | .884 | .738± .038 | .652± .018 | + .116± .037 | + .282± .041 |
| TM2f-6 | 3.09 | 1.186 | 1.018 | .649± .034 | .661± .018 | - .018± .043 | + .186± .038 |
| TM2f-7 | 3.39 | 1.201 | .994 | .768± .040 | .763± .021 | + .006± .042 | + .201± .038 |
| TM2f-8 | 3.46 | 1.198 | .999 | .876± .046 | .876± .025 | + .001± .042 | + .198± .038 |
| TM2f-9 | 4.06 | 1.270 | .880 | 1.012± .053 | .890± .025 | + .120± .037 | + .270± .041 |
| TM2f-10 | 3.68 | 1.233 | .911 | .907± .047 | .826± .023 | + .089± .038 | + .233± .039 |
| **TM13m section (Fig. 29)** | | | | | | | |
| TM13m-1 | 2.18 | 1.007 | 1.589 | .442± .023 | .702± .020 | - .589± .067 | + .007± .032 |
| TM13m-2 | 1.93 | .989 | 1.769 | .309± .016 | .547± .015 | - .769± .078 | - .011± .032 |
| TM13m-3 | 1.97 | 1.018 | 1.755 | .338± .018 | .593± .017 | - .755± .078 | + .018± .032 |
| TM13m-4 | 1.97 | 1.012 | 1.671 | .338± .017 | .559± .016 | - .671± .070 | + .012± .032 |
| TM13m-5 | 2.58 | 1.122 | 1.406 | .460± .024 | .647± .018 | - .406± .059 | + .122± .036 |
| TM13m-6 | 3.29 | 1.168 | 1.125 | .669± .035 | .752± .021 | - .125± .047 | + .168± .037 |
| TM13m-7 | 2.90 | 1.095 | 1.146 | .555± .029 | .635± .018 | - .146± .048 | + .095± .035 |
| TM13m-8 | 3.26 | 1.146 | .969 | .627± .033 | .607± .017 | + .031± .041 | + .146± .037 |
| TM13m-9 | 2.60 | 1.056 | 1.070 | .505± .026 | .540± .015 | - .070± .045 | + .056± .038 |
| TM13m-10 | 2.87 | 1.096 | .977 | .530± .028 | .518± .015 | + .023± .041 | + .096± .035 |
| TM13m-11 | 4.12 | 1.168 | .865 | .800± .042 | .692± .019 | + .135± .036 | + .168± .037 |
| **TM13f section (Fig. 29)** | | | | | | | |
| TM13f-1 | 2.29 | .999 | 1.486 | .438± .023 | .650± .018 | - .486± .062 | - .001± .037 |
| TM13f-2 | 2.01 | 1.017 | 1.729 | .369± .019 | .638± .018 | - .729± .072 | + .017± .033 |
| TM13f-3 | 1.99 | .966 | 1.722 | .331± .017 | .570± .016 | - .722± .072 | - .038± .031 |
| TM13f-4 | 2.01 | .992 | 1.681 | .333± .017 | .562± .016 | - .681± .071 | - .008± .032 |
| TM13f-5 | 2.30 | 1.091 | 1.491 | .443± .023 | .660± .018 | - .491± .063 | + .091± .035 |
| TM13f-6 | 3.14 | 1.186 | 1.203 | .676± .035 | .814± .023 | - .203± .051 | + .186± .038 |



Table 3. Isotopic ratios of uranium and thorium required for U-trend plots

| Sample | U ppm | Activity Ratios: $\frac{^{234}U}{^{238}U}$ | $\frac{^{230}Th}{^{232}Th}$ | $\frac{^{234}U}{^{232}Th}$ | $\frac{^{230}Th}{^{232}Th}$ | $\frac{(^{234}U-^{230}Th)}{^{238}U}$ | $\frac{(^{234}U-^{238}U)}{^{238}U}$ |
|---|---|---|---|---|---|---|---|
| **TM13f section (Fig. 29)** | | | | | | | |
| TM13f-7 | 2.92 | 1.176 | 1.128 | .548±0.029 | .625±0.017 | - .128±0.047 | + .126±0.036 |
| TM13f-8 | 3.51 | 1.211 | .899 | .753± .039 | .673± .018 | + .011± .042 | + .211± .039 |
| TM13f-9 | 2.58 | 1.078 | 1.105 | .513± .026 | .567± .016 | - .105± .041 | + .078± .034 |
| TM13f-10 | 2.90 | 1.122 | .980 | .552± .029 | .541± .018 | + .020± .041 | + .122± .036 |
| TM13f-11 | 3.58 | 1.130 | 1.008 | .724± .038 | .786± .022 | + .008± .044 | + .130± .038 |
| **TM14B upper unit (Fig. 30)** | | | | | | | |
| TM14B-1 | 2.31 | 1.060 | 1.608 | .650± .023 | .724± .020 | - .608± .068 | + .060± .034 |
| TM14B-2 | 3.95 | 1.207 | .990 | .779± .041 | .772± .022 | + .010± .042 | + .207± .039 |
| TM14B-3 | 2.36 | 1.078 | 1.695 | .666± .028 | .790± .022 | - .617± .068 | + .082± .035 |
| TM14B-4 | 2.46 | 1.082 | 1.617 | .688± .025 | .790± .022 | - .617± .068 | + .089± .035 |
| TM14B-5 | 2.46 | 1.089 | 1.625 | .693± .026 | .800± .022 | - .625± .068 | + .089± .035 |
| TM14B-6 | 2.56 | 1.081 | 1.588 | .517± .027 | .812± .023 | - .588± .067 | + .083± .035 |
| TM14B-7 | 2.82 | 1.119 | 1.529 | .567± .029 | .847± .024 | - .529± .066 | + .119± .036 |
| TM14B-8 | 2.89 | 1.127 | 1.498 | .583± .030 | .870± .024 | - .498± .063 | + .127± .036 |
| TM14B-9 | 3.30 | 1.140 | 1.428 | .690± .036 | .986± .028 | - .428± .063 | + .140± .036 |
| **TM14 upper unit (Fig. 31)** | | | | | | | |
| TM14-1 | 2.09 | 1.024 | 1.452 | 0.503± .026 | 0.730± .020 | -0.452± .061 | +0.024± .033 |
| TM14-2 | 2.08 | 1.002 | 1.569 | .435± .023 | .682± .019 | - .569± .066 | + .002± .032 |
| TM14-3 | 2.10 | 1.040 | 1.566 | .436± .023 | .683± .019 | - .566± .066 | + .040± .033 |
| TM14-4 | 2.26 | 1.041 | 1.591 | .456± .024 | .725± .020 | - .591± .067 | + .041± .033 |
| TM14-5 | 2.20 | 1.050 | 1.553 | .440± .023 | .684± .019 | - .553± .065 | + .050± .034 |
| TM14-6 | 2.28 | 1.048 | 1.539 | .468± .024 | .720± .020 | - .539± .065 | + .048± .034 |
| TM14-7 | 2.39 | 1.079 | 1.678 | .470± .024 | .787± .022 | - .678± .070 | + .079± .035 |
| TM14-8 | 2.74 | 1.088 | 1.620 | .565± .029 | .918± .026 | - .620± .068 | + .088± .035 |
| TM14-9 | 3.05 | 1.184 | 1.465 | .655± .034 | .960± .027 | - .465± .062 | + .184± .038 |
| **TM14 section (Fig. 31)** | | | | | | | |
| TM14-10 | 4.63 | 1.314 | .881 | 1.144± .059 | 1.009± .028 | + .119± .037 | + .314± .042 |
| TM14-11 | 4.84 | 1.246 | .758 | 1.378± .072 | 1.044± .029 | + .242± .032 | + .246± .040 |
| TM14-12 | 5.60 | 1.262 | .894 | 2.829± .147 | 2.530± .071 | + .106± .038 | + .262± .040 |
| TM14-13 | 5.83 | 1.265 | .906 | 3.149± .164 | 2.852± .080 | + .094± .038 | + .265± .040 |
| TM14-14 | 4.26 | 1.362 | .938 | 11.29± .59 | 10.60± .30 | + .062± .039 | + .362± .044 |
| TM14-15 | 2.46 | 1.101 | .988 | 1.000± .052 | .998± .028 | + .012± .041 | + .101± .035 |
| TM14-16 | 2.39 | 1.053 | .963 | .838± .044 | .807± .023 | + .037± .040 | + .053± .034 |
| TM14-17 | 2.67 | .972 | .958 | .872± .045 | .835± .023 | + .042± .040 | - .028± .031 |
| TM14-18 | 3.16 | .949 | .980 | .759± .039 | .743± .021 | + .020± .041 | - .051± .030 |
| TM14-19 | 3.40 | .968 | .986 | .916± .048 | .903± .025 | + .018± .041 | - .032± .031 |
| TM14-20 | 3.55 | .952 | .997 | .700± .036 | .697± .020 | + .004± .042 | - .048± .030 |
| TM14-21 | 5.22 | .936 | .999 | 1.345± .069 | 1.345± .038 | + .001± .042 | - .064± .030 |
| TM14-22 | 3.80 | .906 | .947 | .757± .039 | .717± .020 | + .053± .040 | - .094± .029 |

Table 3. Isotopic ratios of uranium and thorium required for U-trend plots

| Sample | U ppm | Activity Ratios $\frac{^{234}U}{^{238}U}$ | $\frac{^{230}Th}{^{232}Th}$ | $\frac{^{234}U}{^{232}Th}$ | $\frac{^{230}Th}{^{232}Th}$ | $(\frac{^{234}U}{^{238}U}-\frac{^{230}Th}{^{232}Th})$ | $(\frac{^{234}U}{^{238}U}-\frac{^{230}Th}{^{238}U})$ |
|---|---|---|---|---|---|---|---|
| **CBQ unit (Fig. 32)** | | | | | | | |
| CBQ-1 | 2.07 | 1.045 | 1.147 | .555±0.020 | .637±0.020 | - .147±0.048 | + .045±0.033 |
| CBQ-2 | 2.46 | 1.121 | .996 | .673± .035 | .671± .021 | + .005± .042 | + .121± .036 |
| CBQ-3 | 2.84 | 1.191 | .848 | .766± .040 | .680± .022 | + .112± .037 | + .191± .038 |
| CBQ-4 | 2.99 | 1.205 | .827 | .884± .044 | .698± .022 | + .173± .035 | + .205± .039 |
| CBQ-5 | 2.54 | 1.151 | .987 | .702± .037 | .693± .022 | + .013± .042 | + .151± .037 |
| CBQ-6 | 2.85 | 1.199 | .955 | .844± .044 | .806± .026 | + .045± .044 | + .199± .038 |
| CBQ-7 | 2.09 | 1.116 | 1.073 | .604± .031 | .648± .021 | - .073± .045 | + .116± .036 |
| CBQ-8 | 2.78 | 1.189 | .975 | .833± .043 | .812± .026 | + .025± .043 | + .189± .038 |
| **FMA unit (Fig. 33)** | | | | | | | |
| AIS-A | 4.79 | 1.295 | 1.189 | .697± .036 | .828± .023 | - .189± .050 | + .189± .038 |
| AIS-B | 3.72 | 1.268 | 1.220 | .499± .026 | .609± .017 | - .220± .051 | + .268± .041 |
| AIS-C | 4.01 | 1.346 | .826 | .737± .038 | .609± .017 | + .174± .035 | + .346± .043 |
| AIS-D | 7.17 | 1.367 | 1.239 | .753± .039 | .933± .026 | - .239± .052 | + .367± .044 |
| AIS-E | 4.41 | 1.346 | 1.542 | .381± .020 | .588± .016 | - .542± .065 | + .346± .043 |
| **SJ unit (Fig. 34)** | | | | | | | |
| SJ-A | 2.90 | 1.241 | 1.209 | 1.035± .054 | 1.251± .035 | - .209± .051 | + .241± .040 |
| SJ-B | 2.82 | 1.215 | 1.524 | .679± .036 | 1.065± .030 | - .524± .068 | + .215± .039 |
| SJ-C | 3.57 | 1.176 | 1.180 | 1.257± .065 | 1.483± .042 | - .180± .050 | + .176± .038 |
| SJ-D | 2.82 | 1.161 | 1.248 | .837± .044 | 1.044± .029 | - .248± .052 | + .161± .037 |
| SJ-E | 2.25 | 1.156 | 1.129 | .744± .040 | .874± .024 | - .129± .047 | + .156± .037 |
| SJ-F | 2.46 | 1.189 | 1.031 | .868± .045 | .895± .025 | - .031± .043 | + .189± .038 |
| SJ-G | 2.33 | 1.173 | 1.032 | .845± .044 | .868± .024 | - .032± .043 | + .173± .038 |
| SJ-H | 2.29 | 1.187 | 1.249 | .803± .042 | 1.003± .028 | - .249± .052 | + .187± .038 |





Table 4. Uranium-trend model parameters and ages of deposition units in NTS area.

| Unit | Description of Deposit | U-trend slope | X intercept | Half period of F(0) (Ka) | Age Ka |
|---|---|---|---|---|---|
| 39 | FFPG unit, eolian surface Frenchman Flat Trench | +0.276 | -0.721 | 73 | 30±30 |
| 40 | S1 unit, alluvium, upper part, Frenchman Flat Trench | + .706 | - .682 | 74 | 60±60 |
| 41 | F2 unit, buried B horizon Frenchman Flat Trench | + .417 | - .[illegible] | 400 | 240±80 |
| 42 | F3 unit, alluvium lower part, Frenchman Flat Trench | + .331 | - .[illegible] | 440 | 190±70 |
| 43 | RV1 section, (A-D) unit Rock Valley Trench 1 | + .238 | - .671 | 74 | 31±10 |
| 44 | RV1 section, (E-I) unit, Rock Valley Trench 1 | + .540 | - .[illegible] | 660 | 310±40 |
| 45 | RV1 section, (J-O) unit, Rock Valley Trench 1 | + .219 | - .[illegible] | 82 | 37±24 |
| 46 | RV1 section, (P-U) unit, Rock Valley Trench 1 | + .759 | - .[illegible] | 250 | 180±40 |
| 47 | RV1 section (V-Z) unit, Rock Valley Trench 1 | + .628 | - .157 | 500 | 270±30 |
| 48 | TSW 307 unit, upper part Rock Valley Trench 2 | + .[illegible] | - .[illegible] | 86 | 38±10 |
| 49 | RV2 section, upper part, Rock Valley Trench 2 | + .250 | - .500 | 84 | 34±20 |
| 50 | RV2 section, lower part Rock Valley Trench 2 | +2.121 | + .004 | 760 | 350±100 |
| 51 | Q2S unit, sand sheet, Jackass Flat Engine Test Trench | + .428 | - .210 | 460 | 160±90 |
| 52 | S9 unit, alluvium, upper part, Jackass Divide Trench | + .[illegible] | - .[illegible] | 560 | 270±35 |
| 53 | JD unit, alluvium, lower part Jackass Divide Trench | -3.87 | + .[illegible] | 660 | 810±60 |

Table 4. Uranium-trend model parameters and ages of deposition units (cont.)

| Unit | Description of Deposit | U-trend slope | X intercept | Half period of F(0) (Ka) | Age Ka |
|---|---|---|---|---|---|
| 54 | SCF4 section, lower unit (upper part) South Crater Flat Trench | -1.78 | + .008 | 730 | 400±50 |
| 55 | SCF4 section, lower unit (lower part) South Crater Flat Trench | -2.38 | - .002 | 730 | 480±60 |
| 56 | TSV 396 unit, carbonate enriched zone Crater Flat Trench 1 | + .400 | - .648 | 76 | 48±20 |
| 57 | CF1 unit, upper unit Crater Flat Trench 3 | + .313 | - .674 | 74 | 40±10 |
| 58 | CF6 unit, lower B horizon Crater Flat Trench 3 | +1.42 | - .290 | 210 | 190±50 |
| 59 | CF2 unit, lower unit Crater Flat Trench 3 | + .985 | - .191 | 440 | 270±30 |
| 60 | YM2 section, upper unit Yucca Mountain Trench 2 | + .401 | - .603 | 77 | 47±18 |
| 61 | YM2 section, lower unit Yucca Mountain Trench 2 | + .594 | - .287 | 220 | 145±25 |
| 62 | YM-13 section, upper unit Yucca Mountain Trench 13 | - .326 | + .723 | 74 | 41±10 |
| 63 | YM13 section, lower unit Yucca Mountain Trench 13 | + .600 | - .197 | 430 | 240±50 |
| 64 | YM14B section, lower B horizon<br>upper & lower B horizons<br>Yucca Mountain Trench 14 | + .314<br>+1.58 | - .841<br>- .612 | 72<br>77 | 38±10<br>55±20 |
| 65 | YM14M section, carbonate enriched zone Yucca Mountain Trench 14 | - .523 | + .675 | 74 | 270±90 |
| 66 | YM14L section, sandy horizon Yucca Mountain Trench 14 | +8.61 | + .040 | 660 | 420±50 |
| 67 | YM14G section, gravel horizon Yucca Mountain Trench 14 | +1.26 | - .027 | 680 | 480±90 |
| 68 | CBQ unit, alluvium, Shoshone, CA Charlie Brown Quarry | + .522 | - .266 | 270 | 160±25 |
| 69 | FHA unit, altered ash Fairbanks Hills, NV | - .303 | +1.17 | 70 | > 600 |
| 70 | S3 unit, QTA terrace Eleana Pediment | - .176 | +2.22 | 70 | > 800 |



Table 5. Summary of stratigraphic units and their U-trend ages in the NTS area

| Stratigraphic unit | Sample Suite | Sample location | U-trend Age (Ka) | Comments |
|---|---|---|---|---|
| Q2 | FFPG | Frenchman Flat | 30 ± 30 | Clayey silt of eolian deposit |
| Q2a | RV1-AD | Rock Valley | 31 ± 10 | Slope wash |
| | RV1-JO | Rock Valley | 37 ± 24 | Buried B-horizon |
| | TSV-307 | Rock Valley | 38 ± 10 | Gravel alluvium |
| | RV2U | Rock Valley | 36 ± 20 | Buried B-horizon |
| | CF1 | Crater Flat | 40 ± 10 | Pebbly fan gravel |
| | YM2U | Yucca Mountain | 47 ± 18 | Buried B-horizon |
| | YM13U | Yucca Mountain | 41 ± 10 | Buried B-horizon |
| | YM14B | Yucca Mountain | 38 ± 10 | Buried B-horizon |
| | YM14U | Yucca Mountain | 55 ± 20 | Buried B-horizon |
| Q2b | S1 | Frenchman Flat | 80 ± 606 | Poor age, unit recollected as F2/3 |
| | F2 | Frenchman Flat | 200 ± 80 | Buried B-horizon |
| | F3 | Frenchman Flat | 190 ± 70 | Pebbly fan gravel |
| | RV1-PU | Rock Valley | 180 ± 40 | Calcareous B-horizon |
| | CF6 | Crater Flat | 190 ± 50 | Buried B-horizon |
| | YM2L | Yucca Mountain | 145 ± 25 | Gravel-alluvium |
| | CBQ | Shoshone, CA | 160 ± 25 | Pebbly alluvium |
| Q2c Younger unit | RV1-EI | Rock Valley | 310 ± 40 | Alluvium |
| | RV1-VZ | Rock Valley | 270 ± 30 | K-horizon |
| | S9 | Jackass Divide | 270 ± 35 | Alluvium |
| | CF2 | Crater Flat | 270 ± 30 | Gravel alluvium |
| | YM13L | Yucca Mountain | 240 ± 50 | Gravel alluvium |
| Q2c Older unit | RV2L | Rock Valley | 390 ± 100 | Gravel alluvium |
| | JD | Jackass Divide | 430 ± 40 | Gravel alluvium |
| | SCF4 | South Crater Flat | 440 ± 60 | Average age of two different facies in alluvium deposit |
| Q2a | QJF5 | Jackass Flat | 160 ± 90 | Large error-higher limit age [illegible] |
| | YM14M | Yucca Mountain | 270 ± 90 | Laminar carbonate--indicates time of calcium carbonate development |
| | YM14L | Yucca Mountain | 420 ± 50 | Cca-horizon in sand deposit |
| | YM14G | Yucca Mountain | 480 ± 90 | Basalt gravel in sand deposit. |
| Q2e | FHA | Fairbanks Hills | >600 | Poor plot, exceeds time range of method |
| QTa | S3 | Eleana Pediment | >800 | Exceeds time range of method |

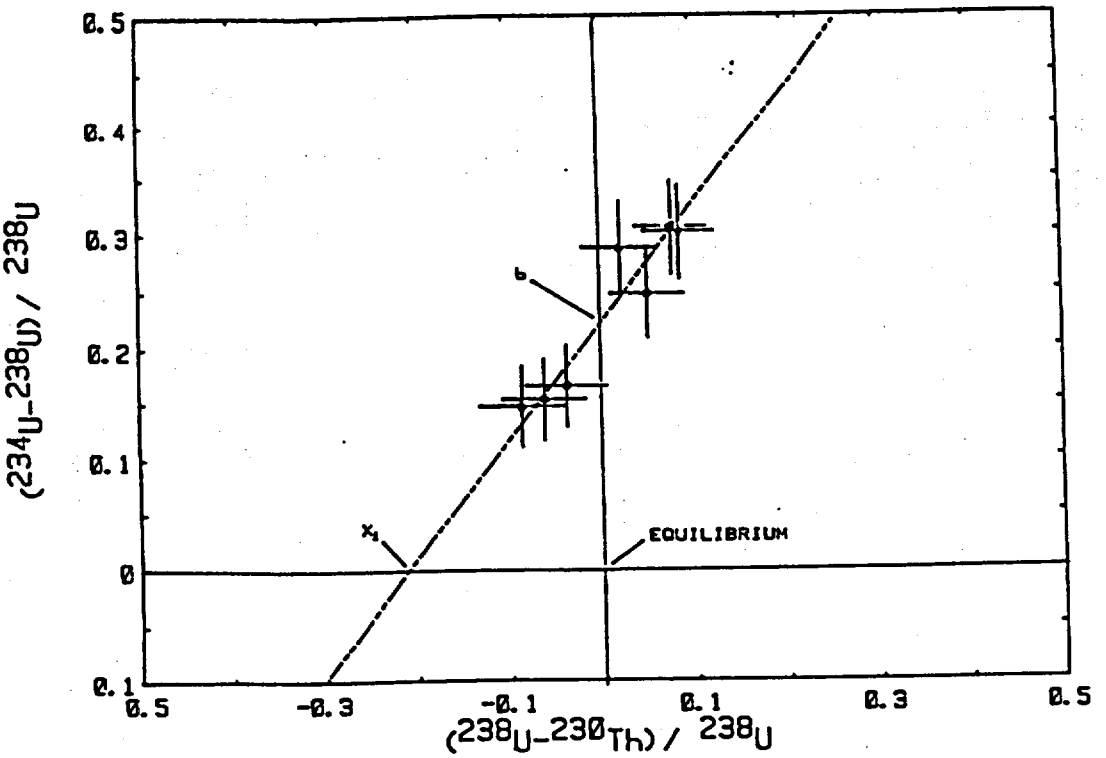


Figure 1. Uranium-trend plot of CF2 alluvium in Crater Flat Trench 3. All samples plotted in terms of activity ratios.

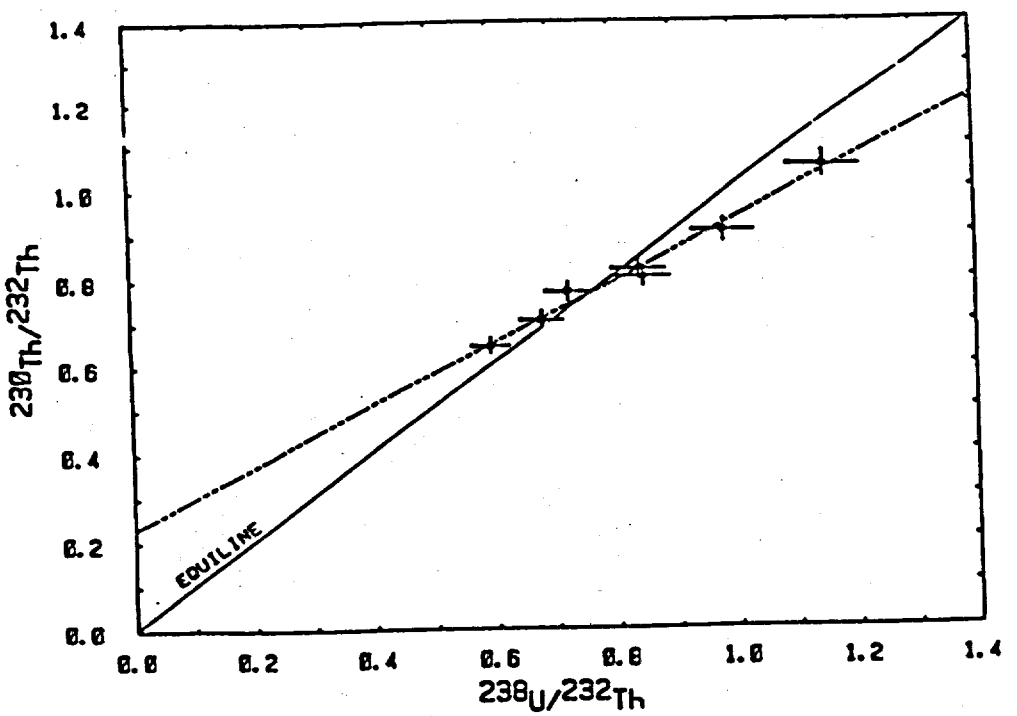


Figure 2. Thorium plot of CF2 alluvium in Crater Flat Trench 3. All samples plotted in terms of activity ratios.

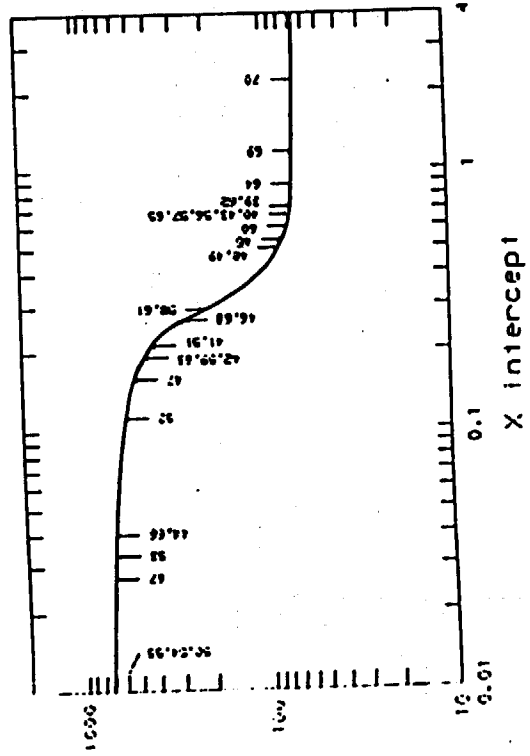


Figure 3. Calibration curve for determination of F(0) from X-intercept value. Indices on curve show unit number from Tables 3 and 4.



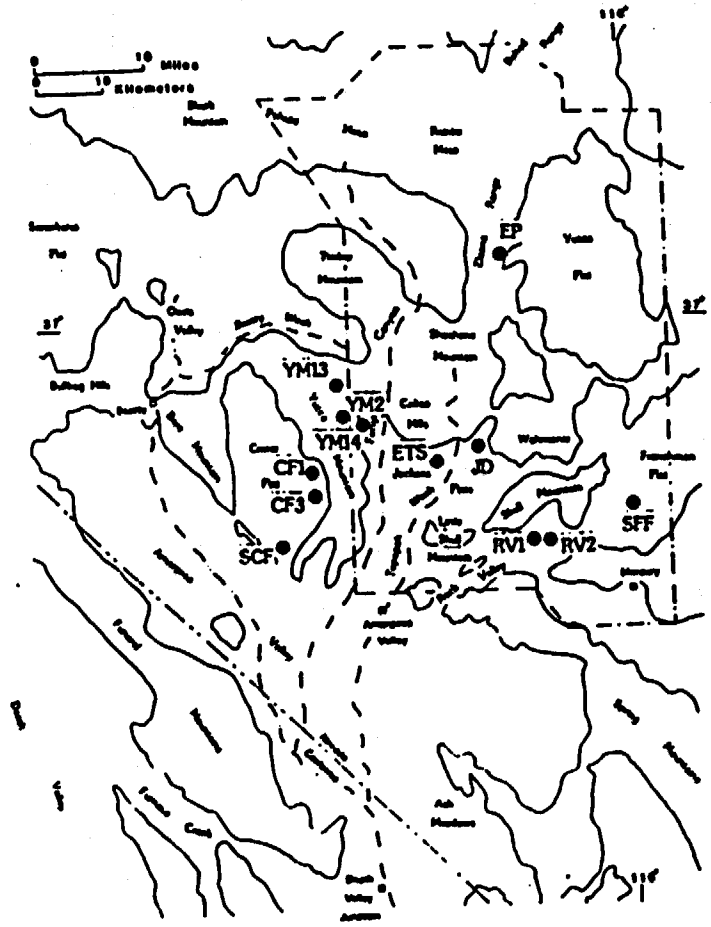


Figure 4. Location of sampling sites (see Table 1) for U-trend dating in the Nevada Test Site area.

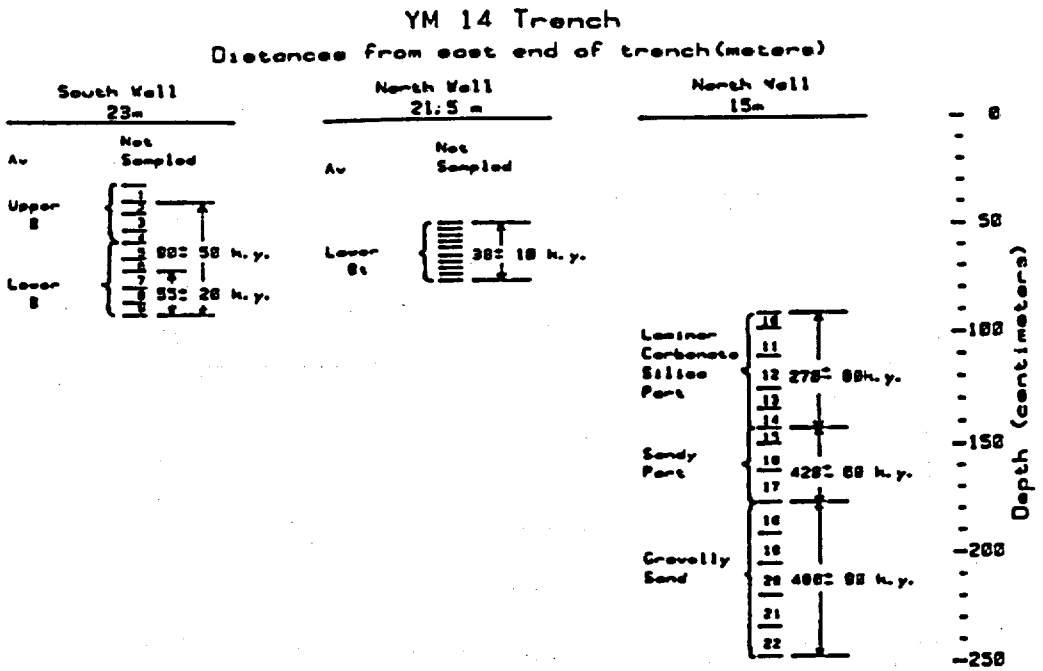


Figure 5. Sample sites in Yucca Mountain Trench 14.

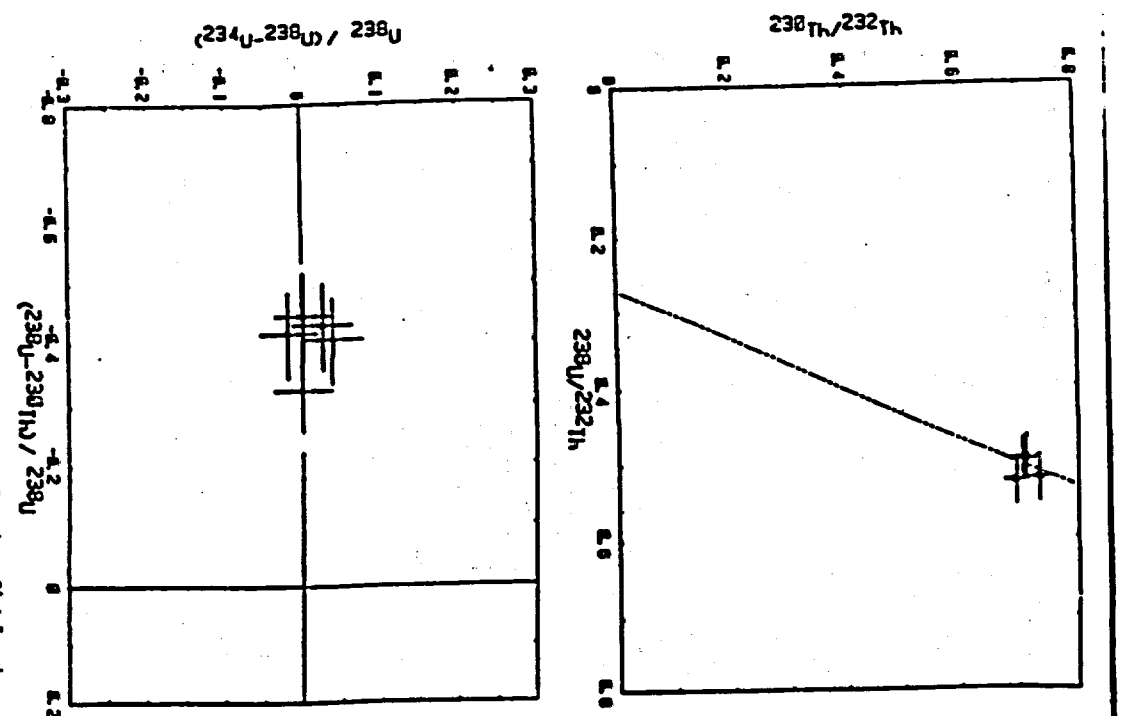


Figure 6. Plots of SFF unit, eolian sand, Frenchman Flat Trench. No age could be calculated because of the circular array of data points.

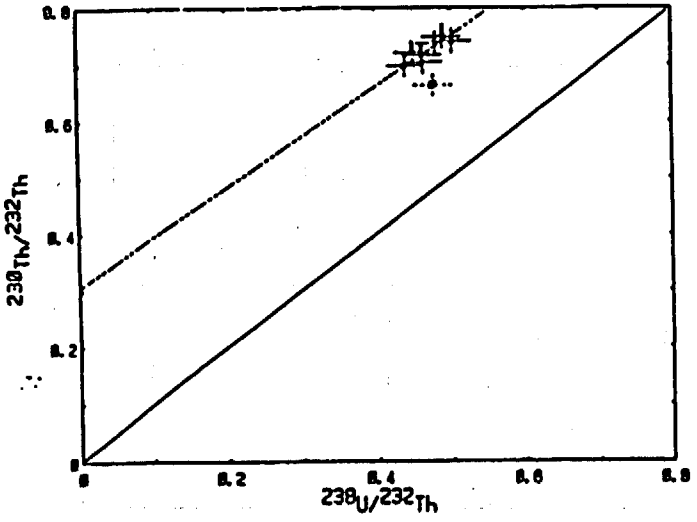


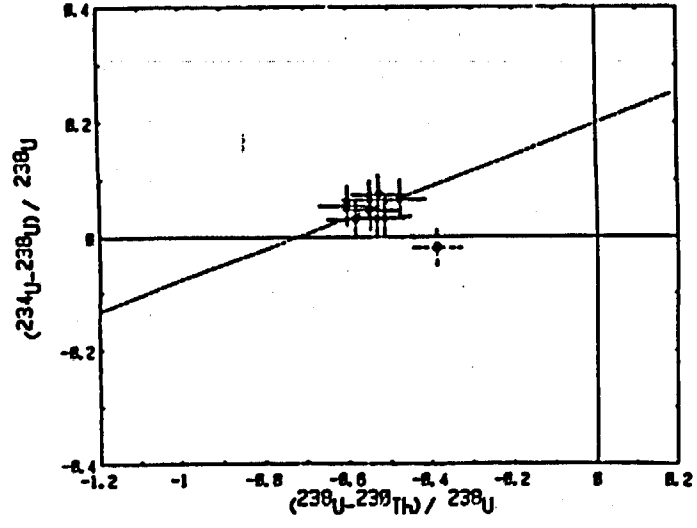


Figure 7. Plots of FFPG unit, eolian sand in Frenchman Flat Trench. The uppermost sample, □, is not included in U-trend slope because it may contain material from overlying deposit.

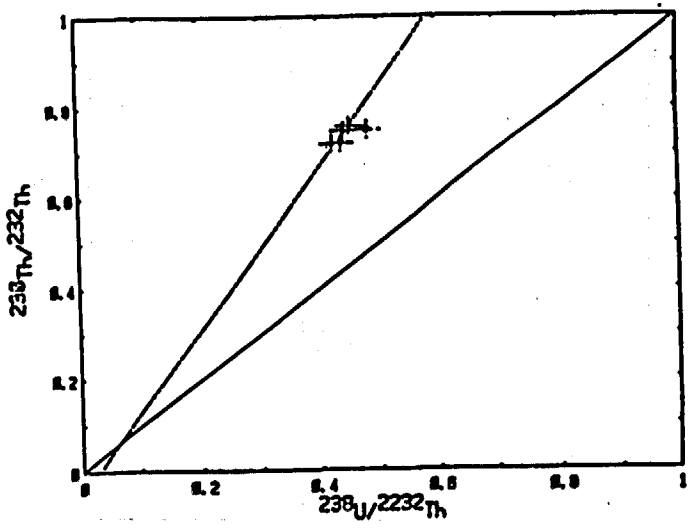


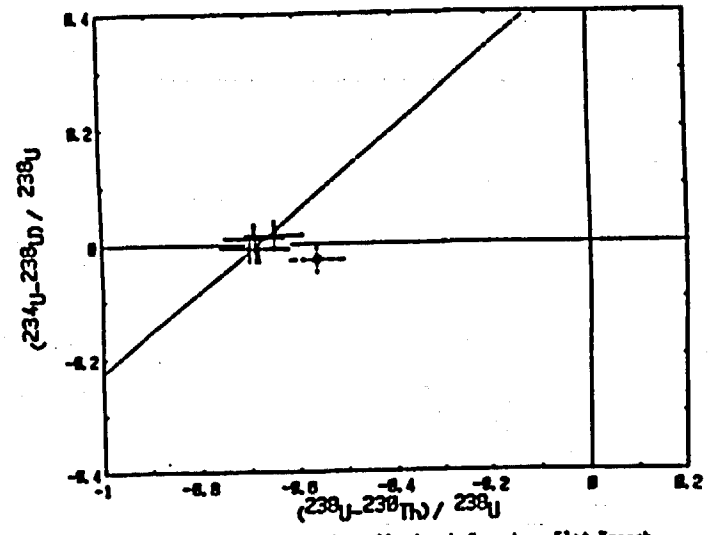


Figure 8. Plots of SI unit, alluvium in Frenchman Flat Trench. The uppermost sample, □, is not included in the U-trend slope because it may contain material from the overlying deposit.

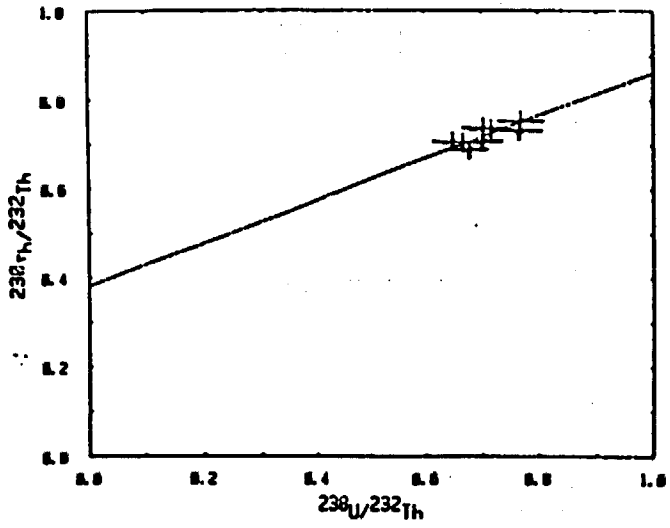


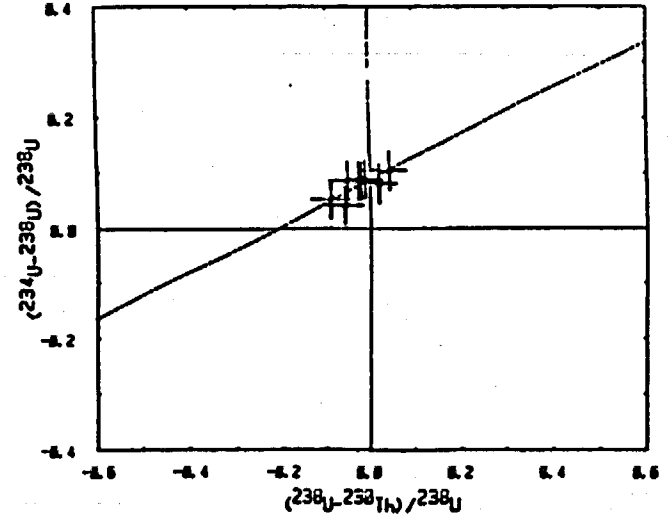


Figure 9. Plots of F2 unit, buried B horizon, Frenchman Flat Trench.

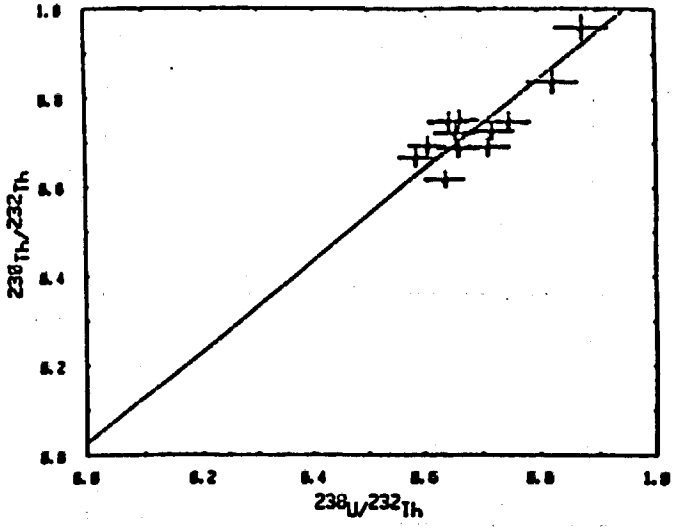


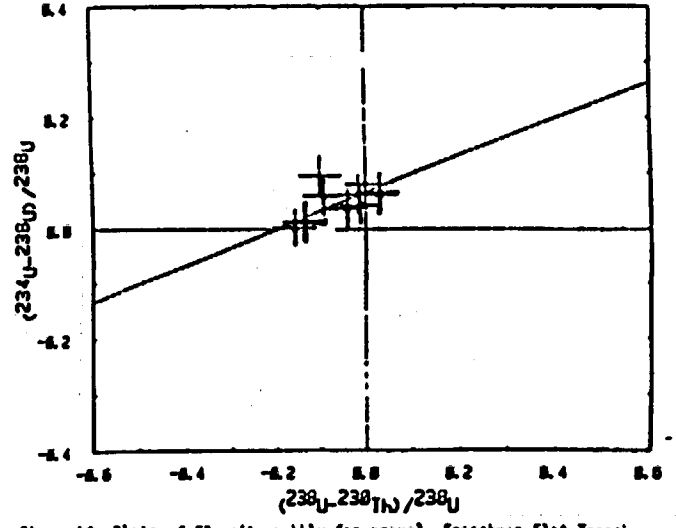


Figure 10. Plots of F3 unit, pebbly fan gravel, Frenchman Flat Trench.

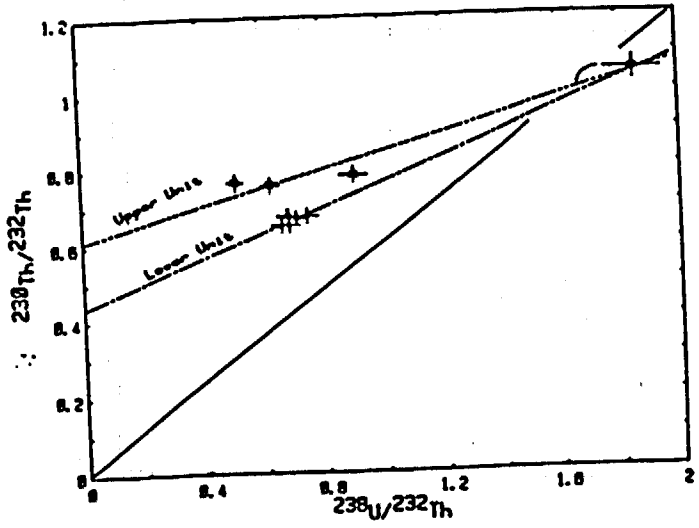


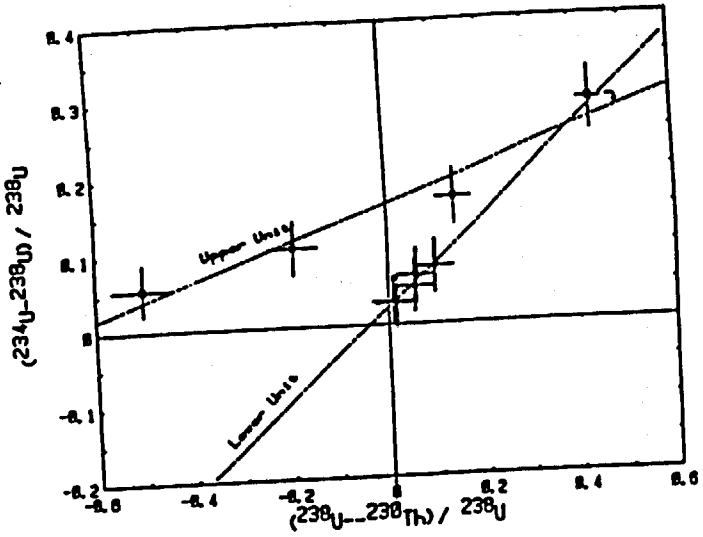


Figure 11. Plots of RV1 section, upper and lower alluvium in Rock Valley Fault Trench 1.

-18

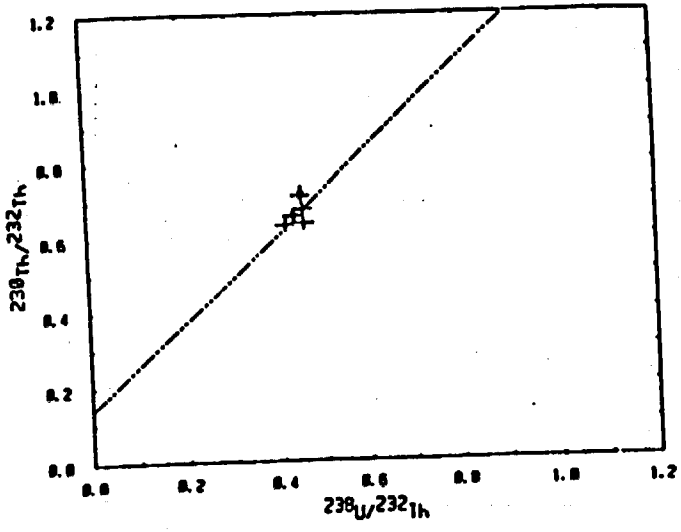


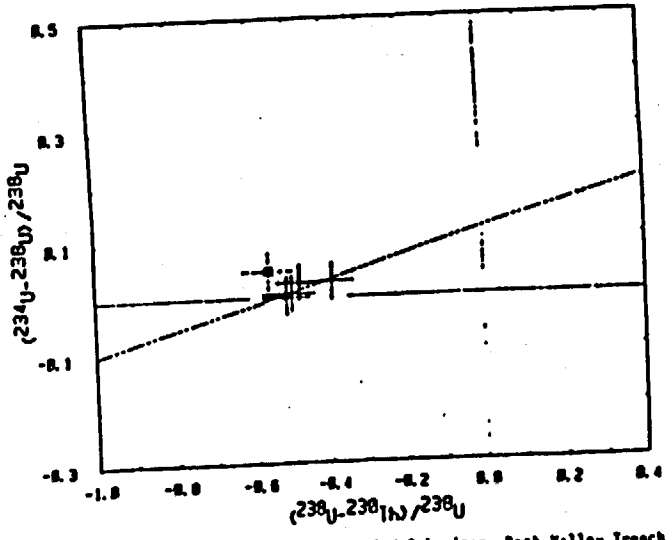


Figure 12. Plots of RV1(J-O) unit, buried A horizon, Rock Valley Trench 1. Upper Sample J, m, is not included in the U-trend slope.

-19

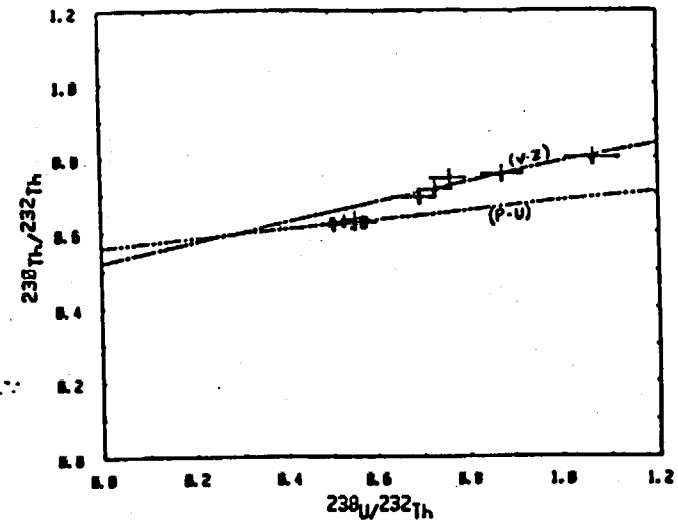


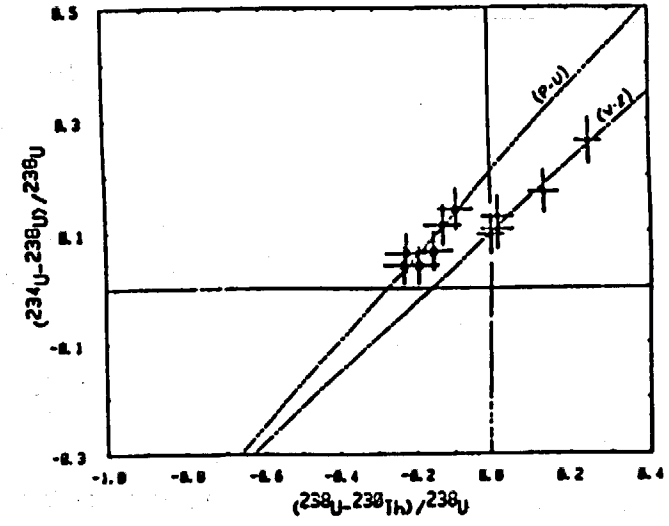


Figure 13. Plots of RV1 section, calcareous B horizon, □(P-U), and K horizon, ○(V-Z), in Rock Valley Trench 1.

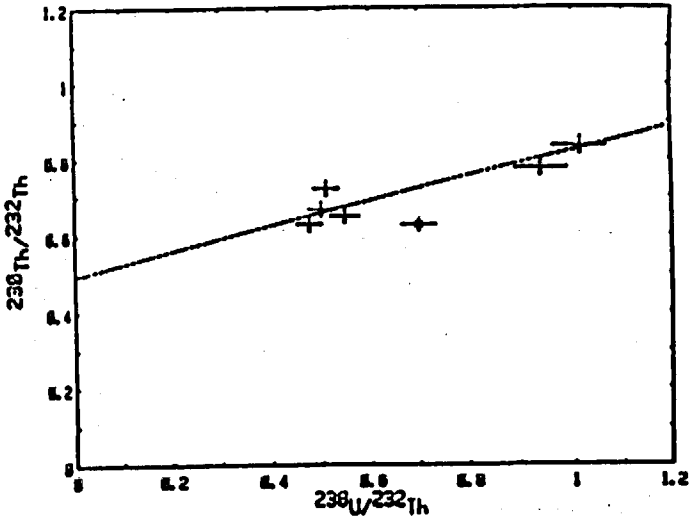


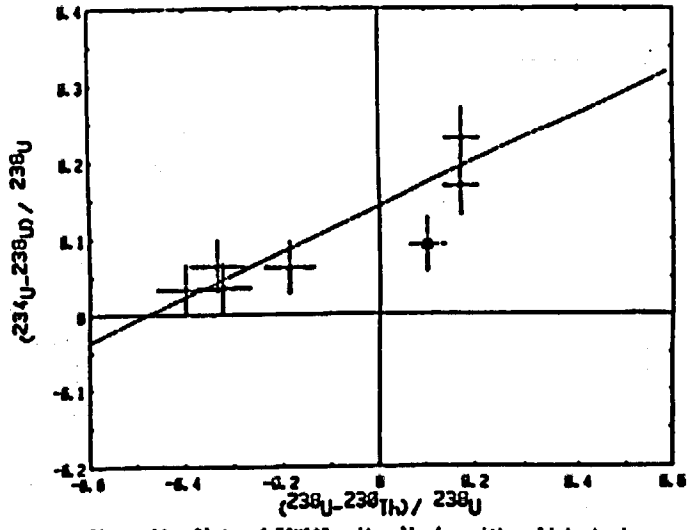


Figure 14. Plots of TSY307 unit, alluvium with caliche horizon in Rock Valley Fault Trench 2. Caliche horizon, □, is not included in U-trend slope.

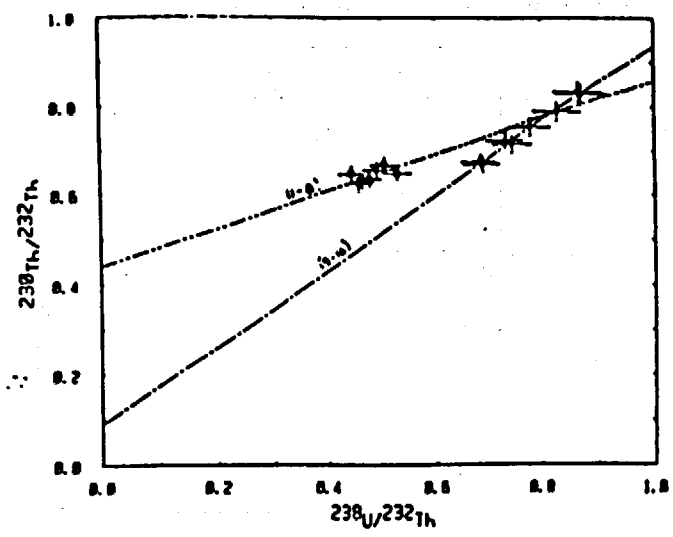


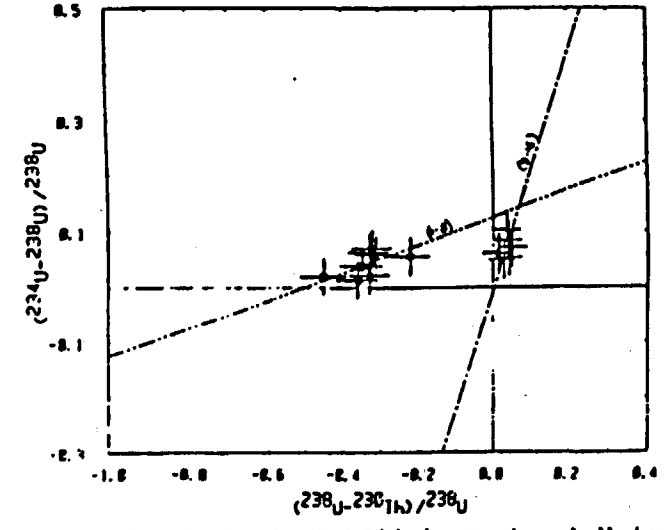


Figure 15. Plots of RV2 Section, buried B horizon □, and gravel alluvium ○, in Rock Valley Trench 2.

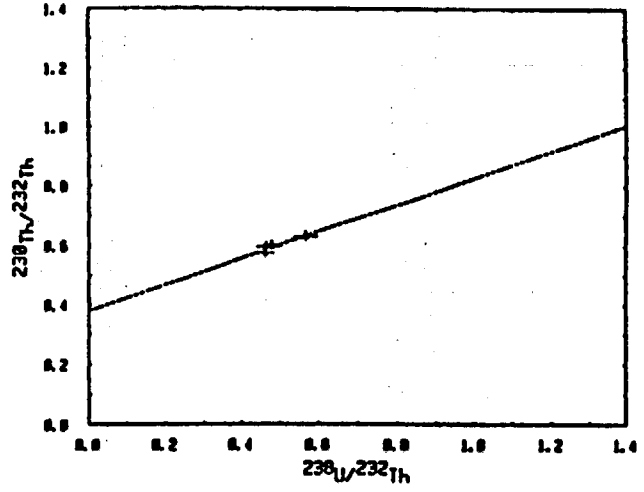


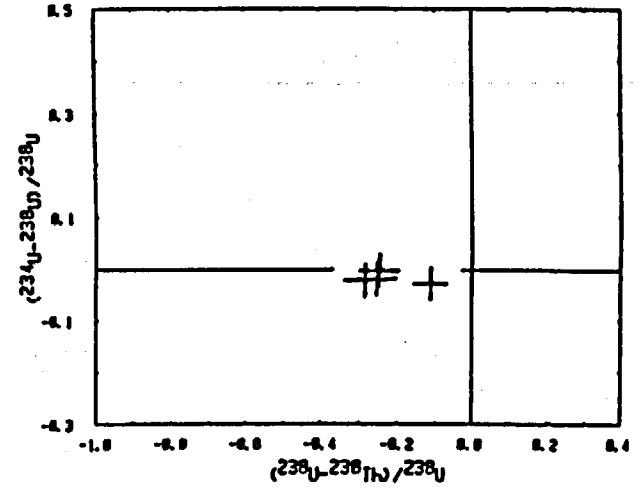


Figure 16. Plots of Q2E unit, sand sheet deposit in Jackass Flat Engine Test Stand Trench. The 4-sample profile was not datable.

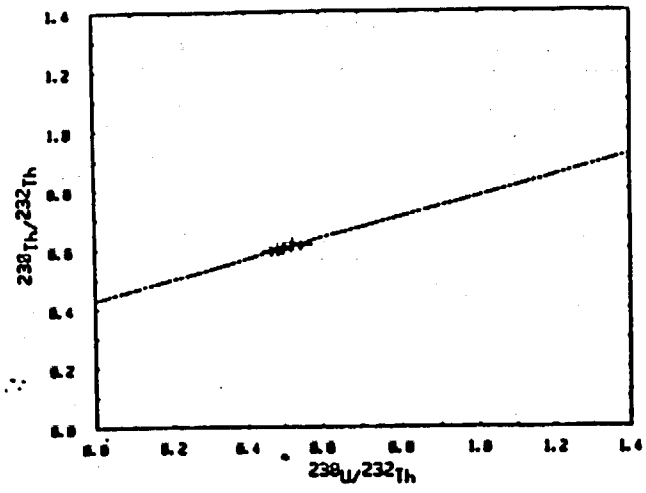


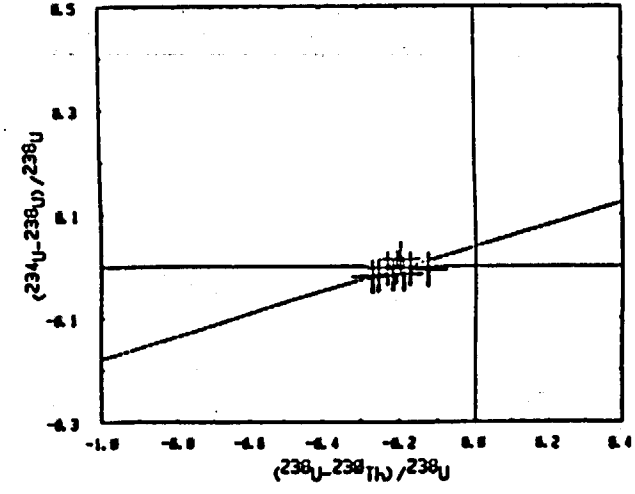


Figure 17. Plots of Q2S unit, sand sheet deposit in Jackass Flat Engine Test Stand Trench.

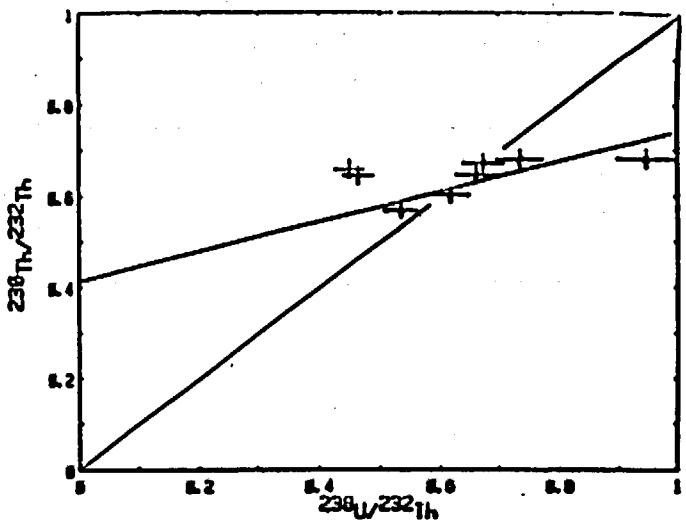


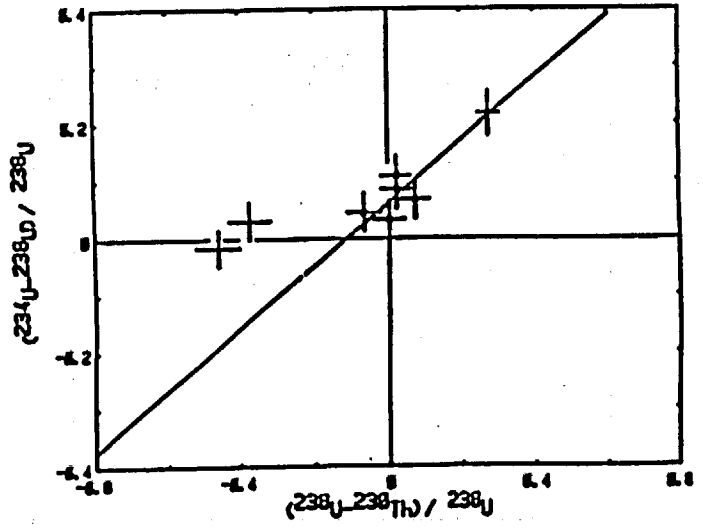


Figure 18. Plots of S9 unit, upper alluvium in Jackass Divide Trench. The upper two samples are not included in the U-trend slope because they do not fit with other samples on the thorium plot.

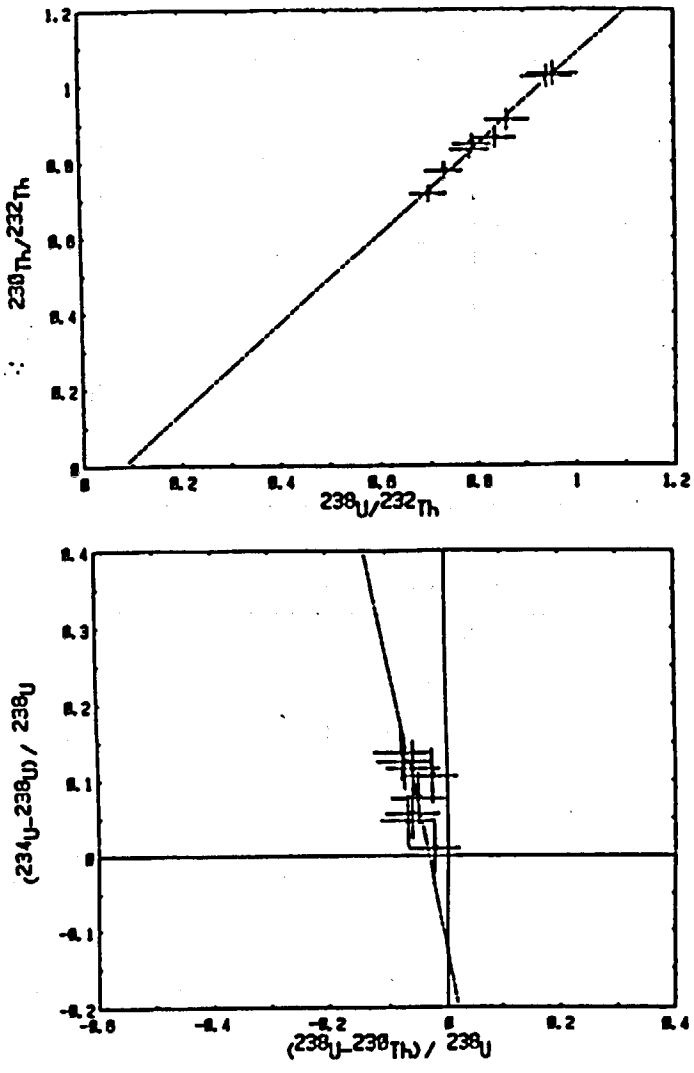


Figure 19. Plots of JD unit, lower alluvium in Jackass Divide Trench.

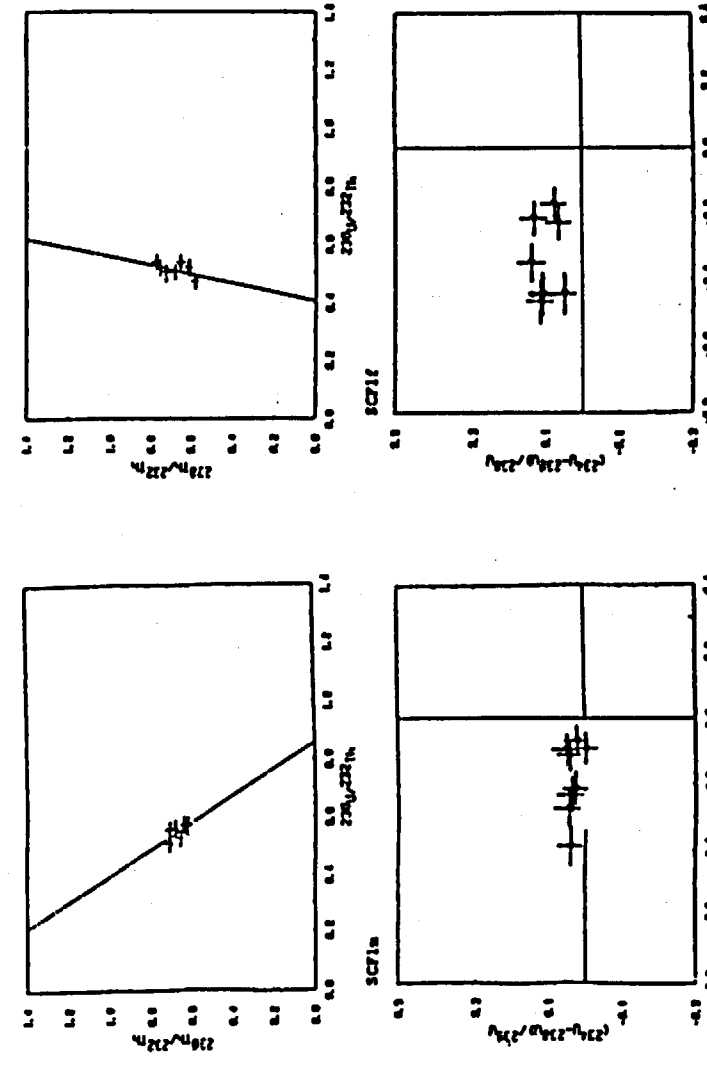


Figure 20. Plots of SCF1 unit, upper alluvium in South Crater Flat West Trench. SCF1a represents samples less than 2 mm size fraction and SCF1f represents samples less than 0.3 mm size fraction; neither fraction was datable by U-trend.

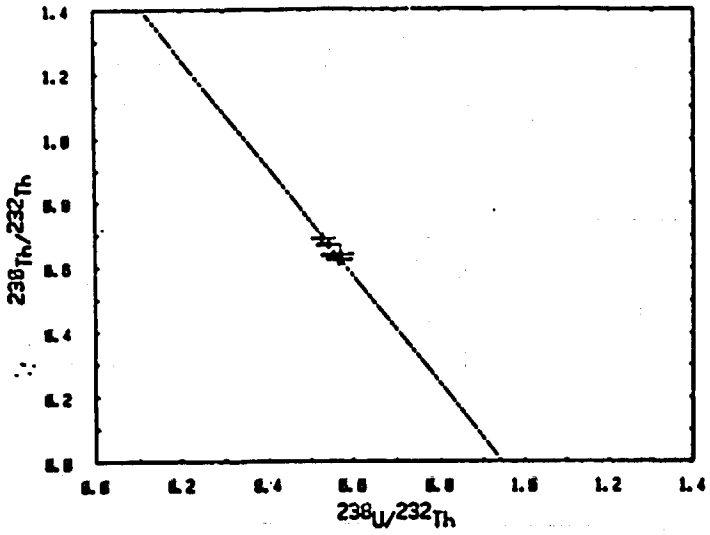


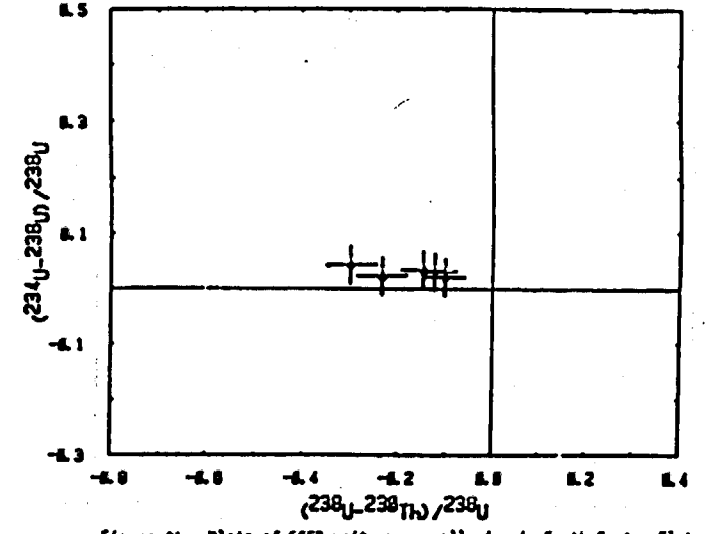


Figure 21. Plots of SCF3 unit, upper alluvium in South Crater Flat West Trench. This profile was not datable because of insufficient variation of $^{234}U/^{238}U$ ratios in 5 samples.



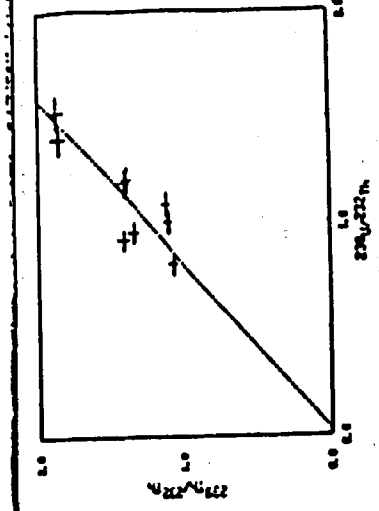

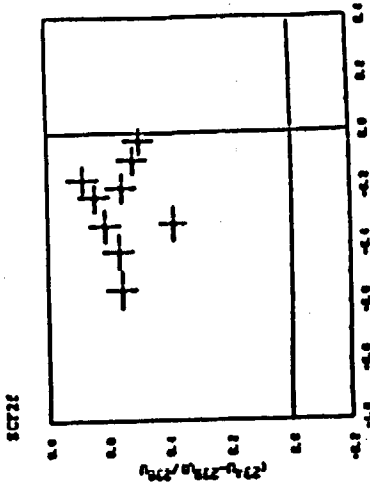


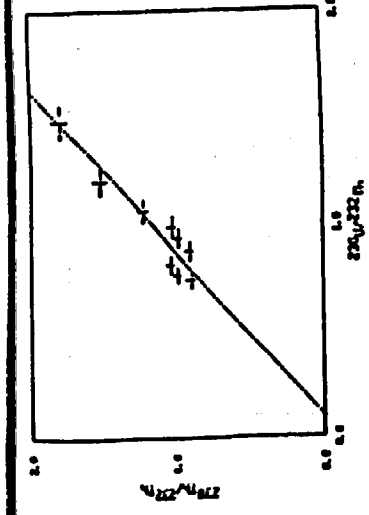

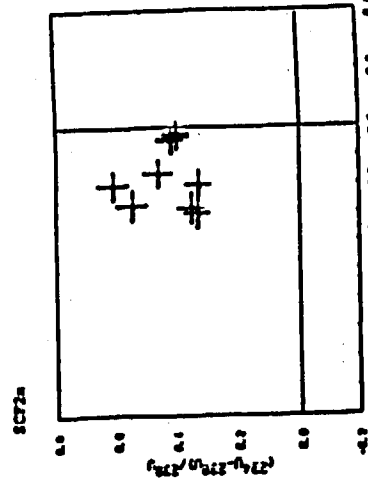


Figure 22. Plots of SCF2 unit, lower alluvium in South Crater Flat West Trench. SCF2m represents samples less than 2 mm size fraction, and SCF2f represents samples less than 0.3 mm size fraction; neither fraction was datable by U-trend.

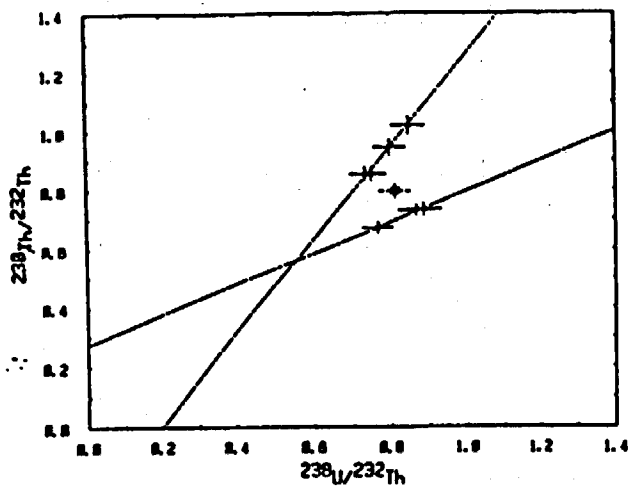


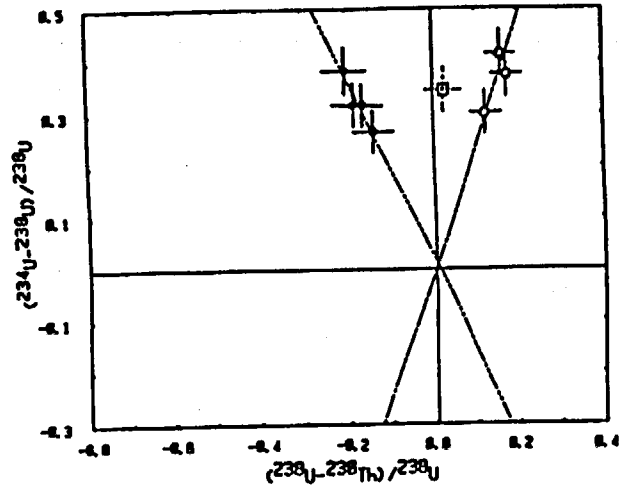


Figure 23. Plots of SCF4 section, lower alluvium in South Crater Flat West Trench. Sample SCF4-5, □, is a mixture of the upper facies, ●, and lower facies, ○, in the unit.

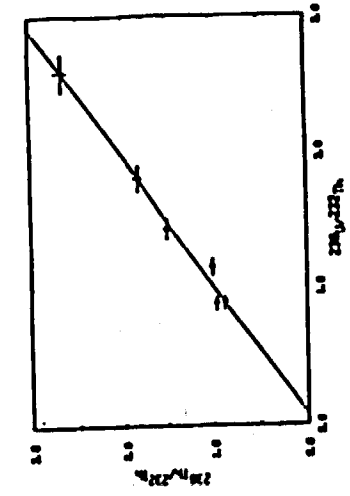

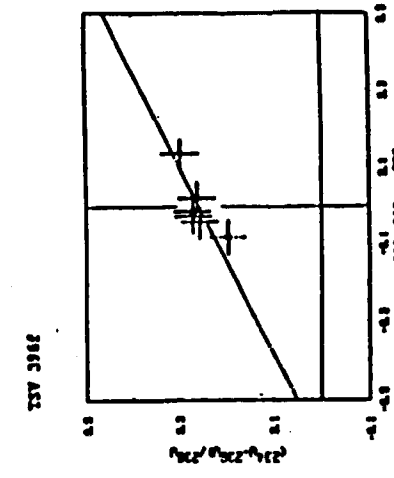


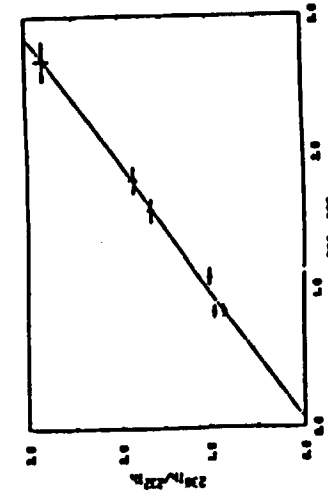

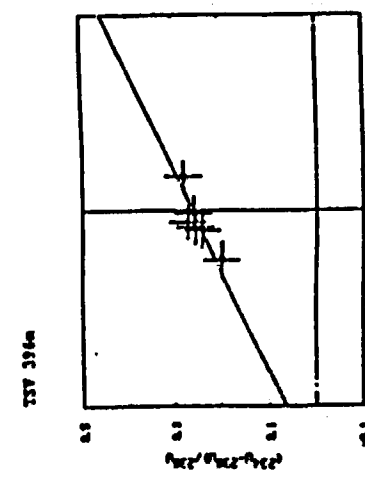


Figure 24. Plots of TSY 396 unit, carbonate-enriched zone in Crater Flat Trench 1. TSY 396a represents samples less than 2 mm size fraction, and TSY 396f represents samples less than 0.3 mm size fraction.

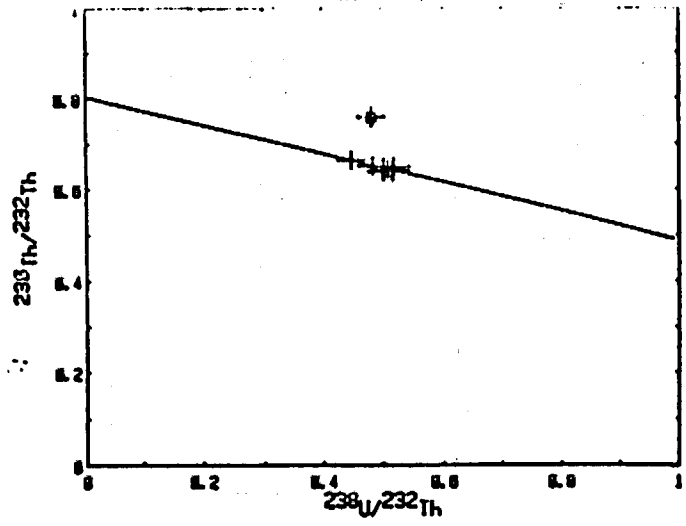


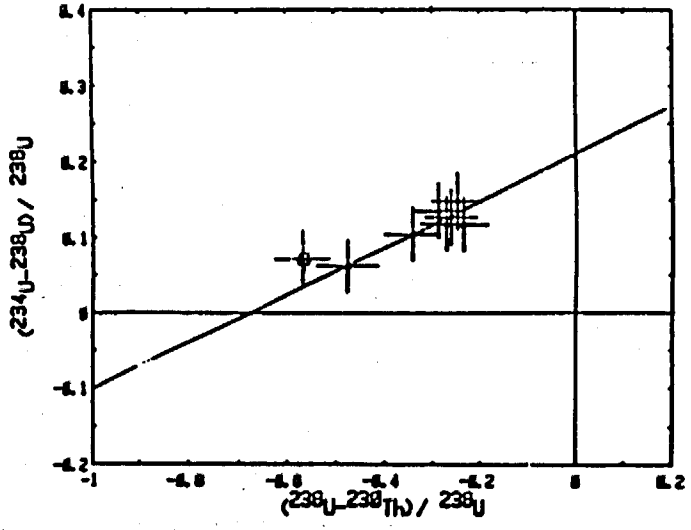


Figure 25. Plots of CF1 unit, upper alluvium in Crater Flat Trench 3. Sample CF1-2, □, is not included in U-trend slope because it does not fit on slope of the thorium plot.

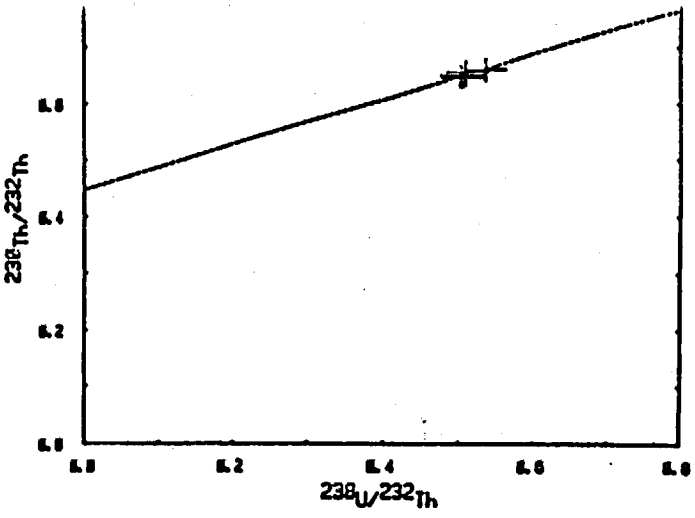


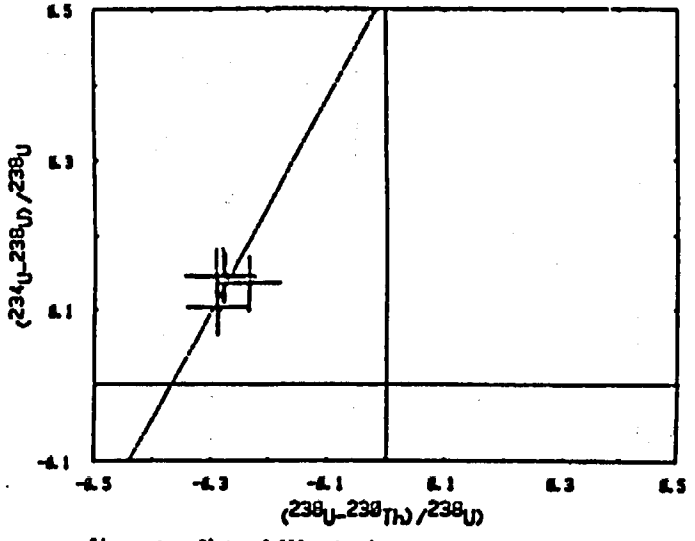


Figure 26. Plots of CF6 unit, lower B horizon exposed in Crater Flat Trench 3.

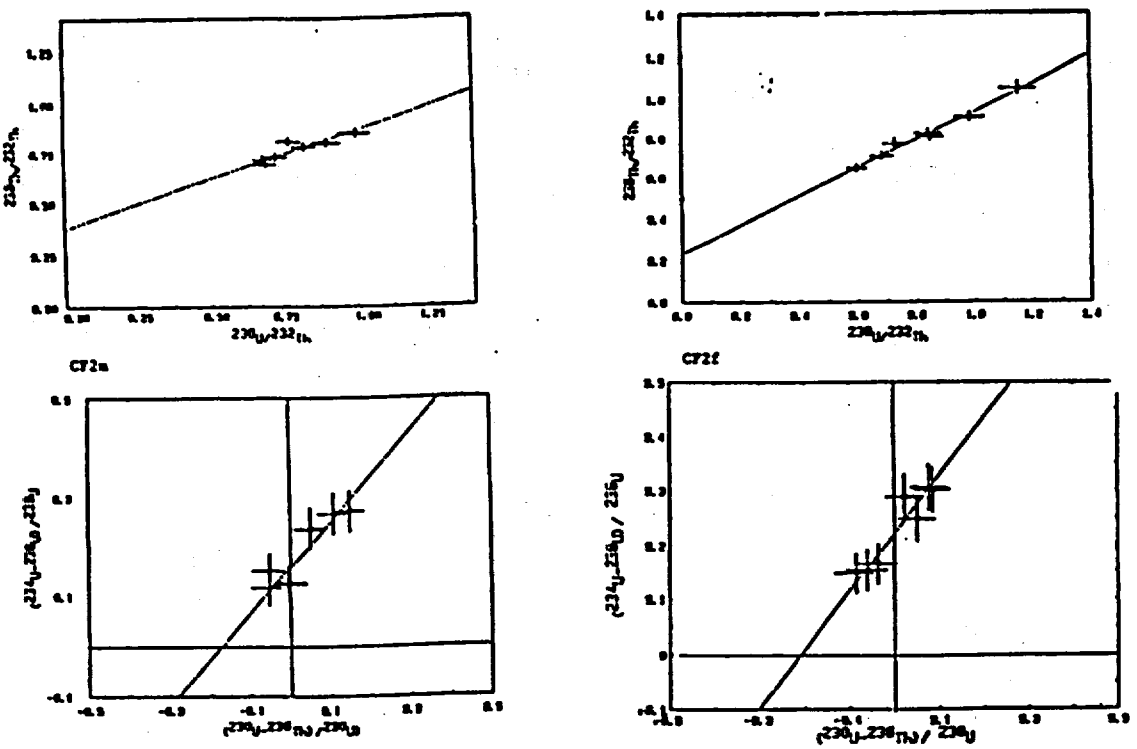


Figure 27. Plots of CF2 unit, lower alluvium in Crater Flat Trench 3. CF2m represents samples less than 2 mm size fraction and CF2f represents samples less than 0.3 mm size fraction.

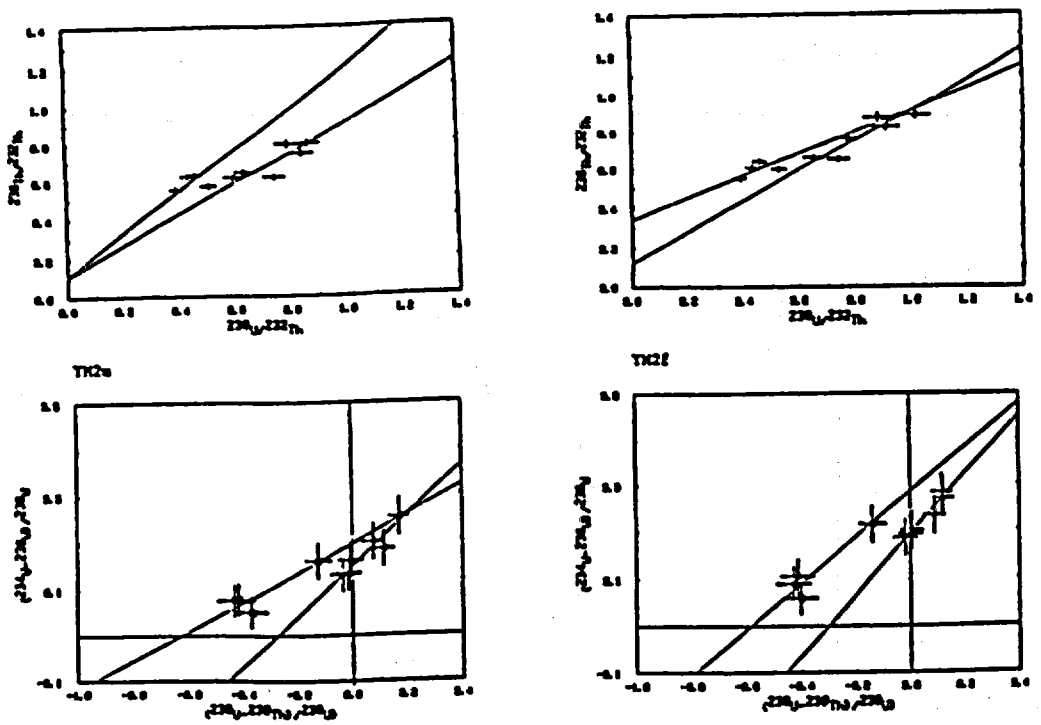


Figure 28. Plots of TM2 section, upper alluvium, □, and lower alluvium, ●, in Yucca Mountain Trench 2. TM2m represents samples less than 2 mm size fraction and TM2f represents samples less than 0.3 mm size fraction.

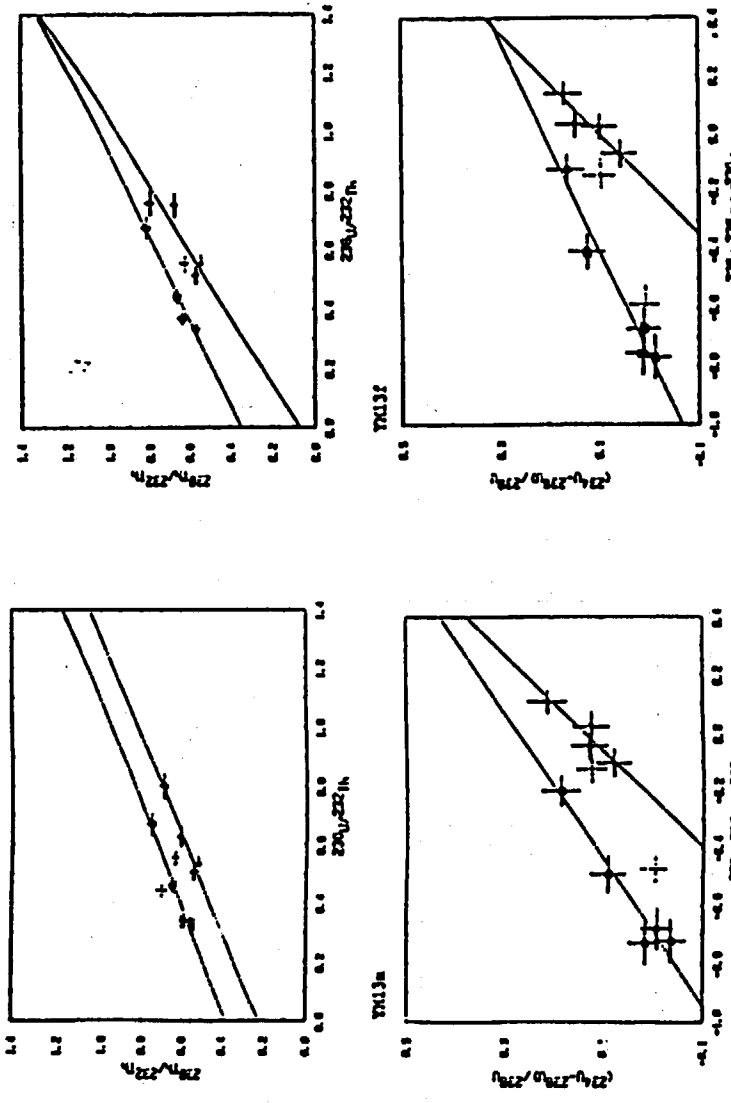


Figure 29. Plots of TN13 section, upper alluvium, □, and lower alluvium, ●, in Yucca Mountain Trench 13. Upper sample in each unit was not included in U-trend slope because of possible mixtures with material from overlying unit.

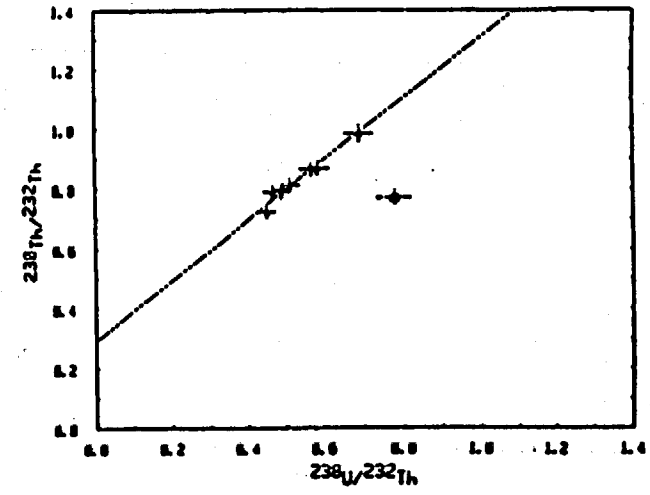


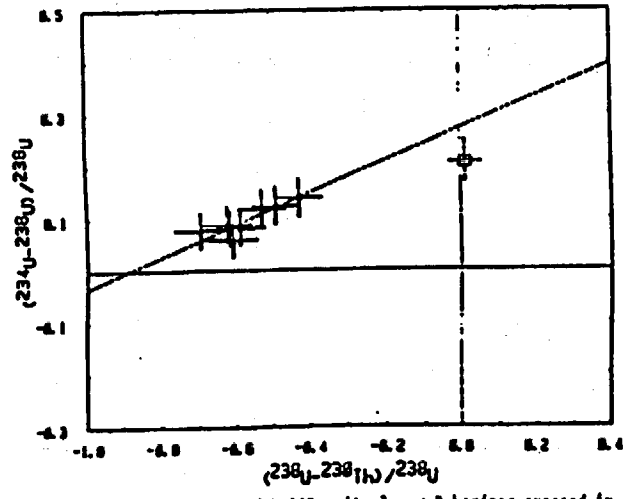


Figure 30. Plots of TN14B unit, lower B horizon exposed in Yucca Mountain Trench 14. Sample TN14B-2, □, is not included in U-trend slope because it does not fit on slope of thorium plot.

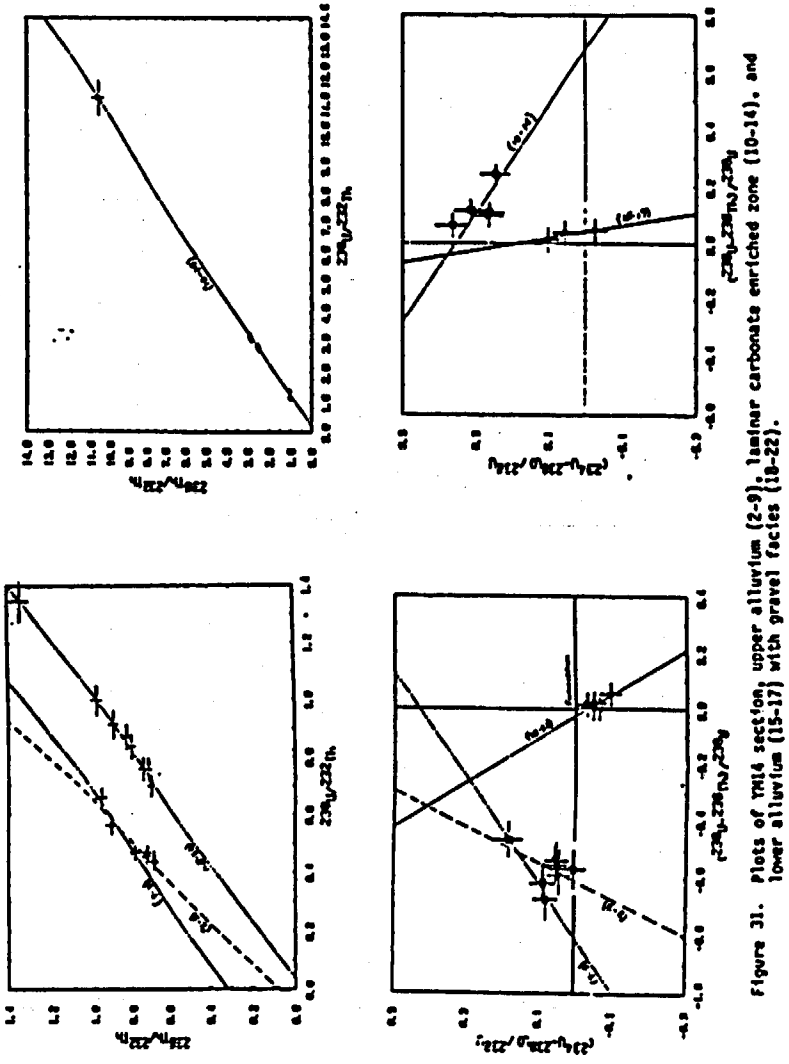

Figure 31. Plots of YM14 section, upper alluvium (2-9); laminar carbonate enriched zone (10-14), and lower alluvium (15-17) with gravel facies (18-22).



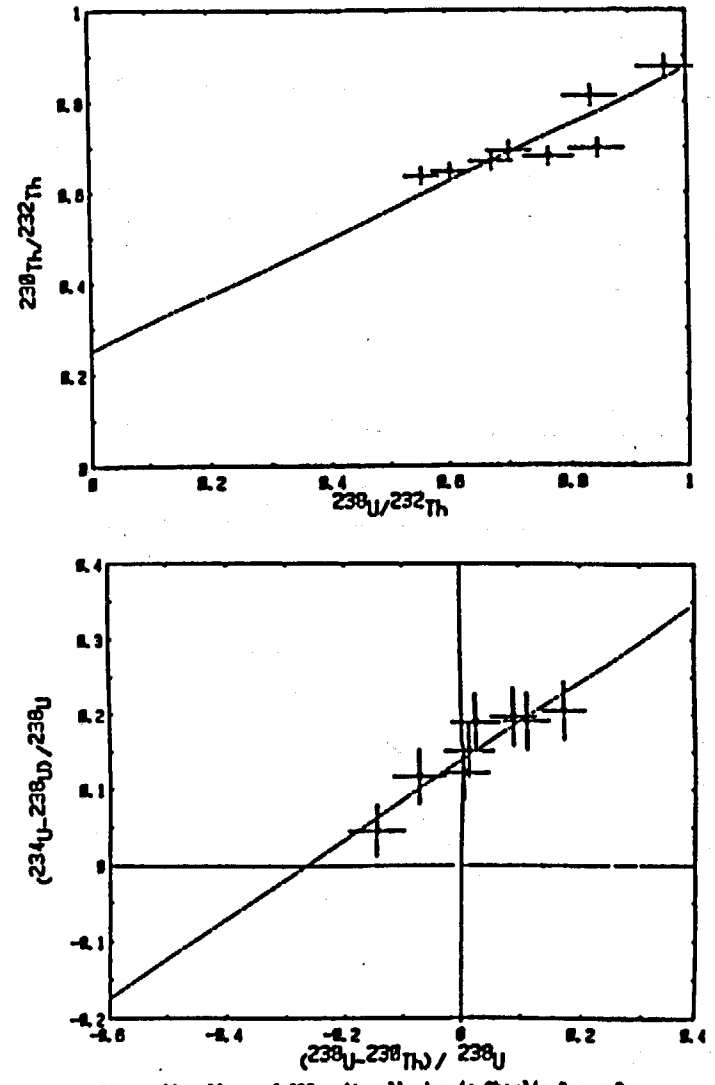


Figure 32. Plots of CBQ unit, alluvium in Charlie Brown Quarry, Shoshone, California.

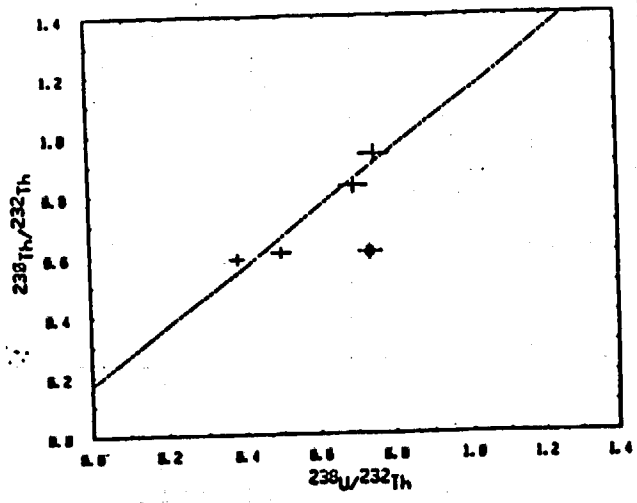


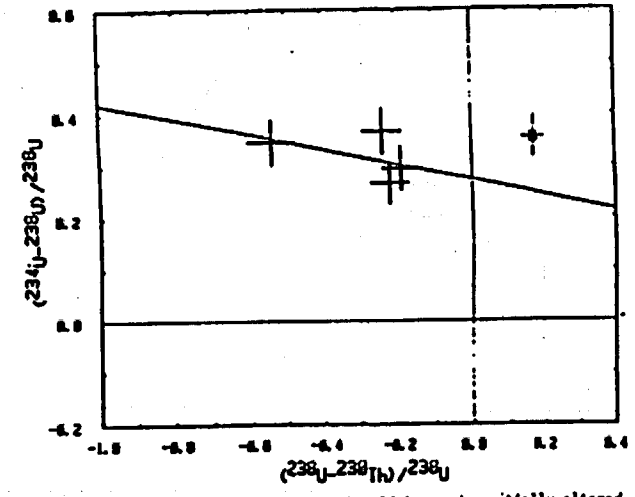


Figure 33. Plots of FHA unit, Bishop ash partially altered to clay exposed in gully at Fairbanks Hills, Nevada. Sample A-15C, □, is not included in U-trend slope because it does not fit on slope of the thorium plot.

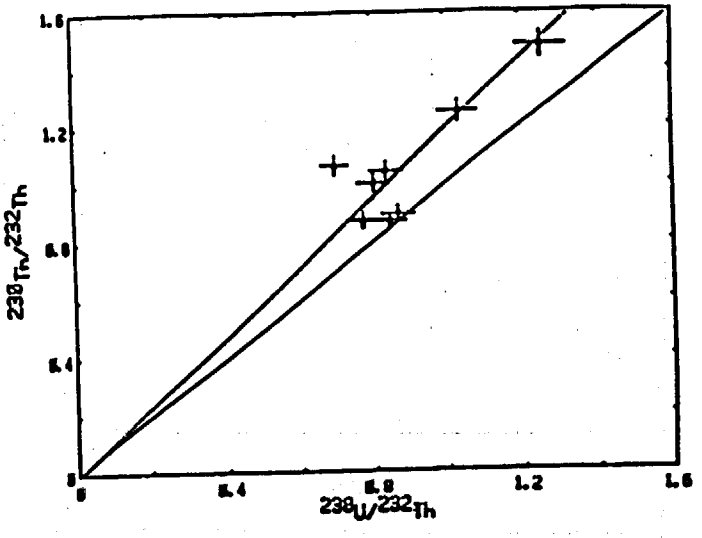


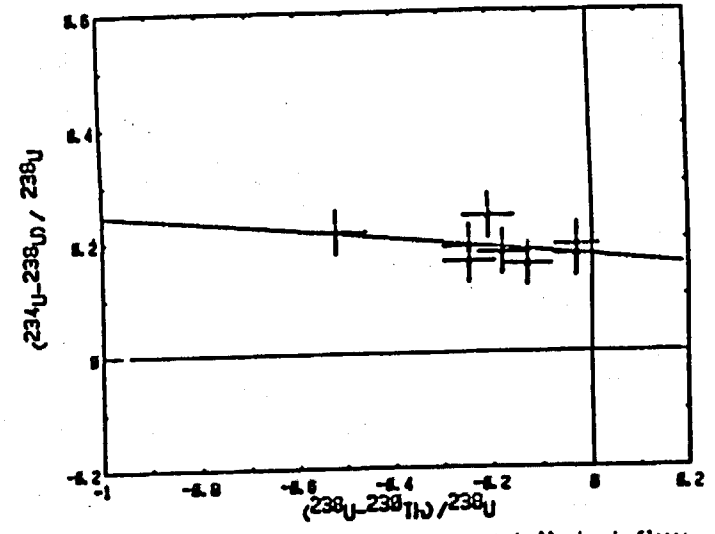


Figure 34. Plots of S3 unit, calcite-cemented alluvium in Eleana Pediment trench.

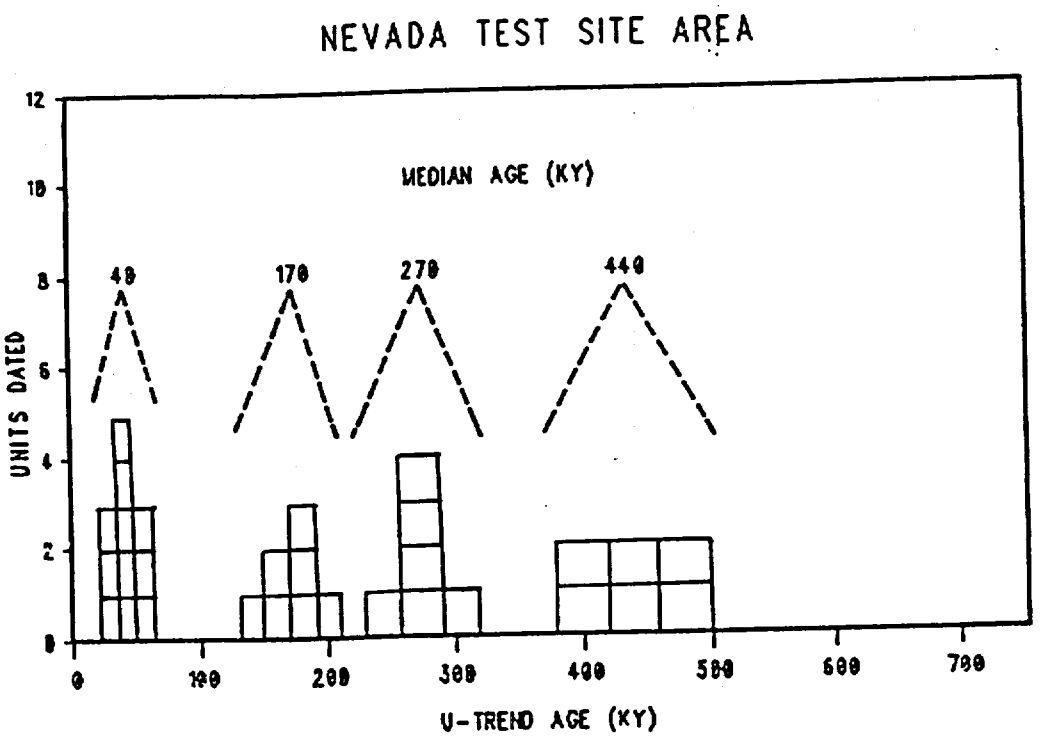


Figure 35. Histogram showing age groups of alluvial units analyzed from the Nevada Test Site area.

# Episodic caldera volcanism in the Miocene southwestern Nevada volcanic field: Revised stratigraphic framework, $^{40}Ar/^{39}Ar$ geochronology, and implications for magmatism and extension



DAVID A. SAWYER *U.S. Geological Survey, M.S. 913, Denver, Colorado 80225*
R. J. FLECK, M. A. LANPHERE *U.S. Geological Survey, M.S. 937, 345 Middlefield Road, Menlo Park, California 94025*
R. G. WARREN, D. E. BROXTON *EES-1, M.S. D462, Los Alamos National Laboratory, Los Alamos, New Mexico 87545*
MARK R. HUDSON *U.S. Geological Survey, M.S. 913, Denver, Colorado 80225*

## ABSTRACT

The middle Miocene southwestern Nevada volcanic field (SWNVF) is a classic example of a silicic multicaldera volcanic field in the Great Basin. More than six major calderas formed between >15 and 7.5 Ma. The central SWNVF caldera cluster consists of the overlapping Silent Canyon caldera complex, the Claim Canyon caldera, and the Timber Mountain caldera complex, active from 14 to 11.5 Ma and centered on topographic Timber Mountain. Locations of calderas older than the Claim Canyon caldera source of the Tiva Canyon Tuff are uncertain except where verified by drilling. Younger peralkaline calderas (Black Mountain and Stonewall Mountain) formed northwest of the central SWNVF caldera cluster. We summarize major revisions of the SWNVF stratigraphy that provide for correlation of lava flows and small-volume tuffs with the widespread outflow sheets of the SWNVF.

New laser fusion $^{40}Ar/^{39}Ar$ isotopic ages are used to refine and revise the timing of eruptive activity in the SWNVF. The use of high-sensitivity mass spectrometry allowed analysis of submilligram-sized samples with analytical uncertainties of ~0.3% (1σ), permitting resolution of age differences as small as 0.07 Ma. These results confirm the revised stratigraphic succession and document a pattern of episodic volcanism in the SWNVF. Major caldera episodes (Belted Range, Crater Flat, Paintbrush, Timber Mountain, and Thirsty Canyon Groups) erupted widespread ash-flow sheets within 100–300 k.y. time spans, and pre- and post-caldera lavas erupted within 100–300 k.y. of the associated ash flows. Peak volcanism in the SWNVF occurred during eruption of the Paintbrush and Timber Mountain Groups, when over 4500 km$^3$ of metaluminous magma was erupted in two episodes within 1.35 m.y., separated by a 750 k.y. magmatic gap. Peralkaline and metaluminous magmatism in the SWNVF overlapped in time and space. The peralkaline Tub Spring and Grouse Canyon Tuffs erupted early, and the peralkaline Thirsty Canyon Group tuffs and Stonewall Flat Tuff erupted late in the history of the SWNVF, flanking the central, volumetrically dominant peak of metaluminous volcanism. Magma chemistry transitional between peralkaline and metaluminous magmas is indicated by petrographic and chemical data, particularly in the overlapping Grouse Canyon and Area 20 calderas of the Silent Canyon caldera complex.

Volcanism in the SWNVF coincided with the Miocene peak of extensional deformation in adjoining parts of the Great Basin. Although regional extension was concurrent with volcanism, it was at a minimum in the central area of the SWNVF, where synvolcanic faulting was dominated by intracaldera deformation. Significant stratal tilting and paleomagnetically determined dextral shear affected the southwestern margin of the SWNVF between the Paintbrush and Timber Mountain caldera episodes. Larger magnitude detachment faulting in the Bullfrog Hills, southwest of the central SWNVF caldera cluster, followed the climactic Timber Mountain caldera episode. Postvolcanic normal faulting was substantial to the north, east, and south of the central SWNVF caldera cluster, but the central area of peak volcanic activity remained relatively unextended in postvolcanic time. Volcanism and extension in the SWNVF area were broadly concurrent, but in detail they were episodic in time and not coincident in space.

## INTRODUCTION

The southwestern Nevada volcanic field (SWNVF) is an outstanding example of a multicaldera silicic volcanic field. The SWNVF has been the focus of intensive scientific study over the past 35 yr, largely as a result of underground nuclear testing at the Nevada Test Site (NTS) and nuclear-waste repository studies at Yucca Mountain. It is well exposed due to Basin and Range faulting and dissection in an arid environment, and it is well known geometrically due to hundreds of deep drill holes (>600 m depth). The history of geologic investigations of the volcanic field was recently summarized by Byers and others (1989). Geochronology of the volcanic rocks of the field was first determined by K-Ar methods (Kistler, 1968). We report initial results of a new generation of isotopic ages determined by the laser-fusion $^{40}Ar/^{39}Ar$ method (Dalrymple and Duffield, 1988) for the principal SWNVF stratigraphic units, and we use these results to confirm significant revisions in the stratigraphic framework of the SWNVF and precisely define episodes of major eruptive activity. Source calderas for the major ash-flow sheets are described for calderas that are well known on the basis of outcrop or drill-hole data. Finally, we summarize the implications of the high-precision ages for the magmatic evolution of the SWNVF, and the temporal and spatial distribution of extensional deformation relative to SWNVF magmatism.

Geological Society of America Bulletin, v. 106, p. 1304–1318, 6 figs., 3 tables, October 1994.

TABLE 1. SUMMARY OF MAJOR STRATIGRAPHIC UNITS OF THE SOUTHWESTERN NEVADA VOLCANIC FIELD

| Assemblage symbol | Current name | Age (Ma) | Estimated erupted magma volumes ($km^3$) | Old (previous usage) | Volcanic center |
|---|---|---|---|---|---|
| Ts | Stonewall Flat Tuff | | 125 | | Stonewall Mountain volcanic center |
| | Civet Cat Canyon Member | | 40 | | |
| | Spearhead Member | | 80 | | |
| Tt | Thirsty Canyon Group | | 300 | | |
| | Gold Flat Tuff | | 20 | Thirsty Canyon Tuff | Black Mountain caldera |
| | Trail Ridge Tuff | | 50 | Gold Flat Member | |
| | Pahute Mesa Tuff | | 100 | Trail Ridge Member | |
| | Rocket Wash Tuff | 9.4 | 100 | Pahute Mesa Member | |
| Tf | Fortymile Canyon assemblage | | 140 | Rocket Wash Member | |
| | Beatty Wash Formation* | | 110 | | Diverse vent areas |
| Tm | Timber Mountain Group | | 2275 | Rhyolite of Beatty Wash | |
| | Ammonia Tanks Tuff | 11.45 | 900 | Timber Mountain Tuff | Timber Mountain Caldera Complex |
| | Rainier Mesa Tuff | 11.6 | 1200 | Ammonia Tanks member | Ammonia Tanks caldera |
| Tp | Rhyolite of the Loop | 12.5 | 40 | Rainier Mesa Member | Rainier Mesa caldera |
| | Paintbrush Group | | 2270 | | |
| | Tiva Canyon Tuff | 12.7 | 1000 | Paintbrush Tuff | |
| | Yucca Mountain Tuff | | 25 | Tiva Canyon Member | Claim Canyon caldera |
| | Pah Canyon Tuff | | 35 | Yucca Mountain Member | Claim Canyon caldera? |
| | Topopah Spring Tuff | 12.8 | 1200 | Pah Canyon Member | Uncertain |
| Ta | Calico Hills Formation* | 12.9 | 160 | Topopah Spring Member | Uncertain |
| | | | | Tuffs and lavas of Calico Hills, Area 20 | |
| Tw | Wahmonie Formation | 13.0 | 90 | | Wahmonie volcano |
| Tc | Crater Flat Group | | 880 | Crater Flat Tuff | Silent Canyon caldera complex |
| | Prow Pass Tuff | | 45 | Prow Pass Member | |
| | Bullfrog Tuff | 13.25 | 650 | Bullfrog Member (and Stockade (Wash Tuff)) | Uncertain |
| | Tram Tuff | | 170 | Tram Member | Area 20 caldera† |
| Tb | Belted Range Group | | 350 | Belted Range Tuff | Prospector Pass caldera complex? |
| | Dead Horse Flat Fm.* | 13.5 | 120 | Tuff and lava of Dead Horse Flat/volcanics of Saucer Mesa | |
| | Grouse Canyon Tuff | 13.7 | | Grouse Canyon Member | |
| | bedded member | | 210 | Tunnel bed 5 | Grouse Canyon caldera† |
| | Comendite of Split Ridge | 13.85 | | Rhyolite of Split Ridge | |
| | | | 20 | | |
| Tr | Lithic Ridge Tuff | 14.0 | 250 | | Uncertain |
| | Lava of Tram Ridge | 14.0 | 60 | Quartz latite lava and unit C tuff | |
| Tn | Tunnel Formation* | | 50 | Tunnel beds 3 and 4 | |
| Tu | Tub Spring Tuff | 14.9 | 130 | Tub Spring Member | Uncertain |
| To | Tuff of Yucca Flat | 15.1 | 50 | | Uncertain |
| | Redrock Valley Tuff | 15.25 | 360 | | Uncertain |

*Note:* No entry in "Old" column indicates that current usage is unchanged.
*Newly defined with formal stratigraphic name.
†The Area 20 and Grouse Canyon calderas only compose the Silent Canyon caldera complex.

## REVISED SWNVF STRATIGRAPHIC FRAMEWORK

Many units of the SWNVF were systematically described by Byers and others (1976a), who discussed in detail only the volcanic rocks they interpreted to be related to the Timber Mountain–Oasis Valley caldera complex. Older metaluminous stratigraphic units were described in Carr and others (1986), but no comprehensive stratigraphic discussion of the older and younger peralkaline units of the SWNVF and their relation to the metaluminous units has been published. The revised stratigraphy of the SWNVF summarized in Table 1 is based on our new petrologic and geochronologic studies.

The stratigraphic changes (Table 1), first, raise formally defined formations of previous usage (Belted Range, Crater Flat, Paintbrush, Timber Mountain, and Thirsty Canyon) to group rank. Petrographically, geochemically, and temporally related lava flows and nonwelded tuffs are associated with their regional welded ash-flow tuff sheets. Second, these well-defined, regionally correlative ash-flow sheets (members of the former formations) are raised to formation rank and given the rank term *Tuff*. Formation rank units are the Tub Spring (now separated from the Belted Range Group), Grouse Canyon, Tram, Bullfrog, Prow Pass, Topopah Spring, Pah Canyon, Yucca Mountain, Tiva Canyon, Rainier Mesa, Ammonia Tanks, Rocket Wash, Pahute Mesa, Trail Ridge, and Gold Flat Tuffs. Civet Cat Canyon and Spearhead Members of the Stonewall Flat Tuff, Wahmonie Formation, Lithic Ridge Tuff, tuff of Yucca Flat, and Redrock Valley Tuff retain the same rank as assigned in the earlier literature (Byers and others, 1976a; Noble and others, 1984; Carr and others, 1986). Newly defined formal stratigraphic units are the Beatty Wash Formation, Calico Hills Formation, Dead Horse Flat Formation, and Tunnel Formation. The stratigraphic units of the SWNVF are described next in older to younger sequence and related to their respective volcanic centers (Table 1).

Major ash-flow sheets of the SWNVF erupted predominantly from calderas (Table 1); lava flows and minor pyroclastic deposits erupted from numerous smaller vents. General consensus exists about the location and approximate geometry of the Silent Canyon caldera complex, the Claim Canyon caldera, the Timber Mountain caldera complex, and the Black Mountain caldera (Fig. 1). Sources for units older than the Tiva Canyon Tuff are completely buried and are documented only where revealed by extensive drilling, as for the Silent Canyon caldera complex in the subsurface of Pahute Mesa (Orkild and others, 1969; Ferguson and others, 1994). Caldera sources for Topopah Spring, Tram, Lithic Ridge, Tub Spring, and Redrock Valley Tuffs remain poorly known, though various source areas have been postulated (Byers and others, 1976a;

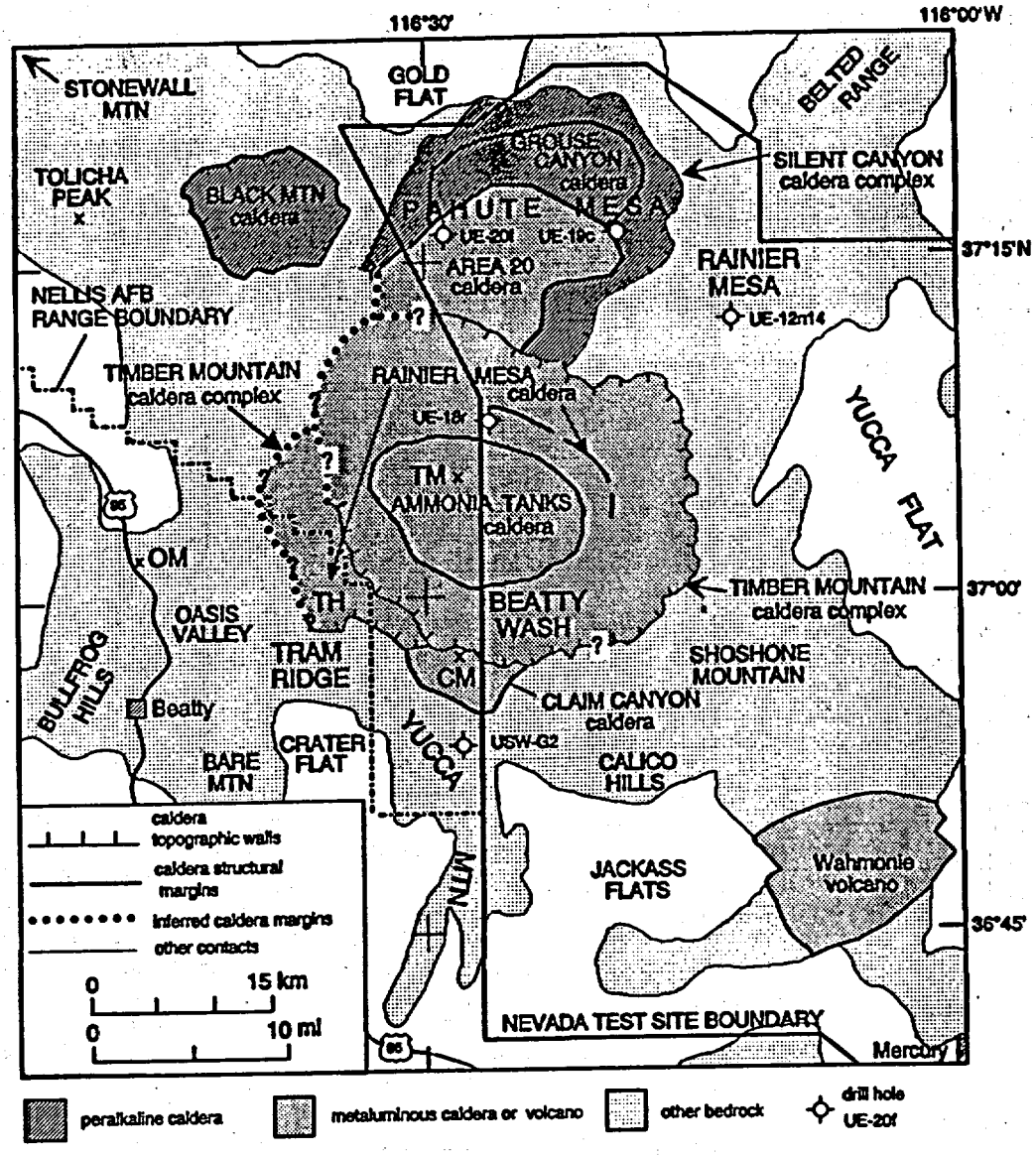


**Figure 1. Location of calderas of the southwestern Nevada volcanic field (SWNVF) and index map to geographic features. Known calderas of the SWNVF are the Timber Mountain–Claim Canyon–Silent Canyon caldera complexes and the Black Mountain caldera. The Timber Mountain caldera complex was the source of the Rainier Mesa Tuff and the Ammonia Tanks Tuff. The Tiva Canyon Tuff was erupted from the Claim Canyon caldera. The Silent Canyon caldera complex consists of an earlier Grouse Canyon caldera and a younger Area 20 caldera, source of the Bullfrog Tuff. The Trail Ridge Tuff was probably erupted during the final collapse of the Black Mountain caldera, but the caldera may have largely formed in response to the eruption of the Pahute Mesa Tuff. Geographic localities mentioned in the text are abbreviated as follows: CM, Chocolate Mountain; OM, Oasis Mountain; TH, Transvaal Hills; TM, Timber Mountain.**

Christiansen and others, 1977; Carr and others, 1986).

The oldest well-characterized metaluminous ash-flow sheets in the SWNVF are the Redrock Valley Tuff and the tuff of Yucca Flat (Byers and others, 1976a; Carr and others, 1986). The oldest peralkaline units in the SWNVF include the Tub Spring Tuff, previously the Tub Spring Member of the Belted Range Tuff (Sargent and others, 1964). We remove this unit from the Belted Range Group because it is 1.2 m.y. older than the Grouse Canyon Tuff and because as much as 200 m of predominantly metaluminous bedded and nonwelded tuffs of the Tunnel Formation separate the Tub Spring and the Grouse Canyon Tuffs at Rainier Mesa. Petrologic and geochemical criteria indicate that the Grouse Canyon and Tub Spring peralkaline ash-flow sheets are not comagmatic (Sawyer and Sargent, 1989). The source of the Tub Spring Tuff is unknown, and intracaldera Tub Spring has not been penetrated in Pahute Mesa, although a few drill holes penetrate the stratigraphic level of the Tub Spring.

The Tunnel Formation, as defined here, is divided into two informal subunits, beds 3 and 4, that are widely used in the Rainier Mesa area and are equivalent to tunnel beds 3 and 4 of the Oak Spring and Indian Trail Formations as used by Gibbons and others (1963) and Hansen and others (1963). The name is derived from the extensive series of tunnels used for underground nuclear testing on the east side of Rainier Mesa. The formation base overlies the top of the Tub Spring Tuff, and the top underlies the base of the bedded member of the Grouse Canyon Tuff on the east side of Rainier Mesa (bed 5 of Gibbons and others, 1963). The Tunnel Formation consists of a diverse sequence of bedded and nonwelded tuffs, predominantly rhyolitic in composition. Drill hole UE-12n14 (Fig. 1), from a depth of 351–508 m, is a reference section for the Tunnel Formation; the type section extends about 1500 m east-northeast from UE-12n14, across the east face of Rainier Mesa. Tephras in the upper part of the Tunnel Formation at Rainier Mesa probably correlate with rhyolitic to dacitic eruptive and intrusive units described below as lava of Tram Ridge. Lithic Ridge Tuff (Carr and

others, 1986) stratigraphically overlies the Tunnel Formation in the Shoshone Mountain area (Fig. 1). The lava of Tram Ridge is a sequence of lava flows and related tuff and intrusive rocks that is present beneath Lithic Ridge Tuff at Tram Ridge (Fig. 1) and as dikes around Crater Flat (quartz latite of Carr and others, 1986). The lava and tuffs correlate with the biotite-hornblende rhyolite west of Split Ridge (Byers and others, 1976b) and unit C tuff in the subsurface of Yucca Mountain (Warren and others, 1984).

The Silent Canyon caldera complex includes the oldest calderas in the SWNVF that are confidently identified. It is completely buried by younger deposits but coincides with a major gravity low (Healey, 1968; Kane and others, 1981; Healey and others, 1987). Existence of this geophysically defined caldera complex has been verified by more than 70 deep (>600 m depth) drill holes in Pahute Mesa (Ferguson and others, 1994). The composite topographic wall of the Silent Canyon caldera complex is expressed at the surface by inward dips of younger Timber Mountain tuffs that were plastered on the walls of the older caldera complex (Orkild and others, 1969; Byers and others, 1976b). The Silent Canyon caldera complex formed by two separate caldera collapses (Sawyer and Sargent, 1989): an initial collapse of the northeastern caldera of the complex related to eruption of the Grouse Canyon Tuff, and a younger collapse of the Area 20 caldera caused by eruption of the Bullfrog Tuff (Fig. 1).

The Grouse Canyon caldera was the source of the peralkaline Grouse Canyon Tuff. Comendite of Split Ridge, previously called the *rhyolite of Split Ridge* (Orkild and others, 1969; Sawyer and Sargent, 1989), is a petrologically related precursor lava to the Grouse Canyon Tuff. The bedded peralkaline tuff beneath the welded part of the Grouse Canyon Tuff is the bedded member of the Grouse Canyon Tuff, replacing *tunnel bed 5* of previous usage (Table 1). Following Grouse Canyon eruption, the northeast Silent Canyon caldera complex was filled and overflowed by postcollapse lava flows. This sequence of peralkaline lava flows and related tuffs, previously termed the *lava and tuff of Dead Horse Flat* (Orkild and others, 1969), are now assigned a formal stratigraphic rank as the Dead Horse Flat Formation, named for an open meadow in the Dead Horse Flat topographic quadrangle. The type section is drill hole UE-19c (depth 725–2249 m, Ferguson and others, in press) in Pahute Mesa (Fig. 1), where the formation overlies the Grouse Canyon Tuff and underlies the Bullfrog Tuff. The Dead Horse Flat Formation includes the extracaldera lavas exposed north of Pahute Mesa that overlie the Grouse Canyon Tuff that were termed *volcanics of Saucer Mesa* by Sawyer and Sargent (1989).

The Bullfrog Tuff is the ash-flow sheet associated with the younger Area 20 caldera (Fig. 1) of the Silent Canyon caldera complex (Sawyer and Sargent, 1989); the intracaldera facies was termed the *lithic-rich ash-flow tuff* by Orkild and others (1969) and is interleaved with thick megabreccia lenses. The intracaldera Bullfrog is more than 600 m thick in three drill holes, including UE-20f (1859–2522 m depth; Ferguson and others, 1994). Boundaries of the Area 20 caldera (Minor and others, 1993) are fixed by drill holes east and north of drill hole UE-20f, but evidence for the caldera south and west of UE-20f and UE-18r (Fig. 1) is concealed by younger units and not delineated by drilling southwest of the NTS boundary. Gravity data (Kane and others, 1981) suggest that the Area 20 caldera extends south under the Timber Mountain caldera complex. The distribution of thick Calico Hills lavas and tephras south of Timber Mountain and at Yucca Mountain is evidence of petrochemically related post–Area 20 caldera volcanism and supports the interpretation of Area 20 caldera collapse extending at least partly beneath Timber Mountain (Warren, 1983). The Stockade Wash Tuff (Byers and others, 1976a) is petrographically similar to both the outflow facies of the Bullfrog Tuff at Yucca Mountain and the intracaldera Bullfrog Tuff on Pahute Mesa. The Stockade Wash Tuff and the Bullfrog Tuff at Yucca Mountain may be separate outflow lobes of a composite ash-flow sheet that represent slightly different parts of the compositional zonation in a single magma chamber. The paleomagnetic signatures of these two geographically discrete ash-flow tuffs are identical and distinct from a typical Miocene direction (Hudson and others, 1994), consistent with eruption at the same time. For these reasons, we correlate the Stockade Wash Tuff with the Bullfrog Tuff, an important unit in the Yucca Mountain area (Warren, 1983; Broxton and others, 1989; Scott, 1990). A caldera source for the Bullfrog Tuff in Crater Flat (Carr and others, 1986) has been contested (Scott, 1990) and is inconsistent with evidence for an Area 20 caldera source.

Caldera sources for other units of the Crater Flat Group are less well known. The northern half of the proposed Prospector Pass caldera complex (near Tram Ridge, Fig. 1) is reasonably supported by field and geophysical evidence (Snyder and Carr, 1984) and may have been the source of the Tram Tuff (Carr and others, 1986). The Prow Pass Tuff does not have an identified source, and it may be small enough (Carr and others, 1986) not to have erupted from a caldera.

The Wahmonie Formation (Poole and others, 1965) is a sequence of andesite and dacite lava flows and related volcaniclastic sedimentary rocks and tephras that erupted from the Wahmonie volcano (Fig. 1) southeast of the Timber Mountain caldera complex (Frizzell and Shulters, 1990; Broxton and others, 1989). Biotite-rich mafic tephras that erupted from the Wahmonie volcano form a widespread, distinctive marker between Crater Flat Group tuffs and Calico Hills Formation tuff. This marker is common in Yucca Flat and Rainier Mesa, is exposed west of Yucca Flat and east of Yucca Mountain (Broxton and others, 1993), but is absent to the northwest in Pahute Mesa (Ferguson and others, 1994).

The Calico Hills Formation combines the tuffs and lavas of Calico Hills (significant at Yucca Mountain) with the tuffs and lavas of Area 20 (significant at Pahute Mesa). These two sequences are stratigraphically and petrologically equivalent (Warren, 1983) and resulted from Crater Flat Group post-caldera volcanism. Throughout the SWNVF they lie stratigraphically between the Wahmonie Formation (or the Crater Flat Group where Wahmonie is absent) and the Paintbrush Group. The type locality for the Calico Hills Formation is the northwestern Calico Hills (Orkild and O'Connor, 1970); reference sections are drill holes USW G-2, at 518–824 m depth at Yucca Mountain (Warren and others, 1984), and UE-20f, at 899–1324 m depth at Pahute Mesa (Ferguson and others, 1994). The Calico Hills Formation consists of rhyolite lava flows, domes, and nonwelded ash-flow and bedded tuffs. It has a maximum thickness of 1306 m and commonly is >600 m thick in western Pahute Mesa drill holes (Fig. 6, Ferguson and others, 1994); in the Yucca Mountain area it is 50–300 m thick (Warren, 1983; Warren and others, 1984; Broxton and others, 1993).

Paintbrush Group tuffs and lavas are one of the most widespread and voluminous caldera-related assemblages in the SWNVF.

Topopah Spring Tuff directly overlies bedded rhyolite tuffs of the Calico Hills Formation at Yucca Mountain and at most localities south of Timber Mountain. A caldera source for the Topopah Spring Tuff is buried and its location uncertain. The Pah Canyon Tuff may have been too small (Byers and others, 1976a) to have formed a caldera; no separate source has been identified. The younger of the widespread Paintbrush Group ash-flow sheets, the Tiva Canyon Tuff, was erupted from the Claim Canyon caldera (Byers and others, 1976a). The Claim Canyon caldera (Fig. 1) is bounded by precaldera rhyolite tuffs and lavas of the Calico Hills Formation to the southeast, and by precaldera tuffs and lavas of the Crater Flat Group to the southwest. Only part of the caldera is exposed because much of the caldera collapsed into the younger Timber Mountain caldera complex to the north (Byers and others, 1976a). The boundary illustrated is approximately the structural boundary of the resurgent intracaldera block; the topographic wall is not exposed (Christiansen and Lipman, 1965). The presence of thick intracaldera Tiva Canyon Tuff, a reversely magnetized unit, is corroborated by a negative aeromagnetic anomaly centered on Chocolate Mountain (Fig. 1); a local gravity high is consistent with the exposed Claim Canyon caldera being a fragment of the resurgent dome (Kane and others, 1981). The Yucca Mountain Tuff, directly beneath the Tiva Canyon, is an early small-volume eruption of the uppermost high-silica rhyolite part of the Tiva Canyon magma chamber (Broxton and others, 1989), probably from the same area of the Claim Canyon caldera.

Climactic ash flows of the Timber Mountain Group were erupted from the Timber Mountain caldera complex. The complex consists of two overlapping, resurgent calderas: an older caldera formed by eruption of the Rainier Mesa Tuff, and a younger, nested caldera formed by eruption of the Ammonia Tanks Tuff (Minor and others, 1993). Intracaldera Rainier Mesa Tuff and caldera-collapse breccias are exposed in the Transvaal Hills, west of Timber Mountain (Byers and others, 1976a, 1976b). These exposures and their inferred subsurface extensions coincide with aeromagnetic lows (Kane and others, 1981), consistent with the reversed remanent magnetic polarity of the Rainier Mesa Tuff (Bath, 1968). We interpret the Transvaal Hills as the western part of a larger resurgent dome formed within the Rainier Mesa caldera. The dome was later truncated and down-dropped on the east by formation of the Ammonia Tanks caldera. The Rainier Mesa caldera structural boundary is buried but can be delimited by geophysical and drill-hole data (UE-18r); the margin (Fig. 1) approximately coincides with the inferred buried cauldron boundary on the Timber Mountain caldera geologic map (Byers and others, 1976b; Minor and others, 1993).

Intracaldera Ammonia Tanks Tuff forms topographic Timber Mountain and was originally identified as the dome of the Timber Mountain caldera (Byers and others, 1976a); it is, more specifically, the resurgent dome of the Ammonia Tanks caldera (Minor and others, 1993). The structural margin or ring-fault zone of the Ammonia Tanks caldera (Fig. 1) is exposed on the east margin of Timber Mountain. The margin was depicted as a tuff dike zone on the Timber Mountain caldera geologic map (Byers and others, 1976b); its continuity as a ring-fault zone around the Ammonia Tanks resurgent dome is clearly demonstrated by subregional gravity and aeromagnetic anomalies (Kane and others, 1981).

Previous studies (Byers and others, 1976a, 1976b, 1989) depicted only the geometry of an "approximate outer cauldron boundary" and a "partial buried inner cauldron fault" for the Timber Mountain caldera complex. As has been documented for calderas in the San Juan volcanic field and many other localities (Lipman, 1984), calderas have a collapse boundary or topographic wall outside of the ring-fault or structural margin. The composite topographic wall of the Timber Mountain caldera complex (Minor and others, 1993) is exposed around 200° of the calderas (Fig. 1); it is covered by younger units on the northwest side of the complex (south and west of drill holes UE-18r and UE-20f and the NTS boundary; Byers and others, 1976b). The distinction between the Ammonia Tanks and Rainier Mesa topographic walls is uncertain along most of the length of this contact. The two collapse features can be clearly distinguished only east and south of the Transvaal Hills (Fig. 1), where the Ammonia Tanks topographic wall swings north to the east of the Transvaal Hills and the Rainier Mesa topographic wall trends west to the south of the Transvaal Hills (Minor and others, 1993) before being covered by younger gravels in Oasis Valley.

Geologic data previously cited as evidence for an Oasis Valley caldera segment (Byers and others, 1976a; Christiansen and others, 1977) are inadequate to confirm its existence (Noble and others, 1991); the gravel-filled basin in Oasis Valley cannot be unequivocally linked to caldera collapses from eruption of the Ammonia Tanks, Tiva Canyon, or Rainier Mesa Tuffs. A lap-out of Ammonia Tanks Tuff against precaldera rocks at Oasis Mountain (Byers and others, 1976b) is probably related to paleotopography generated by syn-volcanic tectonism in the Oasis Valley area (Minor and others, 1993). Proposed caldera walls on the west side and north of Oasis Mountain (Byers and others, 1976b; Noble and others, 1991) do not continue into the exposed Rainier Mesa and Ammonia Tanks topographic walls near Timber Mountain (Fig. 1) according to existing evidence. Aeromagnetic data (Kane and others, 1981; U.S. Geological Survey, 1979) indicate that the arcuate negative magnetic anomaly associated with reversely magnetized intracaldera Rainier Mesa Tuff does not extend west to Oasis Mountain. This anomaly is the basis for the inferred (though buried) western boundary of the Rainier Mesa caldera illustrated in Figure 1. Because no unit can uniquely be attributed to it, we recommend that the concept of an Oasis Valley caldera segment be abandoned and disassociated from the well-characterized Timber Mountain caldera complex formed by eruption of the Ammonia Tanks and Rainier Mesa Tuffs. New subsurface data will be required to unambiguously establish the origin of Oasis Valley.

The newly defined Beatty Wash Formation is part of an informal sequence of units, the Fortymile Canyon assemblage. Assignment of rhyolite lava flows and tuffs previously called the *rhyolite lavas of Fortymile Canyon* on the south side of the Timber Mountain caldera complex (Byers and others, 1976a, 1976b) has been uncertain because field relations to the major ash-flow sheets of the Timber Mountain and Paintbrush Groups are lacking. Most of these units can be correlated with the Timber Mountain and Paintbrush Groups based on detailed petrography and chemistry (Warren and others, 1988). We restrict the Fortymile Canyon assemblage to the sequence of rocks stratigraphically above the Ammonia Tanks Tuff and related lavas of the Timber Mountain Group, and beneath the peralkaline units of the Thirsty Canyon Group. This assemblage is a diverse sequence of rhyolite lava flows and domes, related tephra deposits, minor ash-flow deposits, and basaltic and other mafic lavas erupted from a variety of relatively small-volume

TABLE 2. REPRESENTATIVE $^{40}Ar/^{39}Ar$ ANALYSES

Calico Hills Formation lava/sanidine
Field sample number: RW19f2-m
Irradiation laboratory number LXXXVII:A22; $J$ = 0.003590

| Sample number | Percent $^{40}Ar^*$ | $^{36}Ar$-Ca | $^{40}Ar/^{39}Ar$ | $^{37}Ar/^{39}Ar$ | $^{36}Ar/^{39}Ar$ | $^{40}Ar/^{39}Ar$ Age (Ma) |
|---|---|---|---|---|---|---|
| 90Z0582 | 87.6 | 1.29 | 2.2829 | 0.05373 | 0.00097 | 12.90 ± 0.08 |
| 90Z0583 | 77.4 | 0.54 | 2.5735 | 0.04612 | 0.00197 | 12.85 ± 0.08 |
| 90Z0584 | 86.6 | 0.47 | 2.3218 | 0.02106 | 0.00105 | 12.98 ± 0.08 |
| 90Z0585 | 80.2 | 0.53 | 2.4910 | 0.03815 | 0.00167 | 12.90 ± 0.08 |
| 90Z0586 | 79.1 | 0.62 | 2.5171 | 0.04768 | 0.00178 | 12.86 ± 0.08 |
| 90Z0587 | 71.8 | 0.23 | 2.7693 | 0.02589 | 0.00265 | 12.83 ± 0.08 |
| | | | Weighted mean age and uncertainty (Ma) | | | |
| | | 12.89 ± 0.03 | | s.e.m: 0.02 | | MSWD: 0.458 |

Grouse Canyon Tuff/sanidine
Field sample number: DS18a1
Irradiation laboratory number XCIII:47; $J$ = 0.004055

| Sample number | Percent $^{40}Ar^*$ | $^{36}Ar$-Ca | $^{40}Ar/^{39}Ar$ | $^{37}Ar/^{39}Ar$ | $^{36}Ar/^{39}Ar$ | $^{40}Ar/^{39}Ar$ Age (Ma) |
|---|---|---|---|---|---|---|
| 91Z0410A | 90.3 | 1.60 | 2.0854 | 0.03953 | 0.00066 | 13.72 ± 0.09 |
| 91Z0410B | 88.4 | 1.67 | 2.1246 | 0.05067 | 0.00082 | 13.69 ± 0.10 |
| 91Z0410C | 89.4 | 1.69 | 2.1063 | 0.04626 | 0.00074 | 13.72 ± 0.10 |
| 91Z0410D | 90.3 | 1.94 | 2.0693 | 0.04759 | 0.00066 | 13.62 ± 0.12 |
| 91Z0410E | 79.5 | 0.71 | 2.3878 | 0.04309 | 0.00163 | 13.84 ± 0.14 |
| 91Z0410F | 88.9 | 1.45 | 2.1031 | 0.04140 | 0.00077 | 13.63 ± 0.11 |
| | | | Weighted mean age and uncertainty (Ma) | | | |
| | | 13.70 ± 0.04 | | s.e.m: 0.03 | | MSWD: 0.407 |

Irradiation laboratory number CII:A24; $J$ = 0.002975

| Sample number | Percent $^{40}Ar^*$ | $^{36}Ar$-Ca | $^{40}Ar/^{39}Ar$ | $^{37}Ar/^{39}Ar$ | $^{36}Ar/^{39}Ar$ | $^{40}Ar/^{39}Ar$ Age (Ma) |
|---|---|---|---|---|---|---|
| 91Z1035A | 98.5 | 9.31 | 2.6145 | 0.04548 | 0.00013 | 13.76 ± 0.08 |
| 91Z1035B | 97.9 | 6.56 | 2.6190 | 0.04482 | 0.00018 | 13.70 ± 0.09 |
| 91Z1035C | 97.9 | 3.07 | 2.6171 | 0.01977 | 0.00017 | 13.70 ± 0.09 |
| 91Z1035D | 87.4 | 1.36 | 2.9642 | 0.06386 | 0.00126 | 13.85 ± 0.09 |
| 91Z1035E | 97.5 | 6.79 | 2.6182 | 0.05635 | 0.00022 | 13.64 ± 0.10 |
| 91Z1035F | 99.2 | 14.93 | 2.5990 | 0.03647 | 0.00007 | 13.78 ± 0.09 |
| 91Z1035G | 95.3 | 3.24 | 2.6823 | 0.05112 | 0.00042 | 13.67 ± 0.09 |
| 91Z1035H | 96.3 | 1.95 | 2.6727 | 0.02349 | 0.00032 | 13.76 ± 0.09 |
| | | | Weighted mean age and uncertainty (Ma) | | | |
| | | 13.74 ± 0.03 | | s.e.m: 0.02 | | MSWD: 0.553 |
| | | | Pooled weighted mean age and uncertainty (Ma) | | | |
| | | 13.72 ± 0.03 | | | | MSWD: 0.498 |

*Note:* MSWD is the mean square of weighted deviates; s.e.m. is the standard error of the mean; and $J$ is the neutron flux parameter.

vent complexes. The Beatty Wash Formation is the most significant of these post–Timber Mountain units and consists of rhyolite lava domes and related pyroclastic deposits in the moat of the Ammonia Tanks caldera. The type area is upper Beatty Wash on the Topopah Spring NW quadrangle (Christiansen and Lipman, 1965); the formation also includes the related tuff of Cutoff Road to the west of the Timber Mountain caldera complex adjoining Oasis Valley (Byers and others, 1976b). The Fortymile Canyon assemblage also includes such widely dispersed units (Minor and others, 1993) as the rhyolite of Rainbow Mountain in the Beatty area (Maldonado and Hausback, 1990), the rhyolite of West Cat Canyon west of Timber Mountain, and the mafic lavas at Dome Mountain and the rhyolite lavas of Shoshone Mountain along the southeast margin of the Timber Mountain caldera complex (Byers and others, 1976b).

The Black Mountain caldera, just west of the Silent Canyon caldera complex (Fig. 1), produced the youngest widespread ash-flow sheets in the SWNVF area. Those sheets make up the several moderate-volume peralkaline ash-flow tuffs (Christiansen, 1979; Noble and others, 1984): the Rocket Wash, Pahute Mesa, Trail Ridge, and Gold Flat Tuffs (Table 1) of the Thirsty Canyon Group. Individual collapse boundaries have not been identified due to a lack of dissection of the caldera. The composite topographic wall of the Black Mountain caldera (Fig. 1) is mantled by Trail Ridge Tuff (Minor and others, 1993), indicating that collapse was syn– or pre–Trail Ridge in age. The Stonewall Mountain volcanic center (Noble and others, 1984; Minor and others, 1993) is >50 km northwest of the central SWNVF caldera cluster. Distal Stonewall tuff overlaps the Thirsty Canyon Group tuffs at Black Mountain.

## $^{40}Ar/^{39}Ar$ GEOCHRONOLOGY

Ages reported here were determined at the U.S. Geological Survey laboratories in Menlo Park, California. Two $^{40}Ar/^{39}Ar$ methods (described in the Appendix) were used: laser fusion determination of small sanidine samples and incremental heating determination of larger biotite samples. Twenty-six sanidine samples were analyzed by the laser fusion $^{40}Ar/^{39}Ar$ technique (Dalrymple and Duffield, 1988; Dalrymple, 1989). Analytical results for two representative samples are listed in Table 2: RW19f2, a Calico Hills Formation sanidine from a rhyolite lava north of Timber Mountain, and DS18a1, Grouse Canyon Tuff sanidine irradiated and analyzed twice. Two biotite samples (Wahmonie Formation lava and dacite lava of Tram Ridge, Fig. 2) were analyzed by the incremental heating $^{40}Ar/^{39}Ar$ technique (Dalrymple and Lanphere, 1971; Lanphere, 1988). These biotites yielded undisturbed age plateaus containing >90% of the total gas and have atmospheric argon intercepts on $^{36}Ar/^{40}Ar$-$^{39}Ar/^{40}Ar$ isochron diagrams.

We determined $^{40}Ar/^{39}Ar$ ages for the largest volume, most widespread units of the SWNVF (Table 3). All reported ages are rounded to ±50 ka because additional results for the same units and further refinements of the monitor ages may affect the final ages by as much as 10–50 k.y. due to cumulative J-curve calibration uncertainties and within-unit and within-sample age variations. Sample locations and detailed analytical data for samples other than those listed in Table 2 and Figure 2 are available from the first author upon request. Results for four samples of Topopah Spring Tuff, three samples each of Ammonia Tanks, Rainier Mesa, and Tiva Canyon Tuffs, and two samples of Bullfrog Tuff are reported as error-weighted pooled averages for the absolute age and uncertainty. All $^{40}Ar/^{39}Ar$ ages were measured relative to a monitor age of 513.9 Ma for MMhb-1 (Lanphere and others, 1990; Dalrymple and others, 1993). The $^{40}Ar/^{39}Ar$ results presented here agree well with $^{40}Ar/^{39}Ar$ determinations recently published for a few SWNVF units (Hausback and others, 1990; Noble and others, 1991), when recalculated to the same monitor ages.

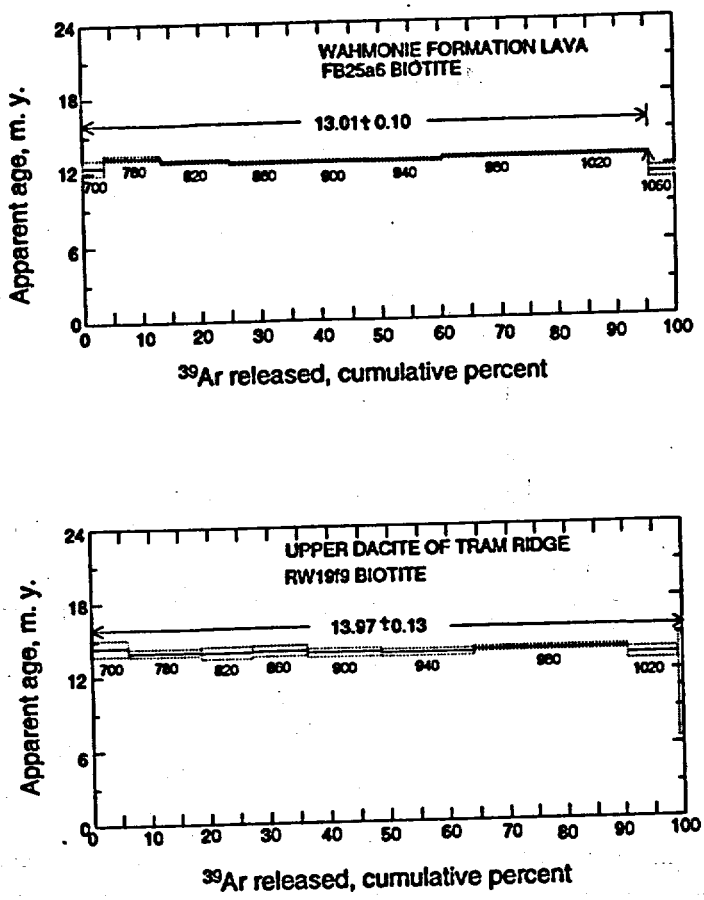


**Figure 2. $^{40}Ar/^{39}Ar$ plateau age spectra for biotite from FB25a6, Wahmonie Formation lava, and from RW19f9, dacite lava of Tram Ridge.**

## DISCUSSION

### Comparison of New $^{40}Ar/^{39}Ar$ and Previous K/Ar Results

Volcanic rocks of the SWNVF have been the subject of many conventional K/Ar geochronology studies since the early 1960s. Over 150 K/Ar determinations have been made on SWNVF units (Kistler, 1968; Marvin and others, 1970, 1973, 1989; Marvin and Cole, 1978; Weiss and others, 1989; Noble and others, 1984, 1991; R. J. Fleck, unpub. data; and F. W. McDowell, University of Texas, 1989, written commun.). Typical reported analytical uncertainties for K/Ar ages average about 3% (Kistler, 1968; Tabor and others, 1985) and thus represent absolute age uncertainties of 0.25–0.50 m.y. for the 7.5–15.25 Ma rocks of the SWNVF. Even if the ~100 units of the SWNVF, or the 20 major ash-flow sheets, or the 13 petrologic assemblages (Table 1) were distributed evenly across this time period, the ages of units would be unresolvable given a 3% uncertainty. Because the interval between eruptions was nonuniform—in fact distinctly episodic (as detailed below)—the actual overlap of uncertainties is even greater. Consequently, conventional K/Ar geochronology discriminates only three episodes of SWNVF volcanism: an early episode including all older volcanic rocks up through the Paintbrush Group (Table 1), a Timber Mountain Group episode, and a younger (but inaccurately dated by K/Ar) Thirsty Canyon Group and basalt episode.

In contrast, analytically distinct $^{40}Ar/^{39}Ar$ ages (Table 3) on SWNVF units are consistent with tight stratigraphic constraints derived from petrographic, geochemical, and field geological studies (Byers and others, 1976a; Warren and others, 1988; Broxton and others, 1989; and Sawyer and Sargent, 1989). Analytical uncertainties for laser-fusion $^{40}Ar/^{39}Ar$ on sanidine range from 20–60 k.y., about an order of magnitude better than those measured by the conventional K/Ar method. Comparison of the new ages determined by $^{40}Ar/^{39}Ar$ and those determined by K/Ar on the same mineral separate or the same unit (Fig. 3) illustrate types of problems with the K/Ar data. The K/Ar ages for sanidine are more discordant with $^{40}Ar/^{39}Ar$ ages than those for biotite. Nearly 45% of sanidine K/Ar determinations are too young by more than the typical 3% uncertainty of the method. Several explanations have been proposed for inaccurately young sanidine K/Ar ages (McDowell, 1983; Hausback and others, 1990), but young sanidine ages exhibit no simple relationship to sanidine chemical composition and are not as common as would be expected if due to a standard analytical problem. A relationship between alkali feldspar structural state and concordance of K/Ar and $^{40}Ar/^{39}Ar$ age determinations may explain the aberrant ages, as the most strongly exsolved sanidines have the most discordant ages (P. W. Lipman, U.S. Geological Survey, 1969, written commun.; F. W. McDowell, 1989, written commun.). More than half of K/Ar biotite age determinations agree

TABLE 3. $^{40}Ar/^{39}Ar$ AGE DETERMINATIONS

| Unit | Sample | Mineral/N | Weighted mean age (Ma) | s.e.m. | Uncertainty |
|---|---|---|---|---|---|
| Spearhead Member | N80A | sanidine/5 | 7.5 | 0.01 | 0.03 |
| Rocket Wash Tuff | Age 11 | sanidine/4 | 9.4 | 0.03 | 0.04 |
| Ammonia Tanks Tuff | Pooled average of 3 | sanidines/19 | 11.45 | 0.03 | 0.03 |
| Rainier Mesa Tuff | Pooled average of 3 | sanidines/16 | 11.6 | 0.03 | 0.03 |
| Rhyolite of Loop | POG2b11 | sanidine/6 | 12.5 | 0.02 | 0.03 |
| Tiva Canyon Tuff | Pooled average of 3 | sanidines/20 | 12.7 | 0.03 | 0.03 |
| Topopah Spring Tuff | Pooled average of 4 | sanidines/21 | 12.8 | 0.02 | 0.03 |
| Calico Hills Formation | RW19f2-m | sanidine/6 | 12.9 | 0.02 | 0.04 |
| Wahmonie Formation | FB25a6 | biotite-plateau/8 | 13.0 | 0.09 | 0.10 |
| Bullfrog Tuff | Pooled average of 2 | sanidines/13 | 13.25 | 0.02 | 0.04 |
| Dead Horse Flat Formation | DS19d15 | sanidine/5 | 13.5 | 0.02 | 0.02 |
| Grouse Canyon Tuff | DS18a1 | sanidine/14 | 13.7 | 0.02 | 0.04 |
| Comendite of Split Ridge | DS19f9 | sanidine/5 | 13.85 | 0.01 | 0.02 |
| Lithic Ridge Tuff | TSV-417B | sanidine/5 | 14.0 | 0.07 | 0.06 |
| Lava of Tram Ridge | RW19f9 | biotite-plateau/7 | 14.0 | 0.35 | 0.13 |
| Tub Spring Tuff | DS15e6 | sanidine/5 | 14.9 | 0.01 | 0.04 |
| Tuff of Yucca Flat | FB16a3 | sanidine/6 | 15.1 | 0.05 | 0.06 |
| Redrock Valley Tuff | Age 13 | sanidine/6 | 15.25 | 0.06 | 0.06 |

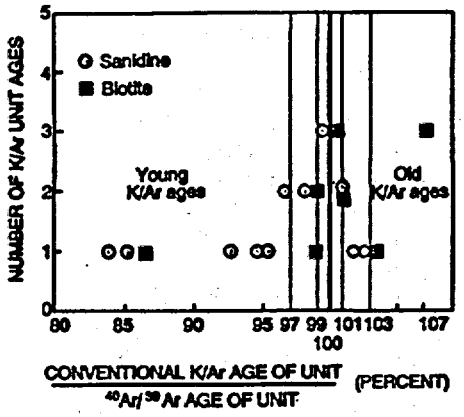


**Figure 3. Comparison of laser fusion $^{40}Ar/^{39}Ar$ ages with previous conventional K-Ar ages for stratigraphic units of the southwestern Nevada volcanic field. K/Ar data are from published sources listed in text and from unpublished data provided by F. W. McDowell (1989, written commun.).**

within 1% of the new $^{40}Ar/^{39}Ar$ ages, but about 30% of the K/Ar biotite ages are >3% older. A probable explanation for these older ages is that they are contaminated by xenocrysts due to fusion of large (>1 g) bulk samples.

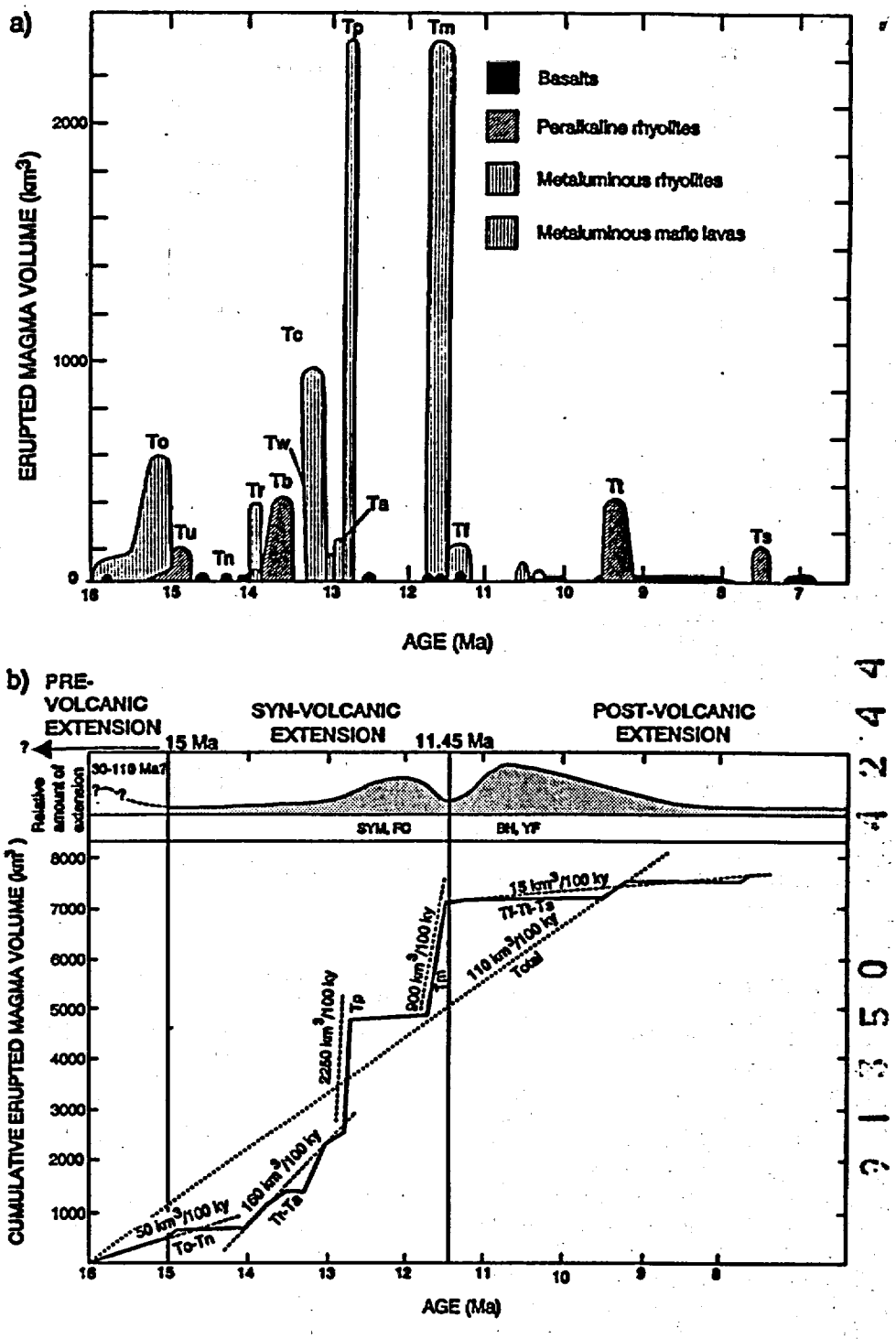


**Figure 4. Episodes of volcanism in the southwestern Nevada volcanic field. (a) Approximate erupted magma volume for each group or assemblage plotted against the age range. Group or assemblage symbols and erupted magma volumes are from Table 1. Area under the curves is not proportional to volume, as width of the bars is solely a function of the age range of the assemblage. (b) Cumulative erupted magma volume and rates of material erupted for volcanic assemblages of the southwestern Nevada volcanic field (SWNVF). Top of figure superimposes episodes of extension and relative magnitude of extension during extensional episodes. Abbreviations for extensional domains described in text and illustrated in Figures 4b and 6 are SYM, southern Yucca Mountain; FC, Fluorspar Canyon; BH, Bullfrog Hills; and YF, Yucca Flat. Group or assemblage symbols as listed in Table 1. Rates of material erupted are derived graphically and listed above dashed lines. Average eruptive rate for the SWNVF over the 7 m.y. history of the field is ~110 km³/100 k.y.**

## Episodicity of Caldera Volcanism

The high-resolution $^{40}Ar/^{39}Ar$ ages reveal for the first time a pattern of episodic volcanic activity in the SWNVF. This pattern is accentuated when erupted magma volumes are considered (Fig. 4a). Magma volume estimates (Table 1) are from Byers and others (1976a), Broxton and others (1989), and Sawyer and Sargent (1989) or are compiled from geologic map data (Ekren and others, 1971; Frizzell and Shulters, 1990) for units not cited in the previous sources. Volume estimates are at best semiquantitative because of the limitations of the calculation method (known area of exposure multiplied

by estimated average thickness). Volumes of major ash-flow sheets older than the Tiva Canyon Tuff have an additional significant uncertainty in that intracaldera tuff is not exposed, and thus intracaldera tuff volumes are not estimated. Volumes of the intracaldera Bullfrog and Grouse Canyon Tuffs have been estimated because they are penetrated by several drill holes in the subsurface of the Silent Canyon caldera complex. Despite these volumetric uncertainties, the general time-volume relationship is decidedly episodic (Fig. 4a).

Eruption of the Paintbrush and Timber Mountain Group magmas was the climax of volcanism in the SWNVF. Over 4500 $km^3$ of magma was erupted in two distinct and subequal episodes separated by a magmatic gap of 750 k.y. Each episode lasted 150 k.y. or less (Fig. 4a). Volume of the remaining units of the SWNVF was dwarfed by the magma erupted as the four large ash-flow sheets of the Paintbrush and Timber Mountain Groups. The cumulative volume of magma erupted prior to the climactic eruptions of the Paintbrush Group was about 2500 $km^3$ erupted over 3.3 m.y. (Fig. 4b). The volume erupted after the Timber Mountain Group was 600 $km^3$ over 4 m.y. during the waning of SWNVF volcanism.

The rate of material erupted gradually increased with time from the initiation of SWNVF at ca. 16 Ma to the eruption of the Paintbrush Group between 12.8 and 12.7 Ma. The first major episode of volcanism occurred between 15.25 and 14.9 Ma when the Redrock Valley Tuff (15.25 Ma), tuff of Yucca Flat (15.1 Ma), and the Tub Spring Tuff (14.9 Ma) were erupted. The rate of eruption was much lower between 14.9 and 14.0 Ma during the accumulation of tephras and distal ash-flow tuffs of the Tunnel Formation (Fig. 4a). During this early volcanism, magma erupted at a time-averaged rate of about 50 $km^3$/100 k.y. (Fig. 4b). At 14.0 Ma, metaluminous lava of Tram Ridge erupted from many centers, followed soon after by the related Lithic Ridge Tuff. Eruption of the peralkaline Grouse Canyon Tuff (13.7 Ma; Fig. 4a) caused the initial caldera collapse in the Silent Canyon caldera complex (Fig. 1), subsequently filled by lavas and tuffs of the peralkaline Dead Horse Flat Formation until 13.5 Ma. Between 14.0 and 12.8 Ma the rate of volcanic eruption increased to about 160 $km^3$/100 k.y. (Fig. 4b), and the greatest number of separate eruptive centers were active. Centers active during this time include the sources of the Crater Flat Group tuffs (ca. 13.25 Ma), the Wahmonie andesitic volcano (13.0 Ma; Fig. 4a), widespread Calico Hills lava vents (12.9 Ma), and Paintbrush Group calderas and lava vents. The peak of early SWNVF volcanism was eruption of Paintbrush Group tuffs and lavas, including the Topopah Spring Tuff (12.8 Ma) and Tiva Canyon Tuff (12.7 Ma), within 100 k.y. The rapid rate of magma extrusion, about 2250 $km^3$/100 k.y. (Table 1; Fig. 4b), was the highest during the lifetime of the SWNVF.

Lava flows that were petrographically similar to the Timber Mountain Group magma (for example, rhyolite of the Loop, Tables 1 and 3) were first erupted at ca. 12.5 Ma, but between 12.45 and 11.7 Ma no eruptions occurred (Fig. 4a) in the SWNVF. This 750 k.y. magma gap probably represents the time of magma generation and accumulation in magma chambers prior to the climactic eruption of the Timber Mountain Group tuffs. Precursory eruptions of rhyolite lava began ca. 11.7 Ma and were followed by the first of two major Timber Mountain Group ash-flow sheets, the Rainier Mesa Tuff, at 11.6 Ma. Rhyolite lava eruptions continued after eruption of the Rainier Mesa Tuff and preceded eruption of the second major Timber Mountain ash-flow sheet, the Ammonia Tanks Tuff, at 11.45 Ma. The Timber Mountain eruptions represent the second major peak of volcanism in the SWNVF, and time-averaged eruption rates on the order of 900 $km^3$/100 k.y. (Fig. 4b) characterized a 250 k.y. period. Significant basalt was first erupted in the SWNVF during Timber Mountain time. Ash flows and postcaldera moat lava flow eruptions related to the Ammonia Tanks Tuff followed soon after; rhyolite lava flows and tuffs erupted primarily west of the caldera.

Local rhyolite lava flows and more widespread basalt eruptions continued after 11.45 Ma during waning SWNVF volcanism. A 2 m.y. gap separates peak Timber Mountain ash-flow eruptions and the next caldera-forming eruptions of the Black Mountain caldera (Fig. 4a). Units of the peralkaline Thirsty Canyon Group, ash-flow sheets that total about 300 $km^3$ in volume, were erupted from the Black Mountain caldera after 9.4 Ma. The Stonewall Mountain caldera erupted almost 2 m.y. later than the Black Mountain caldera (Spearhead Member, 7.5 Ma). Eruption rates (15 $km^3$/100 k.y.) were low during this waning stage of SWNVF volcanism (Fig. 4b).

Episodic volcanic activity observed in the SWNVF is similar to some multicaldera Oligocene to Quaternary volcanic fields but contrasts with temporal patterns observed in others. The Mogollon-Datil volcanic field displays a similar episodicity in major caldera pulses (McIntosh and others, 1992), but caldera sources there had lateral migrations, which contrast with sequential eruptions from a single area of overlapping calderas in the SWNVF (Warren, 1983). The San Juan volcanic field, like the Mogollon-Datil, is composed of several overlapping clusters of calderas, each of which might be considered analogous to the SWNVF. $^{40}Ar/^{39}Ar$ geochronologic data for the central San Juan caldera cluster (Lanphere, 1988) indicate a peak volcanic eruption rate and frequency (the four middle, out of six, caldera eruptions were about 250 k.y. apart) comparable to the SWNVF. The waxing, waning, and eventual extinction of silicic volcanism in the SWNVF contrasts with the time-predictable migration of silicic volcanism along the Yellowstone–eastern Snake River Plain hot-spot track (Pierce and Morgan, 1992).

## Magmatic Evolution of the SWNVF: The Relationship of Peralkaline and Metaluminous Volcanism in Time and Space

Magma composition varied along with eruptive volume during the lifetime of the SWNVF. Peralkaline magmas were erupted at several time intervals interspersed with eruption of the dominant metaluminous magmas, and source areas for the peralkaline magmas overlapped in part the metaluminous sources (Figs. 1 and 5a), in contrast to previous interpretations (Byers and others, 1976a; Christiansen and others, 1977; Noble and others, 1991). Earliest volcanism in the SWNVF produced mainly metaluminous ash-flow tuffs, including the Redrock Valley Tuff and the tuff of Yucca Flat; late in the earliest volcanic episode, however, peralkaline Tub Spring Tuff was erupted. Zirconium concentrations (Fig. 5a) are high in the peralkaline units, whereas modal plagioclase is very low to absent (Fig. 5b). Large-volume metaluminous volcanism began again at 14.0 Ma (Fig. 4a) with the eruption of the lava of Tram Ridge and the Lithic Ridge Tuff; these units have typical low zirconium contents and high modal plagioclase contents (Figs. 5a and 5b). Peralkaline comendite of Split Ridge lava, Grouse Canyon Tuff (the largest peralkaline ash-flow sheet in the SWNVF), and Dead Horse Flat lavas were erupted between 13.85 and 13.5 Ma.

The Grouse Canyon Tuff and lavas of the Dead Horse Flat Formation ponded in the northeastern caldera of the Silent Canyon caldera complex and were subsequently

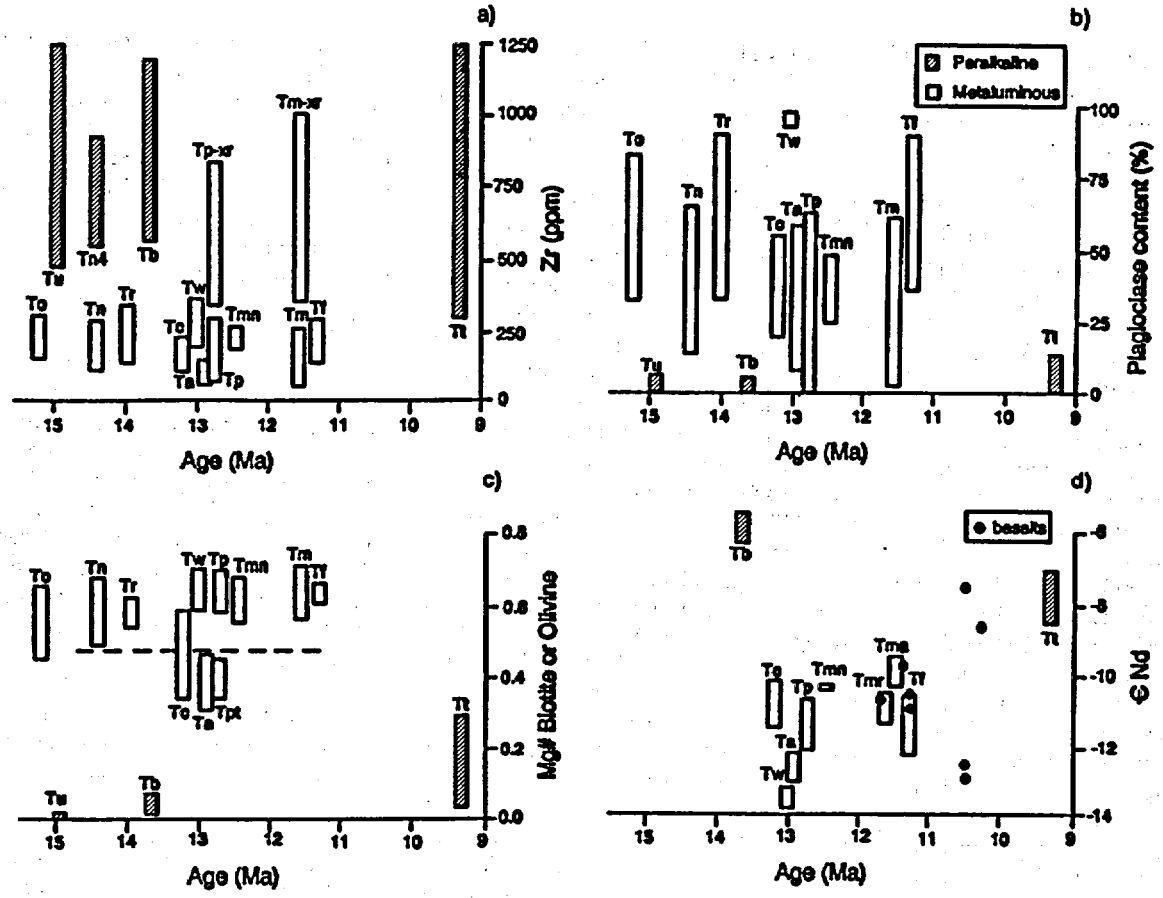


**Figure 5. Ranges for selected chemical, petrographic, and isotopic characteristics of assemblages and units of the southwestern Nevada volcanic field (SWNVF) through time. (a) Ranges of zirconium contents for whole-rock samples. (b) Ranges of median proportions of plagioclase phenocrysts among felsic phenocrysts in units of each assemblage, as determined by petrography. (c) The variation of Mg# [Mg/(Mg + total Fe)] in biotite or olivine. (d) The range of analyzed neodymium isotopic compositions for each assemblage, coeval basalts, and selected units (Tegtmeyer, 1990; Tegtmeyer and Farmer, 1990; Farmer and others, 1991). Symbols from Table 1 except for Tm-xr, Timber Mountain Group, crystal-rich tops of ash-flow sheets; Tmn, transitional Timber Mountain Group lavas (Broxton and others, 1989); Tp-xr, Paintbrush Group, crystal-rich tops of ash-flow sheets; Tma, Ammonia Tanks Tuff; Tmr, Rainier Mesa Tuff; Tpt, Topopah Spring Tuff; and Tn4, Tunnel Formation subunit 4j. Hachured pattern for peralkaline units; metaluminous units unpatterned.**

overlapped by the Area 20 caldera (Fig. 1). Metaluminous Bullfrog Tuff (13.25 Ma) of the Crater Flat Group and the postcaldera Calico Hills Formation lavas and tuffs (12.9 Ma) filled the Area 20 caldera (Warren, 1983). Peralkaline Belted Range Group and metaluminous Crater Flat Group and Calico Hills lavas have typical zirconium and plagioclase contents for their respective magma chemistries (Figs. 5a and 5b), but the mafic mineral chemistry of Crater Flat and Calico Hills units are anomalously iron-rich relative to other metaluminous rocks of the SWNVF (Fig. 5c). Iron enrichment (and corresponding magnesium depletion) of biotite and pyroxene in these metaluminous rocks is transitional to the extreme iron enrichment (Fig. 5c) characteristic of peralkaline mafic minerals (for example, fayalitic olivine and acmite). We interpret this pattern to indicate some degree of magmatic interaction, inheritance, or similarity in origin or evolution between the peralkaline Grouse Canyon magmatic system and the younger, spatially overlapping metaluminous Bullfrog Tuff and Calico Hills Formation magma systems. Iron-enriched mafic minerals also are present in the lower Topopah Spring Tuff (Tpt, Fig. 5c), suggesting a relationship between the Crater Flat/Calico Hills magmas and the initial Paintbrush Group magmas.

Magma chemistry of both Paintbrush and Timber Mountain caldera episodes is fundamentally metaluminous, although all four major ash-flow sheets are zoned from early-erupted high-silica rhyolite to late-erupted moderately alkalic trachytic compositions. Paintbrush Group rhyolites are slightly more alkalic than the Timber Mountain Group rhyolites. The higher zirconium contents of crystal-rich Paintbrush and Timber Mountain magmas (Fig. 5a) reflect accumulation of zircon included in cumulate phenocrysts (Warren and others, 1989) and are not due to high magmatic zirconium contents. Late peralkaline volcanism occurred with the eruption of the Thirsty Canyon Group magmas at 9.4 Ma (Figs. 5a, 5b, and 5c), after a 2 m.y. gap in ash-flow caldera-forming eruptions, during which time small-volume basalts and metaluminous rhyolites were erupted (Fig. 4a, and Tf, Figs. 5a, 5b, and 5c). Basaltic volcanism associated with the peralkaline Black Mountain caldera was more voluminous and widespread than with the two earlier peralkaline ash-flow tuffs. Peralkaline magmatism in the SWNVF occurred principally during the early (Tub Spring Tuff and Grouse Canyon Tuff), waxing phase of volcanism in the SWNVF, and during the late, waning stages of SWNVF activity at the Black Mountain

caldera (Vogel and others, 1983). Peralkaline SWNVF volcanism continued until the 7.5 Ma volcanism at the Stonewall Mountain volcanic center (Noble and others, 1984; Hausback and others, 1990).

The Nd isotopic composition of peralkaline magmas of the SWNVF is distinctive (Fig. 5d) with respect to metaluminous magmas (Tegtmeyer, 1990; Tegtmeyer and Farmer, 1990; Farmer and others, 1991). Peralkaline units have $\varepsilon Nd > -9$, whereas metaluminous units have $\varepsilon Nd < -9$. Metaluminous andesites of the Wahmonie volcano have the lowest εNd values (Farmer and others, 1991) in the SWNVF (Fig. 5d) and are petrographically distinguished by their high modal plagioclase contents (Fig. 5b) and calcic chemistry (Broxton and others, 1989). Spatially, the Wahmonie volcano is southeast of the central SWNVF caldera cluster (Fig. 1). These observations support a derivation of Wahmonie magmas from sources distinct from the rest of the SWNVF (Broxton and others, 1989).

Basaltic eruptions, starting in the metaluminous Timber Mountain episode and continuing through the eruption of peralkaline Thirsty Canyon tuffs, became more voluminous late in the history of the SWNVF (Figs. 4a and 5d). The Nd isotopic compositions of basalts and associated Timber Mountain Group tuffs and post–Timber Mountain rhyolite lavas are similar (Fig. 5d); most vents are south of the Silent Canyon caldera complex (Fig. 1). In contrast, younger basalts generally coeval with the peralkaline Thirsty Canyon tuffs were erupted mainly from volcanic centers on the north side of the SWNVF. Similarity of high values for εNd in young basalt and the peralkaline tuffs (Fig. 5d) and the geographic restriction of peralkaline sources to the northern SWNVF suggest that a lithospheric mantle boundary may exist between the Black Mountain and Grouse Canyon calderas to the north and the Timber Mountain caldera complex to the south.

### Relation of Extension to SWNVF Volcanism

The relationship of Tertiary volcanism to extension in the Great Basin has been the subject of much controversy. Some have asserted that magmatism was prerequisite to large amounts of extension (Gans and others, 1989); others have found little evidence for significant extension during times of peak volcanism (Best and Christiansen, 1991). Extensional deformation in the SWNVF area (Figs. 1 and 6) variously preceded volcanism, was synchronous with volcanism in discrete domains, and postdated caldera volcanism. Probably most extensional deformation in the SWNVF area is middle to late Miocene (16–8 Ma) in age and thus coincides with the peak of extensional deformation (15–5 Ma) in the central Basin and Range of Wernicke (1992) to the south.

Prevolcanic extension is known to have affected several localities in the SWNVF area, but the timing and amount of this extension are difficult to determine because (1) the youngest affected units are Pennsylvanian, (2) structural reconstructions are complicated by Mesozoic thrust-faulting, and (3) exposures of pre-Tertiary rocks are limited (Fig. 6). Low-angle extensional faults cut Paleozoic and older sedimentary rocks around the margins of Yucca Flat (Fig. 6) at Mine Mountain (Hudson and Cole, 1993; Cole and others, 1989), the CP Hills (Caskey, 1991), and in the northern Halfpint Range (J. C. Cole, 1993, oral commun.; Barnes and others, 1963, 1965). Prevolcanic extension at Mine Mountain is older than the Redrock Valley Tuff (15.25 Ma) and younger than Mesozoic thrusting. Gently dipping 27.3 Ma Monotony Tuff and 26.7 Ma Shingle Pass Tuff (Sargent and Orkild, 1973; ages from Best and Christiansen, 1991) and conformable 14.9 Ma Tub Spring Tuff in the northern Halfpint Range depositionally overlie extended late Precambrian and Paleozoic rocks. On the northwest side of the Belted Range, 30°-dipping Monotony and Shingle Pass Tuffs overlie overturned Paleozoic rocks at Limestone Ridge that are cut by low-angle normal faults (Ekren and others, 1971). Thus, at least in the northern Halfpint and the Belted Ranges, early extensional deformation is pre–late Oligocene in age. Evidence from a drill hole at Rainier Mesa suggests that some prevolcanic extension may be pre–Late Cretaceous (Cole and others, 1993). We find no data that support postulated strong Paleogene extension (Axen and others, 1993) within the area of the central SWNVF caldera cluster (Fig. 6).

Synvolcanic normal faulting, minor strike-slip faulting, and tilting took place throughout the main period (14–11.5 Ma) of magmatism in the SWNVF (Fig. 4b), but extensional strain was modest in and near the central SWNVF caldera cluster (Fig. 6). Age constraints for this deformation come from overlap of faults in older units by younger units, from angular unconformities between units, and from thickness changes of units related to growth faulting. We describe below a composite pattern of synvolcanic and postvolcanic deformation (Fig. 4b), but with the following overall characteristics: (1) small cumulative middle to late Miocene extension of the central SWNVF relative to adjoining parts of the Great Basin (Hudson and others, 1994; Wernicke, 1992; Axen and others, 1993) and (2) greater extension in discrete domains (Fig. 6) marginal to the SWNVF at different specific times. These episodic extensional strains were distinctly nonuniform across the area of the SWNVF.

Early synvolcanic extension affected several localities of the SWNVF. Small strains were accommodated by pre-Bullfrog (13.25 Ma) normal faults and spatially limited pre–Tiva Canyon (12.7 Ma) normal and strike-slip faults northwest of Yucca Flat (Minor, 1989). Moderate pre-Bullfrog faulting and northwest tilting also affected an area southeast (Fig. 6) of Tolicha Peak (Minor and others, 1991, 1993). Large subsurface thickness changes of the lower Crater Flat Group tuffs and the Lithic Ridge Tuff reflect growth faulting at northern Yucca Mountain (Fridrich and others, 1994). Warren and others (1985) reported slight (2°–4°) pre–Timber Mountain northeast tilting of Paintbrush Group tuffs and lavas in the subsurface of Pahute Mesa. Calico Hills Formation and Paintbrush Group tuff thicken on the western, downthrown side of different faults at Pahute Mesa. Slight post-Paintbrush extension also occurred at Pahute Mesa where Rainier Mesa Tuff thickens over the same structures.

Late synvolcanic extensional deformation is greater in magnitude (Fig. 4b) on the southwestern margins of the SWNVF. In the Fluorspar Canyon area (Fig. 6), north of Bare Mountain (Monsen and others, 1992), the Bullfrog, Topopah Spring, and Tiva Canyon Tuffs are conformable and tilted east ~30°–60° more than the overlying 11.6–11.45 Ma Rainier Mesa and Ammonia Tanks Tuffs (discordant Timber Mountain tuffs of Carr, 1990, Fig. 4). At Yucca Mountain, Scott (1990) measured differential tilting of 10°–20° between Tiva Canyon Tuff and Timber Mountain Group tuffs at the south end of Yucca Mountain; the Tiva Canyon Tuff was rotated ~25° clockwise about a vertical axis, whereas rotation of the Ammonia Tanks Tuff (6° ± 13°) was much less (Rosenbaum and others, 1991; Hudson and others, 1994).

Postvolcanic extension (defined as younger than the 11.45 Ma Ammonia Tanks Tuff, Fig. 4b) was locally large in magnitude but was restricted to areas marginal to the central SWNVF caldera cluster (Fig. 6). Moderate to large postvolcanic extension occurred in the Bullfrog Hills and Fluorspar Canyon areas (Fig. 6). Extension was ex-

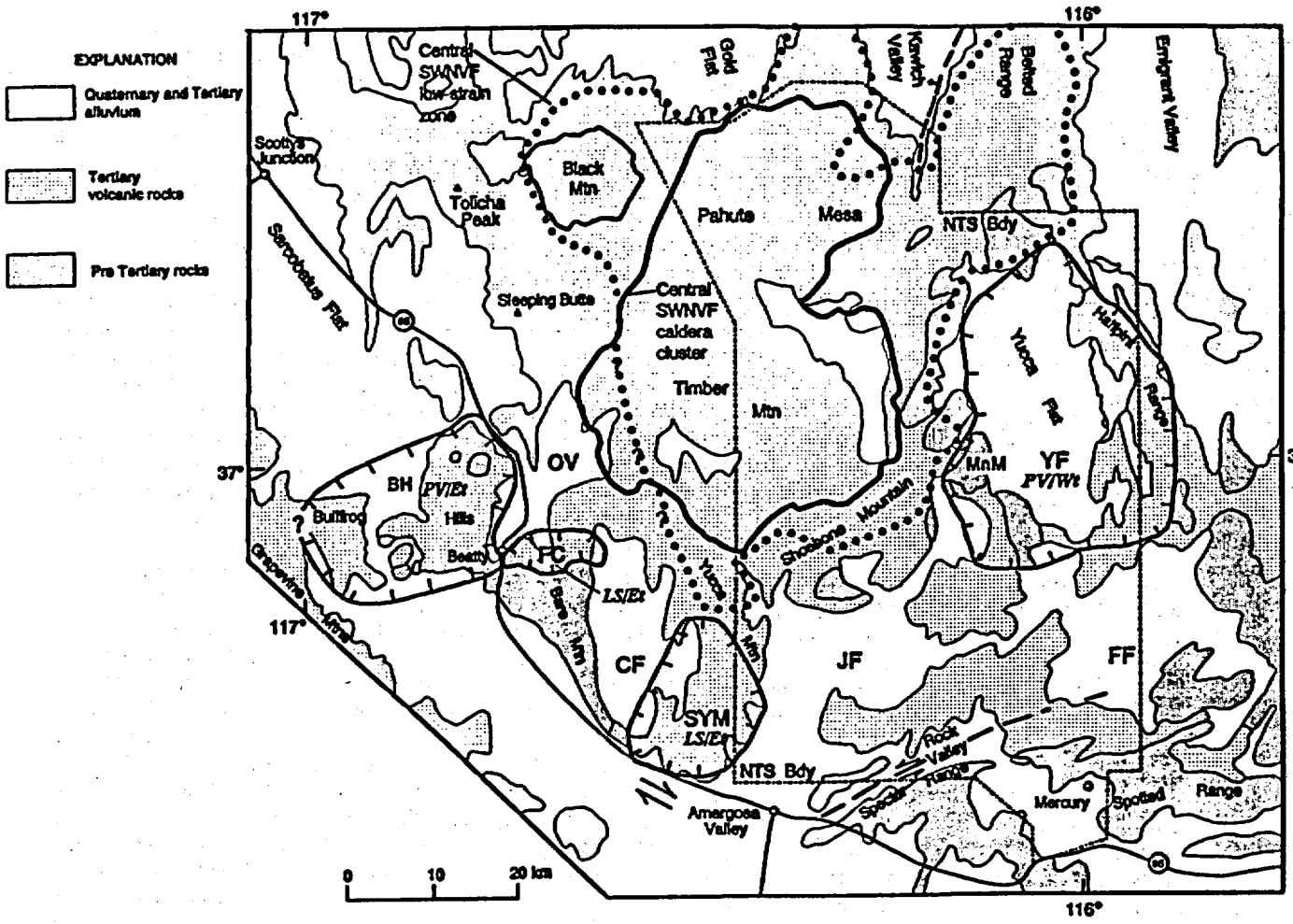


**Figure 6. Map illustrating the central southwestern Nevada volcanic field (SWNVF) caldera cluster and outlining the area showing weak (<10° of tilt or vertical-axis rotation) syn- and postvolcanic deformation, and some marginal domains (enclosed by hachured lines) of moderate to large amounts of late synvolcanic (*LS*) and postvolcanic (*PV*) extension. Tilt direction of beds is indicated by *Et*, east tilt, and *Wt*, west tilt. Abbreviations for labeled domains are from Figure 4b. Additional postvolcanic domains of moderate extension that formed alluvial basins include OV, Oasis Valley; CF, Crater Flat; JF, Jackass Flats; FF, Frenchman Flat; but boundaries for these domains are not completely delimited at present. The area of prevolcanic extension at Mine Mountain is abbreviated as MnM; Nevada Test Site is abbreviated as NTS. The map is not a comprehensive depiction of all synvolcanic and postvolcanic extensional domains in the SWNVF but represents the domains that can be identified at present, relative to the central SWNVF low-strain zone.**

treme in the Bullfrog Hills, where 60°–90° east tilts are observed in conformable sequences ranging from pre–Lithic Ridge Tuff to the Ammonia Tanks Tuff (Maldonado, 1990), but largely predated 10 Ma latite flows (Maldonado and Hausback, 1990). In the western Fluorspar Canyon area (Monsen and others, 1992), Ammonia Tanks Tuff is tilted east as much as 30°. Farther east in Crater Flat, across Yucca Mountain, and southeast of Timber Mountain, the Timber Mountain Group tuffs are generally tilted 10°–30° (Carr, 1990, Fig. 4). Postvolcanic extension was minimal at Pahute Mesa, where Timber Mountain tuffs tilt east <4° (Warren and others, 1985). Slight normal faulting there (offsets >60–80 m on principal faults) and slight (<2°) tilting affected the 9.4 Ma Thirsty Canyon Group (Orkild and others, 1969).

Fault-controlled, post–Ammonia Tanks alluvial sedimentary basins formed on the margins of the SWNVF but do not overlap the central SWNVF caldera cluster. The Yucca Flat basin–Halfpint Range fault system, east of the central SWNVF, is a post–Ammonia Tanks alluvial basin filled by late Miocene and younger sedimentary deposits (Barnes and others, 1963) to 400 m depth, and locally as much as 1200 m (McKeown and others, 1976). In Yucca Flat (Fig. 6) and the Halfpint Range, units of the SWNVF are cut by similar down-to-the-east normal faults and exhibit stratal tilts of 10°–25° west (Frizzell and Shulters, 1990, and sources cited therein). Similar alluvial basins of late Miocene to Quaternary age are present north (Gold Flat, Kawich Valley, and Emigrant Valley) and south (Crater Flat, Jackass Flat, and Frenchman Flat) of the central SWNVF (Fig. 6), but their controlling faults did not propagate across the area of peak volcanism and caldera formation. The central SWNVF is one of the largest areas in the Great Basin unbroken by middle Miocene and younger alluvial basins (Stewart and Carlson, 1978); the northern Basin and Range pattern of paired late Neogene north-south ranges and basins terminates at the north margin of SWNVF. Rainier Mesa Tuff is repeated in fault blocks at about the

same elevation over an east-west distance of 100 km, from the Bullfrog Hills to the Halfpint Range, with no headwall breakaway zones or regions of uplifted lower plate rocks (W. B. Hamilton, 1993, written commun.).

Volcanism and extension that postdate the central SWNVF have different patterns in time and space. Christiansen and Lipman (1972) suggested that extension and volcanism in the SWNVF area occurred after a transition from magmatism generated by subduction to a regime characterized by extension and bimodal basalt-rhyolite volcanism. Magmatism and extension in the SWNVF area also occurred as the Mendocino fracture zone migrated north as a locus for magmatism and extension (Glazner and Bartley, 1984). Detailed plate tectonic reconstructions (Severinghaus and Atwater, 1990) indicate that during the main episode of volcanism (14–11.5 Ma) the SWNVF was located north of the Mendocino fracture zone. In the SWNVF area at this time, the Pacific plate was still being subducted beneath an extending western North America, analogous to the Lassen–Shasta–Medicine Lake Highlands region of northern California today. Younger SWNVF calderas (Black Mountain, 9.4 Ma, and Stonewall Mountain, 7.5 Ma) were peralkaline in composition and small in volume (Fig. 4b), and they migrated northwestward, consistent with a melting locus associated with the movement of the Mendocino fracture zone. Late Miocene and Pliocene silicic caldera volcanism in the southern Great Basin (6 Ma Silver Peak volcanic center) migrated west-northwest toward the Pliocene and Quaternary Long Valley–Mono Basin volcanic system (Luedke and Smith, 1981), whereas younger extension and strike-slip faulting migrated west toward the Death Valley region (Hamilton, 1988).

In contrast to models by Gans and others (1989), we find that the area of greatest magma input to upper crust—within the overlapping Silent Canyon–Claim Canyon–Timber Mountain caldera complexes (Fig. 6)—is the area of least upper crustal extension. Several factors may have led to retardation of extension in the area of the central SWNVF caldera cluster. The caldera complexes are probably rooted in batholith cupolas (Lipman, 1984). After crystallization and cooling, such batholiths could act as buttresses (Wernicke, 1992; Hamilton and Myers, 1966), strengthening the upper crust against regional extensional stress. Crustal strengthening probably best explains retardation of postvolcanic (post–Ammonia Tanks Tuff) extension in the central SWNVF. A strengthening of the crust during synvolcanic extension, however, would require that magmas were emplaced and cooled quickly relative to deformation. This might be possible at shallow crustal levels, as described by Davis and others (1993) for a pluton that intruded and terminated slip on a coeval Miocene detachment fault in the eastern Mojave Desert. For synvolcanic extension, silicic magma input and inflation of the batholithic magma chamber roof also may have affected the regional stress field, reducing the regional deviatoric stress (Parsons and Thompson, 1991) and decreasing regional strain. Quaternary volcanic fields that exhibit similar deformational patterns include the Yellowstone Plateau volcanic field, where neotectonic late Pleistocene and Holocene regional normal faults splay, decrease in displacement, and terminate to the north approaching the 0.6 Ma third-cycle Yellowstone caldera (Pierce and Morgan, 1992, Plate 1), and the Long Valley–Mono Basin volcanic system (Bursik and Sieh, 1989; Dixon and others, 1993).

Miocene extension in the SWNVF occurred in a mosaic of local domains. South and west margins of the field were affected by a dextral shear transfer zone (Rosenbaum and others, 1991; Hudson and others, 1994) that is a northern boundary for the high-strain Death Valley extensional corridor (Wernicke and others, 1988). In general, SWNVF volcanism and regional extension were coeval. In detail, however, age, magnitude, and polarity of extension varied among the more strongly deformed domains marginal to the field. Both volcanism and extensional deformation in the SWNVF were episodic in nature as has been recognized in the eastern Great Basin (Taylor and others, 1989).

## SUMMARY

Volcanic activity in the SWNVF, as revealed by new high-resolution $^{40}Ar/^{39}Ar$ age determinations, was distinctly episodic: very large volumes of magma (up to 2000 $km^3$) were erupted in fairly short periods of <100–300 k.y. separated by longer quiescent periods. For example, two episodes of caldera-forming ash-flow magmatism, separated by a 750 k.y. magma gap, produced the large-volume tuffs of the Paintbrush and Timber Mountain Groups during a 1.35 m.y. time period. New $^{40}Ar/^{39}Ar$ ages corroborate the stratigraphic succession of units within the SWNVF based upon petrographic, geochemical, and field geologic studies (Byers and others, 1976a; Warren and others, 1988; Broxton and others, 1989; Sawyer and Sargent, 1989; Minor and others, 1993). We have revised the stratigraphy of major SWNVF units based upon this new framework, combining major ash-flow sheets with petrologically related lava flows and nonwelded tuff deposits into stratigraphic groups. Newly defined formal stratigraphic units are the Beatty Wash Formation, Calico Hills Formation, Dead Horse Flat Formation, and Tunnel Formation. The revised stratigraphy and ages demonstrate that peralkaline volcanism in the SWNVF was closely associated in time and space with the waxing and waning of metaluminous volcanism. Petrologic and chemical data provide evidence of hybridization between distinct peralkaline and metaluminous magmas during the 7 m.y. span of SWNVF volcanism.

Minor to moderate extension can be demonstrated during the history of the SWNVF, but the slight synvolcanic extension of the central SWNVF contrasts markedly with the synextensional magmatism described by Gans and others (1989) for limited areas of highly extended volcanic rocks in the Great Basin. Best and Christiansen (1991) concluded that the Oligocene and early Miocene peak of volcanism in the Great Basin correlated with only limited extension in east-central Nevada. For the SWNVF, we extend their conclusions in that only limited extension occurred during peak middle Miocene volcanism in the southwestern Great Basin. Within the SWNVF, the central area of coalescing calderas and proximal caldera margins was minimally extended from middle Miocene to the present. Synvolcanic strain was dominated by local magma chamber roof deformation or caldera subsidence (Lipman, 1984). The outer margins of the SWNVF locally were more deformed in discrete extensional domains. An inferred subcaldera batholith may have acted as an upper crustal buttress with respect to regional extensional deformation. Intense middle Miocene volcanism and subjacent plutonism apparently strengthened the upper crust in the central SWNVF area, because it stands today as a high plateau unbroken by regional middle Miocene and younger normal faulting that formed young alluvial basins. Magmatism in the SWNVF and regional extension, although coeval, were not genetically linked to form a zone of highly extended upper crust. The two processes

overlapped in time and space but were not correlated in amount.

## ACKNOWLEDGMENTS

J. C. Cole, P. P. Orkild, and G. A. Izett provided encouragement and guidance in the formulation of the study. We thank G. B. Dalrymple for the opportunity to work on the "GLM" at the U.S. Geological Survey in Menlo Park. The support of Gerry Cebula and Jack Groen for superb mineral separations; of James Saburomaru, Jerry von Essen, and Malcolm Pringle in the lab; of Ray Sabala for scientific illustrations; and from H. Dickensheets, R. Durham, and D. Welch of the U.S. Air Force in providing access is gratefully acknowledged.

Review comments by V. M. Glanzman, W. D. Johnson Jr., P. P. Orkild, Marge MacLachlan, Tom Judkins, Dave Schleicher, Ed du Bray, W. J. Carr, F. M. Byers Jr., J. C. Cole, S. A. Minor, C. J. Fridrich, C. M. Johnson, W. McIntosh, S. Mertzman, A. G. Sylvester, and J. R. LeCompte helped correct many errors of commission and omission; however, the conclusions and any remaining errors remain the responsibility of the authors. This project was funded under Interagency Agreement DE-AI08-91NV11040 between the U.S. Geological Survey and the Department of Energy, Nevada Operations Office.

## APPENDIX: ANALYTICAL METHODS

Sanidine separates for this study were prepared by Kistler (1968), Marvin and others (1970, 1973, 1989), Marvin and Cole (1978), and Fred McDowell (University of Texas, 1989, written commun.) and were previously analyzed by the conventional K/Ar method, were new sanidine separates prepared at Los Alamos National Laboratory, or were new sanidine and biotite prepared at the U.S. Geological Survey (USGS) mineral separation facility in Denver, Colorado. Sanidine separates were leached with dilute HF followed by ultrasonic cleaning to remove volcanic glass and other surface impurities. Only a few milligrams of sanidine were encapsulated in aluminum foil for irradiation; biotite samples for incremental heating weighed about 100 mg. The sanidine and biotite capsules were placed in fused silica vials with flux monitor standards (Taylor Creek Rhyolite sanidine, Fish Canyon Tuff sanidine, and SB-3 biotite) placed at regular intervals and were irradiated in the USGS TRIGA reactor in Denver, Colorado, using the procedures described in Dalrymple and others (1981) over the course of four irradiations (LXXXIV, LXXXVII, XCIII, and CII) between 1989 and 1991; all pooled results of multiple samples are from the first two irradiations. Typical irradiation time was 16 hr and resulted in total neutron doses of about $1 \times 10^{18}$ nvt (nvt = neutron density × neutron velocity × irradiation time).

Dalrymple and Duffield (1988) and Dalrymple (1989) described the analytical capabilities of the SW Ar-ion continuous laser $^{40}Ar/^{39}Ar$ laboratory in Menlo Park. Analysis of sanidine generally involved fusing 6–8 grains of sanidine; in a few cases up to 15 grains of finer-size sanidine (<100 mesh) were fused, and for several samples large single crystals were analyzed. Approximate masses of sanidine fused in each analysis were 0.005–0.4 mg. Typically, each age determination represents the weighted mean of 4–6 sanidine laser-fusion analyses (Table 3). Mass analyses were performed on a MAP 216 mass spectrometer at a sensitivity of about $2 \times 10^{-14}$ mol/V. The incremental heating/age spectrum $^{40}Ar/^{39}Ar$ technique (Dalrymple and Lanphere, 1971; Lanphere, 1988) was used to degas ~100 mg biotite samples in a resistance-heated furnace in 8–12 temperature increments; temperatures were measured using a thermocouple. Argon isotopic ratios were measured on a 6 in. (15.2 cm) radius, 60° sector, Nier-type single-collector mass spectrometer. Corrections for undesirable interferences of $^{36}Ar$, $^{39}Ar$, and $^{40}Ar$ isotopes caused by nuclear reactions of K and Ca were made using standard calculations (Dalrymple and others, 1981). All $^{40}Ar/^{39}Ar$ ages have been measured relative to a monitor age of 513.9 Ma for MMhb-1 (Lanphere and others, 1990; Dalrymple and others, 1993). An age of 27.92 Ma was calculated for the internal monitor standard Taylor Creek Rhyolite sanidine 85G003.

Uncertainties in weighted means are the inverse variance-weighted 1σ standard error of the mean (Taylor, 1982) for multiple laser fusion analyses or fractions of an incremental-heating age spectrum and include propagation of the J-curve calibration uncertainty. Pooled ages for multiple samples of a unit are weighted means of several determinations. Estimates of errors assigned to individual age measurements (internal errors) are made by propagating well-documented errors from all aspects of each analysis (Cox and Dalrymple, 1967; Taylor, 1982). Reproducibility of ages (external error) in highly radiogenic samples such as sanidine and biotite is generally as good or better than internal errors unless geologic factors such as contamination or argon loss are present. The cited best estimate uncertainty of the weighted mean is the square root of the sum of the weighting factors (Taylor, 1982) and represents a 1σ (68.27%) confidence interval of the mean. These uncertainties are analogous to the standard error of the mean (s.e.m., Table 3) for arithmetic means except that they only include internal errors and thus do not include excess dispersion of the measured ages. External error in excess of the internal estimates is alternatively incorporated using the mean square of weighted deviates (MSWD, McIntyre and others, 1966) as a measure of dispersion. Where MSWD is >1.0, estimated uncertainties are adjusted to incorporate the external error component, multiplying them by the square root of MSWD (Ludwig, 1988). Resulting uncertainties produce a MSWD of 1.0, maintaining the weighted mean and relative magnitudes of the error estimates for individual samples.

## REFERENCES CITED

Axen, G. J., Taylor, W. J., and Bartley, J. M., 1993, Space-time patterns and tectonic controls of Tertiary extension and magmatism in the Great Basin of the western United States: Geological Society of America Bulletin, v. 105, p. 56–76.

Barnes, H., Houser, F. N., and Poole, F. G., 1963, Geologic map of the Oak Spring quadrangle: U.S. Geological Survey Map GQ-214, scale 1:24 000.

Barnes, H., Christiansen, R. L., and Byers, F. M., Jr., 1965, Geologic map of the Jangle Ridge quadrangle: U.S. Geological Survey Map GQ-363, scale 1:24 000.

Bath, G. D., 1968, Aeromagnetic anomalies related to remanent magnetism in volcanic rock, Nevada Test Site, *in* Eckel, E. B., ed., Nevada Test Site: Geological Society of America Memoir 110, p. 135–146.

Best, M. G., and Christiansen, E. H., 1991, Limited extension during peak Tertiary volcanism, Great Basin of Nevada and Utah: Journal of Geophysical Research, v. 96, no. N8, p. 13 509–13 528.

Broxton, D. E., Warren, R. G., Byers, F. M., Jr., and Scott, R. B., 1989, Chemical and mineralogical trends within the Timber Mountain–Oasis Valley caldera complex—Evidence for multiple cycles of chemical evolution in a long-lived silicic magma system: Journal of Geophysical Research, v. 94, p. 5961–5986.

Broxton, D. E., Chipera, S. J., Byers, F. M., Jr., and Rautman, C. A., 1993, Geologic evaluation of six nonwelded tuff sites in the vicinity of Yucca Mountain, Nevada for a surface-based test facility for the Yucca Mountain Project: Los Alamos National Laboratory Report LA-12542-MS, 83 p.

Bursik, M., and Sieh, K., 1989, Range front faulting and volcanism in the Mono Basin, eastern California: Journal of Geophysical Research, v. 94, p. 15 587–15 609.

Byers, F. M., Jr., Carr, W. J., Orkild, P. P., Quinlivan, W. D., and Sargent, K. A., 1976a, Volcanic suites and related cauldrons of Timber Mountain–Oasis Valley caldera complex, southern Nevada: U.S. Geological Survey Professional Paper 919, 70 p.

Byers, F. M., Jr., Carr, W. J., Orkild, P. P., Quinlivan, W. D., and Sargent, K. A., 1976b, Geologic map of the Timber Mountain caldera area: U.S. Geological Survey Miscellaneous Investigation Series Map I-891, scale 1:48 000.

Byers, F. M., Jr., Carr, W. J., and Orkild, P. P., 1989, Volcanic centers of southwestern Nevada—Evolution of understanding, 1960–1988: Journal of Geophysical Research, v. 94, p. 5908–5924.

Carr, W. J., 1990, Styles of extension in the Nevada Test Site region, southern Walker Lane belt—An integration of volcano-tectonic and detachment fault models, *in* Wernicke, B. P., ed., Basin and Range extensional tectonics near the latitude of Las Vegas, Nevada: Geological Society of America Memoir 176, p. 283–304.

Carr, W. J., Byers, F. M., Jr., and Orkild, P. P., 1986, Stratigraphic and volcano-tectonic relations of the Crater Flat Tuff and some older volcanic units: U.S. Geological Survey Professional Paper 1323, 28 p.

Caskey, S. J., 1991, Mesozoic and Cenozoic structural geology of the CP Hills, Nevada Test Site, Nye County, Nevada—And regional implications [M.S. thesis]: Reno, University of Nevada, 90 p.

Christiansen, R. L., 1979, Cooling units and composite sheets in relation to caldera structure, *in* Chapin, C. E., and Elston, W. E., eds., Ash-flow tuffs: Geological Society of America Memoir 180, p. 29–42.

Christiansen, R. L., and Lipman, P. W., 1965, Geologic map of the Topopah Spring Northwest quadrangle, Nye County, Nevada: U.S. Geological Survey Geologic Quadrangle Map GQ-444, scale 1:24 000.

Christiansen, R. L., and Lipman, P. W., 1972, Cenozoic volcanism and plate tectonic evolution of the Western United States—Part 2, Late Cenozoic: Royal Society of London Philosophical Transactions, ser. A, v. 271, p. 249–284.

Christiansen, R. L., Lipman, P. W., Carr, W. J., Byers, F. M., Jr., Orkild, P. P., and Sargent, K. A., 1977, The Timber Mountain–Oasis Valley caldera complex of southern Nevada: Geological Society of America Bulletin, v. 88, p. 943–959.

Cole, J. C., Wahl, R. R., and Hudson, M. R., 1989, Structural relations within the Paleozoic basement of the Mine Mountain block: Implications for interpretation of gravity data in Yucca Flat, Nevada Test Site, *in* Olsen, C. W., and Carter, J. A., eds., Proceedings, Fifth Symposium on Containment of Underground Nuclear Explosions: Lawrence Livermore National Laboratory Report CONF-8909163, v. 2, p. 431–455.

Cole, J. C., Harris, A. G., Lanphere, M. A., Barker, C. E., and Warren, R. G., 1993, The case for pre-middle Cretaceous extensional faulting in northern Yucca Flat, southwestern Nevada: Geological Society of America Abstracts with Programs, v. 25, no. 5, p. 22.

Cox, A., and Dalrymple, G. B., 1967, Statistical analysis of geomagnetic reversal data and the precision of potassium-argon dating: Journal of Geophysical Research, v. 72, p. 2603–2614.

Dalrymple, G. B., 1989, The GLM continuous laser system for $^{40}Ar/^{39}Ar$ dating: Description and performance characteristics: U.S. Geological Survey Bulletin 1890, p. 89–96.

Dalrymple, G. B., and Duffield, W. A., 1988, High precision $^{40}Ar/^{39}Ar$ dating of Oligocene rhyolites from the Mogollon-Datil volcanic field using a continuous laser system: Geophysical Research Letters, v. 15, p. 463–466.

Dalrymple, G. B., and Lanphere, M. A., 1971, $^{40}Ar/^{39}Ar$ technique of K-Ar dating—A comparison with the conventional technique: Earth and Planetary Science Letters, v. 12, p. 300–308.

Dalrymple, G. B., Alexander, E. C., Lanphere, M. A., and Kraker,

G. P., 1981, Irradiation of samples for $^{40}Ar/^{39}Ar$ dating using the Geological Survey TRIGA reactor: U.S. Geological Survey Professional Paper 1176, 55 p.

Dalrymple, G. B., Izett, G. A., Snee, L. W., and Obradovich, J. D., 1993, $^{40}Ar/^{39}Ar$ age spectra and total-fusion ages of tektites from Cretaceous-Tertiary rocks in the Beloc Formation, Haiti: U.S. Geological Survey Bulletin 2065, 20 p.

Davis, G. A., Fowler, T. K., Bishop, K. M., Brudos, T. C., Friedmann, S. J., Burbank, D. W., Parke, M. A., and Burchfiel, B. C., 1993, Pluton pinning of an active Miocene detachment fault system, eastern Mojave Desert, California: Geology, v. 21, p. 627–630.

Dixon, T. H., Bursik, M., Wolf, S. K., Heflin, M., Webb, F., Farina, F., and Robaudo, S., 1993, Constraints on deformation of the resurgent dome, Long Valley caldera, California from Space Geodesy, *in* Smith, D. E., and Turcotte, D. L., eds., Contribution of Space Geodesy to geodynamics—Crustal dynamics: American Geophysical Union Geodynamics Series, v. 23, p. 193–214.

Ekren, E. B., Anderson, R. E., Rogers, C. L., and Noble, D. C., 1971, Geology of northern Nellis Air Force Base Bombing and Gunnery Range: U.S. Geological Survey Professional Paper 651, 91 p., scale 1:125 000.

Farmer, G. L., Broxton, D. E., Warren, R. G., and Pickthorn, William, 1991, Nd, Sr, and O isotopic variations in metaluminous ash-flow tuffs and related volcanic rocks at the Timber Mountain/Oasis Valley caldera complex, SW Nevada—Implications for the origin and evolution of large-volume silicic magma bodies: Contributions to Mineralogy and Petrology, v. 109, p. 53–68.

Ferguson, J. F., Cogbill, A. H., and Warren, R. G., 1994, A geophysical-geological transect of the Silent Canyon caldera complex, Pahute Mesa, Nevada: Journal of Geophysical Research, v. 99, p. 4323–4339.

Fridrich, C. J., Dudley, W. W., Jr., and Stuckless, J. S., 1994, A hydrogeologic analysis of the saturated zone ground-water system under Yucca Mountain, Nevada: Journal of Hydrology, v. 154, p. 133–168.

Frizzell, V. A., and Shulters, J., 1990, Geologic map of the Nevada Test Site, southern Nevada: U.S. Geological Survey Miscellaneous Investigations Series Map I-2046, scale 1:100 000.

Gans, P. B., Mahood, G. A., and Schermer, E., 1989, Synextensional magmatism in the Basin and Range province—A case study from the eastern Great Basin: Geological Society of America Special Paper 233, 53 p.

Gibbons, A. B., Hinrichs, E. N., Hansen, W. R., and Lemke, R. W., 1963, Geology of the Rainier Mesa quadrangle, Nye County, Nevada: U.S. Geological Survey Geologic Quadrangle Map GQ-215, scale 1:24 000.

Glazner, A. F., and Bartley, J. M., 1984, Timing and tectonic setting of Tertiary low-angle normal faulting and associated magmatism in the southwestern United States: Tectonics, v. 3, p. 385–396.

Hamilton, W. B., 1988, Detachment faulting in the Death Valley region, California and Nevada: U.S. Geological Survey Bulletin 1790, p. 51–85.

Hamilton, W. B., and Myers, W. B., 1966, Cenozoic tectonics of the western United States: Reviews of Geophysics, v. 4, p. 509–549.

Hansen, W. R., Lemke, R. W., Cattermole, J. M., and Gibbons, A. B., 1963, Stratigraphy and structure of the Rainier and USGS tunnel areas: U.S. Geological Survey Professional Paper 382-A, 49 p., scale 1:6000.

Hausback, B. P., Deino, A. L., Turrin, B. T., McKee, E. H., Frizzell, V. A., Jr., Noble, D. C., and Weiss, S. I., 1990, New $^{40}Ar/^{39}Ar$ ages for the Spearhead and Civet Cat Canyon Members of the Stonewall Flat Tuff, Nye County, Nevada—Evidence for systematic errors in standard K-Ar determinations on sanidine: Isochron/West, no. 56, p. 3–7.

Healey, D. L., 1968, Application of gravity data to geologic problems at Nevada Test Site, *in* Eckel, E. B., ed., Nevada Test Site: Geological Society of America Memoir 110, p. 147–156.

Healey, D. L., Harris, R. N., Ponce, D. A., and Oliver, H. W., 1987, Complete Bouger gravity map of the Nevada Test Site and vicinity, Nevada: U.S. Geological Survey Open-File Report 87-506, scale 1:100 000.

Hudson, M. R., and Cole, J. C., 1993, Kinematics of faulting in the Mine Mountain area of southern Nevada: Evidence for pre-middle Miocene extension: Geological Society of America Abstracts with Programs, v. 25, no. 5, p. 55.

Hudson, M. R., Sawyer, D. A., and Warren, D. A., 1994, Paleomagnetism and rotation constraints for the middle Miocene southwestern Nevada volcanic field: Tectonics, v. 13, p. 258–277.

Kane, M. F., Webring, M. W., and Bhattacharyya, B. K., 1981, A preliminary analysis of gravity and aeromagnetic surveys of the Timber Mountain area, southern Nevada: U.S. Geological Survey Open-File Report 81-189, 40 p., scale 1:48 000.

Kistler, R. W., 1968, Potassium-argon ages of volcanic rocks in Nye and Esmeralda counties, Nevada, *in* Eckel, E. B., ed., Nevada Test Site: Geological Society of America Memoir 110, p. 252–262.

Lanphere, M. A., 1988, High-resolution $^{40}Ar/^{39}Ar$ chronology of Oligocene volcanic rocks, San Juan Mountains, Colorado: Geochimica et Cosmochimica Acta, v. 52, p. 1425–1434.

Lanphere, M. A., Dalrymple, G. B., Fleck, R. J., and Pringle, M. S., 1990, Intercalibration of mineral standards for K-Ar and $^{40}Ar/^{39}Ar$ age measurements [abs.]: Eos (Transactions, American Geophysical Union), v. 71, p. 1658.

Lipman, P. W., 1984, Roots of ash-flow calderas—Windows into granitic batholiths: Journal of Geophysical Research, v. 89, p. 8801–8841.

Ludwig, K. R., 1988, ISOPLOT for MS-DOS, A plotting and regression program for radiogenic-isotope data, for IBM-PC compatible computers, v. 1.00: U.S. Geological Survey Open-File Report 88-557, 44 p.

Luedke, R. G., and Smith, R. L., 1981, Map showing distribution, composition, and age of late Cenozoic volcanic centers in California and Nevada: U.S. Geological Survey Miscellaneous Investigations Map I-1091-C, scale 1:1 000 000.

Maldonado, F., 1990, Structural geology of the upper plate of the Bullfrog Hills detachment system: Geological Society of America Bulletin, v. 102, p. 992–1006.

Maldonado, F., and Hausback, B. P., 1990, Geologic map of the northeast quarter of the Bullfrog 15-minute quadrangle, Nye County, Nevada: U.S. Geological Survey Miscellaneous Investigations Series Map I-2049, scale 1:24 000.

Marvin, R. F., and Cole, J. C., 1978, Radiometric ages—Compilation "A," U.S. Geological Survey: Isochron West, no. 22, p. 3–14.

Marvin, R. F., Byers, F. M., Jr., Mehnert, H. H., Orkild, P. P., and Stern, T. W., 1970, Radiometric ages and stratigraphic sequence of volcanic and plutonic rocks, southern Nye and western Lincoln Counties, Nevada: Geological Society of America Bulletin, v. 81, p. 2657–2676.

Marvin, R. F., Mehnert, H. H., and McKee, E. H., 1973, A summary of radiometric ages of Tertiary volcanic rocks in Nevada and eastern California. Part III—Southeastern Nevada: Isochron/West, no. 6, p. 1–30.

Marvin, R. F., Mehnert, H. H., and Naeser, C. W., 1989, U.S. Geological Survey radiometric ages—Compilation "C," Part three—California and Nevada: Isochron/West, no. 52, p. 3–11.

McDowell, F. W., 1983, K-Ar dating—Incomplete extraction of radiogenic argon from alkali feldspar: Isotope Geoscience, v. 1, p. 119–126.

McIntosh, W. C., Chapin, C. E., Ratte, J. C., and Sutter, J. F., 1992, Time-stratigraphic framework for the Eocene-Oligocene Mogollon-Datil volcanic field, southwest New Mexico: Geological Society of America Bulletin, v. 104, p. 851–871.

McIntyre, G. A., Brooks, C., Compston, W., and Turek, A., 1966, The statistical assessment of Rb-Sr isochrons: Journal of Geophysical Research, v. 71, p. 5459–5468.

McKeown, F. A., Healey, D. L., and Miller, C. H., 1976, Geologic map of the Yucca Lake quadrangle: U.S. Geological Survey Geologic Quadrangle Map GQ-1327, scale 1:24 000.

Minor, S. A., 1989, Paleostress investigation near Rainier Mesa, Nevada Test Site, *in* Olsen, C. W., and Carter, J. A., eds., Proceedings, Fifth Symposium on Containment of Underground Nuclear Explosions: Lawrence Livermore National Laboratory Report CONF-8909163, v. 2, p. 457–482.

Minor, S. A., Sawyer, D. A., Orkild, P. P., Coe, J. A., Wahl, R. R., and Frizzell, V. A., 1991, Neogene migratory extensional deformation revealed on new map of the Pahute Mesa 1:100,000-scale quadrangle, southern Nevada [abs.]: Eos (Transactions, American Geophysical Union), v. 72, p. 469.

Minor, S. A., Sawyer, D. A., Wahl, R. R., Frizzell, V. A., Schilling, S. P., Warren, R. G., Orkild, P. P., Coe, J. A., Hudson, M. R., Fleck, R. J., Lanphere, M. A., Swadley, W. C., and Cole, J. C., 1993, Preliminary geologic map of the Pahute Mesa 30' × 60' quadrangle: U.S. Geological Survey Open-File Report 93-299, 39 p., scale 1:100 000.

Monsen, S. A., Carr, M. D., Reheis, M. C., and Orkild, P. P., 1992, Geologic map of Bare Mountain, Nye County, Nevada: U.S. Geological Survey Miscellaneous Investigations Map I-2201, scale 1:24 000.

Noble, D. C., Vogel, T. A., Weiss, S. I., Erwin, J. W., McKee, E. H., and Younker, L. W., 1984, Stratigraphic relations and source areas of ash flow sheets of the Black Mountain and Stonewall volcanic centers, Nevada: Journal of Geophysical Research, v. 89, p. 8593–8602.

Noble, D. C., Weiss, S. I., and McKee, E. H., 1991, Magmatic and hydrothermal activity, caldera geology, and regional extension in the western part of the southwestern Nevada volcanic field, *in* Raines, G. L., Lisle, R. E., Schaefer, R. W., and Wilkinson, W. H., eds., Geology and ore deposits of the Great Basin, Symposium Proceedings: Reno, Geological Society of Nevada, p. 913–934.

Orkild, P. P., and O'Connor, J. T., 1970, Geologic map of the Topopah Spring quadrangle, Nye County, Nevada: U.S. Geological Survey Geologic Quadrangle Map GQ-849, scale 1:24,000.

Orkild, P. P., Sargent, K. A., and Snyder, R. P., 1969, Geologic map of Pahute Mesa, Nevada Test Site and vicinity, Nye County, Nevada: U.S. Geological Survey Miscellaneous Investigations Series Map I-567, scale 1:48 000.

Parsons, T., and Thompson, G. A., 1991, The role of magma overpressure in supressing earthquakes and topography—Worldwide examples: Science, v. 253, p. 1399–1402.

Pierce, K. L., and Morgan, L. A., 1992, The track of the Yellowstone hot spot—Volcanism, faulting, and uplift, *in* Link, P. K., Kuntz, M. A., and Platt, L. B., eds., Regional geology of eastern Idaho and western Wyoming: Geological Society of America Memoir 179, p. 1–53.

Poole, F. G., Carr, W. J., and Elston, D. P., 1965, Salyer and Wahmonie Formations of southeastern Nye County, Nevada, *in* Contributions to stratigraphy 1965: U.S. Geological Survey Bulletin 1224-A, p. A36–A44.

Rosenbaum, J. G., Hudson, M. R., and Scott, R. B., 1991, Paleomagnetic constraints on the geometry and timing of deformation at Yucca Mountain, Nevada: Journal of Geophysical Research, v. 96, p. 1963–1979.

Sargent, K. A., and Orkild, P. P., 1973, Geologic map of the Wheelbarrow Peak–Rainier Mesa area, Nye County, Nevada: U.S. Geological Survey Miscellaneous Investigations Map I-754, scale 1:48 000.

Sargent, K. A., Noble, D. C., and Ekren, E. B., 1964, Belted Range Tuff of Nye and Lincoln Counties, Nevada: U.S. Geological Survey Bulletin 1224-A, p. 32–36.

Sawyer, D. A., and Sargent, K. A., 1989, Petrologic evolution of divergent peralkaline magmas from the Silent Canyon caldera complex: Journal of Geophysical Research, v. 94, p. 6021–6040.

Scott, R. B., 1990, Tectonic setting of Yucca Mountain, southwest Nevada, *in* Wernicke, B. P., ed., Basin and Range extensional tectonics near the latitude of Las Vegas, Nevada: Geological Society of America Memoir 176, p. 251–282.

Severinghaus, J., and Atwater, T., 1990, Cenozoic geometry and thermal state of subducting slabs beneath western North America, *in* Wernicke, B. P., ed., Basin and Range extensional tectonics near the latitude of Las Vegas, Nevada: Geological Society of America Memoir 176, p. 1–22.

Snyder, D. B., and Carr, W. J., 1984, Interpretation of gravity data in a complex volcano-tectonic setting, southwestern Nevada: Journal of Geophysical Research, v. 89, p. 10 193–10 206.

Stewart, J. H., and Carlson, J. H., 1978, Geologic map of Nevada: U.S. Geological Survey, scale 1:500 000.

Tabor, R. W., Mark, R. K., and Wilson, R. H., 1985, Reproducibility of the K-Ar ages of rocks and minerals—An empirical approach: U.S. Geological Survey Bulletin 1654, 5 p.

Taylor, J. R., 1982, An introduction to error analysis: Mill Valley, California, University Science Books, 269 p.

Taylor, W. J., Bartley, J. M., Lux, D. R., and Axen, G. J., 1989, Timing of Tertiary extension in the Railroad Valley–Pioche transect, Nevada—Constraints from $^{40}Ar/^{39}Ar$ ages of volcanic rocks: Journal of Geophysical Research, v. 94, p. 7757–7774.

Tegtmeyer, K. J., 1990, Regional variation in the Nd and Sr isotopic compositions of Tertiary peralkaline rhyolites from the Great Basin, western U.S. [abs.]: Eos (Transactions, American Geophysical Union), v. 71, p. 1682.

Tegtmeyer, K. J., and Farmer, G. L., 1990, Nd isotopic gradients in upper crustal magma chambers: Evidence for in situ magma–wall-rock interaction: Geology, v. 18, p. 5–9.

U.S. Geological Survey, 1979, Aeromagnetic map of the Timber Mountain area, Nevada: U.S. Geological Survey Open-File Report 79-587, scale 1:62 500.

Vogel, T. A., Noble, D. C., and Younker, L. W., 1983, Chemical evolution of a high-level magma system—The Black Mountain volcanic center: Lawrence Livermore Laboratory Report UCRL-53444, 49 p.

Warren, R. G., 1983, Geochemical similarities between volcanic units at Yucca Mountain and Pahute Mesa—Evidence for a common magmatic origin for volcanic sequences that flank the Timber Mountain caldera, *in* Olsen, C. W., compiler, Proceedings, Second Symposium on the Containment of Underground Nuclear Explosions: Lawrence Livermore Laboratory Report CONF-830882, v. 1, p. 213–244.

Warren, R. G., Byers, F. M., Jr., and Caporuscio, F. A., 1984, Petrography and mineral chemistry of units of the Topopah Spring, Calico Hills, and Crater Flat tuffs, and older volcanic units with an emphasis on samples from USW G-1, Yucca Mountain, Nevada Test Site: Los Alamos National Laboratory Report LA-10003-MS, 78 p.

Warren, R. G., Byers, F. M., Jr., and Orkild, P. P., 1985, Post-Silent Canyon caldera structural setting for Pahute Mesa, *in* Olsen, C. W., and Donohue, M. L., eds., Proceedings, Third Symposium on the Containment of Underground Nuclear Explosions: Lawrence Livermore National Laboratory CONF-850953, v. 2, p. 31–45.

Warren, R. G., McDowell, F. W., Byers, F. M., Jr., Broxton, D. E., Carr, W. J., and Orkild, P. P., 1988, Episodic leaks from Timber Mountain caldera—New evidence from rhyolite lavas of Fortymile Canyon, SW Nevada volcanic field [abs.]: Geological Society of America Abstracts with Programs, v. 20, p. 240.

Warren, R. G., Byers, F. M., Jr., Broxton, D. E., Freeman, S. H., and Hagan, R. C., 1989, Phenocryst abundances and glass and phenocryst compositions as indicators of magmatic environments of large-volume ash flow sheets in southwestern Nevada: Journal of Geophysical Research, v. 94, p. 5987–6020.

Weiss, S. I., Noble, D. C., and McKee, E. H., 1989, Paleomagnetic and cooling constraints on the duration of the Pahute Mesa–Trail Ridge eruptive event and associated magmatic evolution: Journal of Geophysical Research, v. 94, p. 6075–6084.

Wernicke, B. P., 1992, Cenozoic extensional tectonics of the U.S. Cordillera, *in* Burchfiel, B. C., Lipman, P. W., and Zoback, M. L., eds., The Cordilleran orogen: Conterminous U.S.: Boulder, Colorado, Geological Society of America, Geology of North America, v. G-3, p. 553–581.

Wernicke, B. P., Axen, G. J., and Snow, J. K., 1988, Extensional tectonics at the latitude of Las Vegas, Nevada: Geological Society of America Bulletin, v. 100, p. 1738–1757.

MANUSCRIPT RECEIVED BY THE SOCIETY FEBRUARY 17, 1993
REVISED MANUSCRIPT RECEIVED FEBRUARY 15, 1994
MANUSCRIPT ACCEPTED FEBRUARY 24, 1994

Printed in U.S.A.